Designed experiments for efficient engines

Designed Experiments for Efficient Engines

PROEFSCHRIFT

ter verkrijging van de graad van doctor aan de Technische Universiteit Eindhoven,
op gezag van de rector magnificus, prof.dr.ir. F.P.T. Baaijens,
voor een commissie aangewezen door het College voor Promoties,
in het openbaar te verdedigen op vrijdag 4 september 2020 om 16:00 uur

door

Robbert Christian Willems

geboren te Apeldoorn

Dit proefschrift is goedgekeurd door de promotoren en de samenstelling van de promotiecommissie is als volgt:

Voorzitter:	prof.dr. L.P.H. de Goey	
1e promotor:	dr.ir. L.M.T. Somers	
2e promotor:	prof.dr.ir. N.G. Deen	
Copromotor:	prof.dr.ir. F.P.T. Willems	
Leden:	prof.dr.ir. D.M.J. Smeulders	
	prof.dr. Ö. Andersson	(Lunds Universitet)
	dr. A. García-Martínez	(Universitat Politècnica de València)
Adviseur:	dr. B.A. Albrecht	(DAF Trucks NV)

Het onderzoek dat in dit proefschrift wordt beschreven is uitgevoerd in overeenstemming met de TU/e Gedragscode Wetenschapsbeoefening.

Designed Experiments for Efficient Engines
by Robbert Willems
Technische Universiteit Eindhoven, 2020

A catalogue record is available from the Eindhoven University of Technology Library
ISBN: 978-90-386-5101-9
Printed by ADC Dereumaux
Cover design by Paul Verspaget

This research is funded by the Dutch Research Council (NWO), domain Applied and Engineering Sciences (TTW) under project number 14927: Towards a HiEff Engine. Industry support is given by TNO Automotive, DAF Trucks, Shell Global Solutions and Delphi Technologies.

Dissertation summary

Designed Experiments for Efficient Engines

Carbon dioxide (CO_2) regulations on heavy-duty vehicles are introduced in essentially all markets within the next decade. The resulting drive for highly efficient engines has moved research towards new combustion concepts. A promising concept is reactivity controlled compression ignition (RCCI), which utilizes two fuels of different reactivities to control the combustion process. RCCI holds great promise for high thermal efficiency and emitting very low levels of nitrogen oxides (NO_x) and soot. Moreover, RCCI has a fuel flexible character, which offers the possibility to employ low carbon fuels for further CO_2 reduction. However, conventional diesel combustion (CDC) has maintained a firm position in the heavy-duty market and is still incrementally improved. The future of heavy-duty diesel engines is thus far from clearly set out. The goal of the work described in this dissertation is to experimentally chart, understand and compare the capabilities of both combustion regimes to maximize the gross indicated efficiency (GIE) within legislative limits of emissions and mechanical constraints. The experiments are performed at load-speed points that correspond to highway cruising and using practical fuels, i.e., fuels that are compatible with current engine hardware and have an existing infrastructure. First, the focus is directed towards injection rate shaping in CDC. Thereafter, the potential of RCCI is explored through optimization of air path and fuel injection parameters. The tests were systematically conducted using the design of experiments (DOE) methodology and regression analysis was employed to study multiple operating parameters and their corresponding interactions. This approach sets itself apart from varying one factor at a time, which is a widely used method in research, but induces the chance of missing relevant interactions. Identifying relations among operational parameters is crucial for a comprehensive understanding of engine behavior.

The use of post injections in CDC operation, i.e., one or more small injections after a larger main injection, has gained a lot of attention in engine research. Post injections have previously displayed ambiguous outcomes in literature regarding efficiency and pollutant emissions. Reductions of soot emissions were most frequently reported, but the actual efficacy differed between publications. A few of the previous studies also showed reductions of NO_x emissions and fuel consumption. Several obscurities are clarified in this dissertation by studying the impact of operational settings on post-injection efficacy. The results confirmed complex interactions of the post-injection timing and quantity with other settings like the main injection timing, common rail pressure, rate of exhaust gas recirculation (EGR) and intake manifold pressure. These interactions were effectively identified using DOE in combination with multiple regression analysis. The results indicated that a short-dwell, large-split post injection at low load showed promise for simultaneous reductions of fuel consumption and pollutant emissions.

A propitious next step is applying continuous injection rate shaping in the CDC regime, for which a specialized double solenoid fuel injector was tested. This injector allows to adjust the fuel rate within a single injection event without flow

interruption. The tests were focused on ramped rates versus traditional square rates under various settings of the EGR rate and fuel pressure. Ramped rates were created by delaying the start of actuation of one solenoid valve with respect to the other, while the ramp duration was varied by changing the actual start delay. The results indicated that essentially equal gross indicated efficiencies are reached with both rate shapes, although at an elevated engine speed the ramped profiles attained peak GIE at lower engine-out NO_x emissions. Heat transfer loss was shown to be reduced with the application of ramped rates, but a concurrent longer burn duration increased the exhaust loss, rendering the peak GIE equal to that using square rates. Ramped rates generally also lead to higher soot emissions. More importantly, rates of heat release showed that a substantial extension of ignition delays in ramped rate operation caused limited control over separate combustion phases, despite well-controlled injection events. Future work should aim on improving burn rate controllability by reducing the ignition delays.

The use of gasoline as low reactivity fuel in RCCI was optimized using air path and fuel injection settings and was subsequently compared to optimal CDC operation. At intake manifold pressures that are comparable with modern turbocharger capabilities, CDC outperformed RCCI except for NO_x emissions, which are superiorly low in RCCI operation. When the intake air is further boosted, RCCI surpasses CDC on all fronts except for higher emissions of unburned hydrocarbons and carbon monoxide. The GIE in RCCI operation was shown to primarily benefit from extremely low heat transfer budgets through low local temperatures. Still, issues in controlling combustion phasing using fueling parameters were substantial and required the use of excessive EGR rates. This ultimately resulted in limitations of the peak GIE due to low values of the specific heat capacity ratio.

Therefore, further experiments focused on the application of E85, which has a substantially higher octane rating than gasoline. The utilization of E85 showed evident benefits for combustion control. EGR addition was demonstrated to be redundant for proper combustion phasing. A comprehensive analysis revealed that the rates of heat release display specific shapes at different degrees of reactivity stratification, which is in turn controlled by the fuel injection settings. These shapes were characterized using a metric called the burn ratio and showed that a relatively gradual first stage of combustion followed by a fast burnout is most favorable for optimal GIE. Furthermore, regression analysis indicated that heavy intake air boosting needs to be combined with a sufficiently early diesel injection to fully exploit the low heat transfer ability of RCCI combustion, although some reactivity stratification remains necessary for acceptable combustion efficiency.

The influence of the direct injection nozzle specifications on RCCI combustion was finally investigated on a new single-cylinder engine setup. Several direct injectors with different spray included angles were tested and compared under different intake manifold pressures, diesel injection timings and E85 mass percentages. The results suggest that an angle slightly narrower than the original CDC nozzle is best suited for RCCI because of an optimized distribution of diesel. Yet, peak GIE was limited on this setup due to a slow burnout of the charge, which is possibly linked to large amounts of fuel ending up in the crevices between piston and liner. Future work needs to address this slow burnout by improving the port fuel injection.

RCCI shows promise to improve GIE compared to CDC at highway cruising conditions. CDC, on the other hand, has the advantage of being a robust and established principle and displays potential for extracting extra efficiency points. To comply with future CO_2 and pollutant emission legislation, it is likely that engine hardware complexity needs to increase with, e.g., waste heat recovery systems. Furthermore, mode-switching between RCCI, conventional dual-fuel operation and CDC can aid in the optimization over the entire range of loads and speeds. This will require several development steps and vast amounts of resources. Indisputable CO_2 reductions can be made by switching to sustainable fuels, but a well-to-wheel mandate is necessary to make full use of this opportunity.

Contents

Chapter 1

Engine efficiency in context

Introduction

The diesel engine has been an extremely reliable power source for over a century. It has been notably utilized in the heavy-duty transport sector, where it remains the dominant technology to date. Diesel engine efficiency has increased steadily throughout the decades since its invention, which has inherently led to lower carbon dioxide emissions per amount of injected fuel. However, the growing use of internal combustion engines and fossil fuels in general have a clear impact on global warming and air quality, which has led to the worldwide adoption of greenhouse gas and pollutant emission regulations. The question that arises is: can the diesel engine facilitate a sustainable future of heavy-duty transport? Although the use of alternative fuels can account for a considerable reduction of the carbon footprint, attaining a highly efficient thermodynamic cycle is crucial to the task. The experimental work described in this dissertation investigates several pathways to increase the gross indicated efficiency of heavy-duty diesel engines. Advanced fuel injection strategies to improve conventional diesel combustion are explored, as well as the potential of a very promising dual-fuel concept known as reactivity controlled compression ignition.

1.1 A brief history of diesel engine development

The invention of the diesel engine marked the beginning of significant efficiency enhancements of reciprocating heat engines. At the end of the nineteenth century, steam engines were the dominant stationary power source for industry, although reciprocating combustion engines were already widely used as well. Both engine types typically yielded brake efficiencies around 10% and had low power-to-weight ratios. In his earliest efforts, Rudolf Diesel envisioned a piston engine working with the Carnot cycle, but he soon discovered that theory and reality did not match. Many practical limitations rendered such operation impossible and in his second attempt, he adopted the idea of isobaric combustion. After many trials, the first acceptance test of his engine in 1897 confirmed a brake efficiency of roughly 26%, which was more than double of the standard at the time [1].

Many others saw the potential of the diesel engine too, and when the first patents expired in 1908, its development expanded rapidly. Notable progress began with the mass production of the inline fuel pump by Robert Bosch GmbH [2], which allowed much higher fuel pressures to be reached. The diesel fuel could now be properly atomized during injection, which ensured stable compression ignition operation, but also raised the brake efficiency. The way to high speed appliances in the transportation sector was paved. The use of diesel engines only went up since then, first in ships and trucks, and later also in passenger cars.

Major progress continued when turbochargers became more widely applied in the years after the Second World War, although the technology had been around for several decades after being invented by Swiss engineer Alfred Büchi in 1905. Some of the residual energy in the exhaust gas could now be used for boosting the intake air, initially as a means to extend the maximum load [3]. After the oil crises of 1973 and 1979, however, the benefits of forced air induction were gratefully exploited for optimizing efficiency and emissions too [4]. The common problem of a slow response at low speeds (i.e., turbo lag) was eventually alleviated by the application of turbines with variable geometries.

Fuel injection equipment incrementally improved over the years, resulting in better mixing of fuel and air [5]. Electronically controlled fuel pumps and injectors provided more flexibility in selecting injection pressure and timing, which proved crucial for optimizing combustion to comply with directives for exhaust emissions, first introduced in 1992. These electronic components also gave the possibility of multiple injections and precise quantification of fuel pulses. A valuable addition came in the form of the common rail. This technology decoupled the injection pressure and timing from the engine speed, essentially giving full calibration flexibility.

1.2 Environmental impact of diesel engines

1.2.1 Air quality

Nowadays, global society and its economy rely heavily on the use of combustion engines and fossil fuels. Diesel engines are the preferred choice when it comes to the transportation of goods over large distances, because of their reliability, low maintenance cost, high power-to-weight ratio and, of course, their excellent brake efficiency. Their principal downside is that relatively high levels of particulate matter (PM) and nitrogen oxides (NO_x) are emitted, both of which severely affect local air quality, especially in urban areas where traffic density is high. These pollutants have been linked to cardiovascular and respiratory diseases, through which they can cause premature death [6]. These concerns led to the introduction of emission standards in the European Union (EU) that have been tightened over the course of the last three decades. Figure 1.1 shows these increasingly strict limits of PM and NO_x for heavy-duty diesel engines over the years. Additional clean air legislation in the EU has resulted in the formation of low-emission zones in urban areas [7], where mainly vehicles equipped with older diesel engines may no longer enter. Only few studies have assessed the impact of these measures, but do report modest benefits for air pollution and public health [8, 9]. Large scale nitrogen deposition is of concern as well, which finds its origin in both agricultural ammonia and traffic-related NO_x emissions. Such nitrogen deposits threaten biodiversity [10], and thus, the need for not only highly efficient, but also very clean diesel engines is evident.

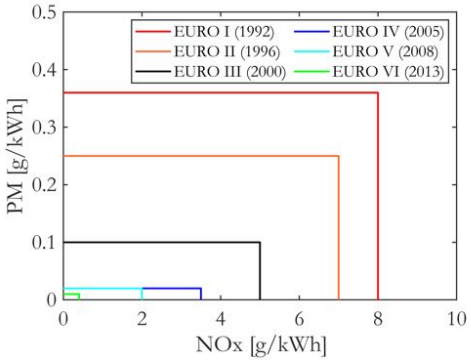

Figure 1.1: Emission standards in the European Union for heavy-duty diesel engines in on-road applications including the year that each standard became effective.

1.2.2 Global warming

On a global scale, the atmospheric concentration of carbon dioxide (CO_2) is known to increase due to human activities [11]. The use of fossil fuels in combustion engines for transportation is one of the main components in this trend. The associated global warming causes rising sea levels and climate change, of which the effects on the world's ecosystems are alarming [12]. For these reasons,

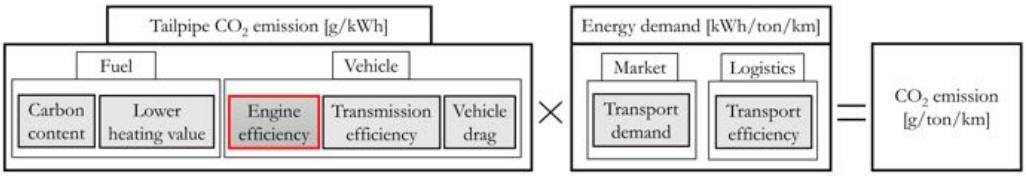

Figure 1.2: Categorization of factors influencing the total tank-to-wheel CO_2 emission of freight transportation. Reductions can be accomplished in many aspects of transport, of which the engine is only one part.

CO_2 emission legislation is introduced in essentially all markets, for both light-duty and heavy-duty vehicles [13]. After signing the Paris Agreement in 2015, the EU has adopted standards for heavy-duty vehicles, mandating a 15% tailpipe CO_2 reduction in 2025 relative to a baseline in 2019 [14]. In addition, a reduction of at least 30% compared to that same 2019 baseline is set for 2030. Figure 1.2 displays a categorization of factors influencing the total CO_2 emission. Vast reductions can obviously be accomplished by improving the efficiency of getting goods from one place to the other. Market demand evidently is the main driver in transportation activity, and thus customer awareness plays a role as well. The use of bio-fuels has the potential to considerably reduce the carbon footprint of freight transportation, but legislation currently aims at tailpipe emissions, thereby demoting the fuel impact considerably. The CO_2 abatements must partly come from design changes on a vehicle level, such as improved aerodynamics, but it is certain that engine efficiency will have to increase significantly in the coming years, while keeping pollutant emissions within legislative limits. This is the challenge that lies ahead.

1.3 Fundamentals of engine efficiency

1.3.1 Efficiency definitions

This dissertation engages in optimizing the gross indicated efficiency (GIE) of heavy-duty diesel engines. The idea is visualized in Figure 1.3, where the highlighted parts indicate the focus area of this work. First, the chemical energy of the fuel is converted to heat by combustion, which increases the pressure inside the combustion chamber. Partially oxidized components like unburned hydrocarbons (UHC) and carbon monoxide (CO) may still be present after the combustion process, yielding some unexploited chemical energy. The generated heat then needs to be converted to useful work by expansion of the working gas. The hot gas also transfers heat to the cylinder walls during the combustion cycle; this energy is not used for work generation. Furthermore, some energy in the form of heat is left after expansion, which is expelled via the exhaust. The heat transfer and exhaust loss together determine the thermal efficiency. Hence, three energy loss channels need to be considered for GIE optimization. Figure 1.3 also displays how the eventual brake efficiency is reached. Some work is needed for exchanging the combustion products with a fresh charge, which results in pumping losses that are related to the gas exchange efficiency. Friction of piston rings and bearings also brings about losses that limit the brake work. Parasitic losses like fuel pump work are often grouped under friction losses and the associated mechanical efficiency. The gas exchange and mechanical efficiency are not considered in this dissertation.

1.3.2 Engine thermodynamics

Let us now consider the theory behind the thermal efficiency of a diesel engine. Two processes play a particular crucial role: combustion and heat transfer. The combustion event is most often described using the rate of heat release (ROHR), whereas the rate of heat transfer (∂Q_{ht}) specifies the heat flux through the combustion chamber walls. In essence, these two processes need to be optimized

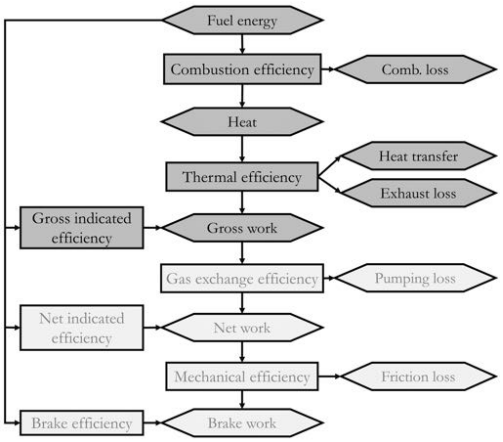

Figure 1.3: Flow chart of separate efficiency constituents and energy loss channels. The work in this dissertation focuses on the highlighted section.

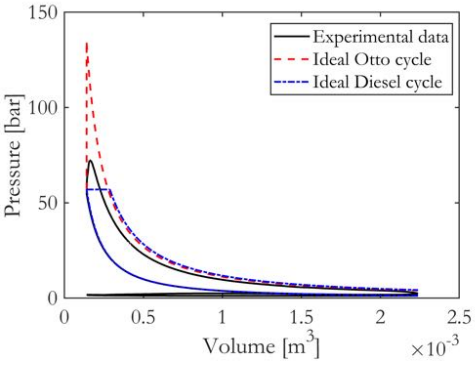

Figure 1.4: An example of a pressure-volume diagram. A measured pressure trace is shown, alongside the Otto and Diesel cycles for the same initial conditions and fuel amount as in the experiment.

for the engine to yield maximal thermal efficiency. The first law of thermodynamics, applied to the closed cycle of an engine, relates the change of internal energy ($\mathrm{d}U$) to heat transfer (δQ_{ht}) and rate of work ($p\mathrm{d}V$) by

$$\mathrm{d}U = \delta Q_{ht} - p\mathrm{d}V \tag{1.1}$$

The term $\mathrm{d}U$ is related to the ROHR ($\sum u_i \, \mathrm{d}m_i$) and the temperature change ($\mathrm{d}T$) via

$$\mathrm{d}U = mC_v\mathrm{d}T + \sum u_i \mathrm{d}m_i \tag{1.2}$$

where m is the total charge mass, C_v is the specific heat capacity at constant volume, u_i and m_i are the specific energies and masses of the gas constituents, respectively.

The gross indicated efficiency is defined as the ratio of the gross indicated work output and the fuel energy input. The former follows from integration of the pressure-volume (p-V) diagram over the compression and expansion strokes. Its surface area thus needs to be maximized for a given amount of injected fuel. An example diagram is shown in Figure 1.4, where an actual measured pressure trace is plotted together with two ideal thermodynamic cycles: the Otto cycle and the Diesel cycle. These ideal cycles are characterized by isochoric (Otto) and isobaric (Diesel) heat addition. For these ideal cycles, it is assumed that there is no heat flux into or out of the system ($\delta Q_{ht} = 0$), all fuel is converted to heat and the working fluid is an ideal gas. Without going into the details of its derivation, it can be graphically confirmed that the Otto cycle provides the largest amount of work of the three cases. That notion adds another feature to the ideal situation: instantaneous combustion at top dead center (TDC). While in principle the centroid of heat release can be tuned to occur at TDC, the combustion process always takes a finite amount of time. This puts the first restraint on attaining the theoretical maximum efficiency, known as the Otto efficiency (η_{Otto}) expressed by

$$\eta_{Otto} = 1 - \frac{1}{r_c^{\gamma-1}} \tag{1.3}$$

Equation 1.3 indicates that the theoretical thermal efficiency is dependent on the compression ratio (r_c) of the engine and the ratio of specific heat capacities (γ) of the working gas. By increasing r_c, the working gas is compressed to higher pressure, hence reaching higher combustion pressures. This is ultimately limited by mechanical constraints at higher loads due to excessive peak pressures. More-

over, the expansion ratio is at the same time enlarged, and together these effects readily increase the p-V surface area. For γ also counts that higher values increase the thermal efficiency. Its value is related to the degrees of freedom (f) of a molecule ($\gamma = 1 + 2/f$). Monatomic gases, such as noble gases ($f = 3$), possess the highest possible value ($\gamma = 5/3$), which is the reason for increased interest in the argon power cycle [15] in recent years. For diatomic gases, like the primary constituents of air, molecular nitrogen (N_2) and oxygen (O_2), $f = 5$ at room temperature. Hence, air retains $\gamma = 1.4$ at standard atmospheric conditions. In an ideal cycle, this value is treated as a constant, but for real gases there is a temperature dependency. For temperatures typically encountered in combustion, vibrational degrees of freedom are activated and this lowers γ, thereby also decreasing the maximum efficiency. In certain cases where it is necessary to recirculate exhaust gases back into the cylinder, triatomic combustion products (CO_2 and H_2O) are added to the working gas, inherently increasing f and thus leading to even lower γ values.

Even before considering heat transfer, the actual efficiency further deviates from the Otto efficiency for reasons that are not directly related to the thermal efficiency characteristics. The exchange of gases occurs through poppet valves that open and close the combustion system. Due to mechanical restrictions (e.g., valves cannot open and close instantaneously) and particular valve timing requirements for an efficient gas exchange, the valves do not open or close exactly at bottom dead center (BDC) or TDC. The intake valve is typically closed several degrees after BDC, which lowers the pressure at the end of compression and consequently also the peak combustion pressure. The exhaust valves, on the other hand, are usually opened several crank angle degrees before BDC, thereby not completing expansion entirely.

1.3.3 Heat transfer

The energy balance shown in Equation 1.1 becomes considerably more intricate with the inclusion of heat transfer. In engine combustion, it is assumed that convection dominates the process of heat transfer from the gas to the cylinder walls, which is expressed by

$$\delta Q_{ht} = h_c A \left(T_{gas} - T_{wall} \right) \tag{1.4}$$

where A is the combustion chamber wall surface area, T_{gas} is the global gas temperature and T_{wall} is the wall temperature. The heat loss coefficient (h_c) is often calculated by correlations for spatially-averaged values using

$$Nu = a Re^m Pr^n \tag{1.5}$$

where a, m and n are model-specific fit constants. The Nusselt number (Nu, the ratio of convective to conductive heat transfer) is related to the Reynolds number (Re, the ratio of inertial to viscous forces) in a power law, as first proposed by Annand [16]. The Prandtl number (Pr) is almost constant for gases and is most often neglected in this relation. Equation 1.5 can be rewritten as

$$\frac{h_c L}{k} = a \left(\frac{\rho v L}{\mu} \right)^m \tag{1.6}$$

where Pr is left out, L is a characteristic length scale, k is the thermal conductivity of the gas, ρ is the in-cylinder density, v is a characteristic velocity and μ is the dynamic viscosity of the gas. Both k and μ are temperature dependent quantities. Especially the selection of L and v has been debated [17], since representative values are needed to properly condense h_c into a spatially-averaged value.

As the rate of heat transfer is strongly influenced by both density and temperature in the combustion chamber, it is not so certain that very rapid combustion at TDC will yield maximum thermal efficiency in a real cycle. To prevent excessive temperatures and pressures, the combustion phasing is actually often delayed into the expansion stroke by several crank angle degrees, which evidently limits the attainable thermal efficiency further. However, delaying combustion is not only

necessary to optimize the thermal efficiency, but also serves to prevent excessive peak pressures to remain within mechanical constraints and lower peak temperatures in order to mitigate NO_x formation. Reverting to Figure 1.4 learns that in a real situation, approaching the ideal Diesel cycle has a favorable element, since the compression ratio can be well increased without extremely raising peak pressure and temperature. It is conceivable that peak thermal efficiency is reached using a mix of isochoric "Otto" and isobaric "Diesel" combustion, of which the relative proportions will depend on specific operational conditions for an optimal balance of heat transfer and the expansion ratio.

Despite that the heat flux from the working gas to combustion chamber walls is generally estimated using spatially-averaged values, it is certainly a surface process that is besides affected by intricate flow phenomena. Because temperature and flow properties are not homogeneous, heat transfer proceeds in different ways under various operational conditions and combustion regimes. After all, it matters where it gets hot, and how high local temperatures reach. This dissertation aims to understand the peak GIE potential of two fundamentally different combustion regimes. One is the conventional diesel combustion (CDC) regime, characterized by a high temperature, turbulent diffusion flame. The other is the reactivity controlled compression ignition (RCCI) concept, which utilizes a large degree of charge dilution and fuel premixing prior to combustion. In the following, these combustion regimes are outlined to further address their fundamental differences.

1.4 Conventional diesel combustion

Regardless of appreciable advancements in diesel engine technology, the principles of operation and the combustion process remained largely unchanged over the years [18]. A schematic representation of a four stroke, compression ignition engine is shown in Figure 1.5. Air alone, or an air and exhaust gas mixture, is inducted into the cylinder via the intake manifold. Thereafter, the charge is compressed to high pressure and temperature

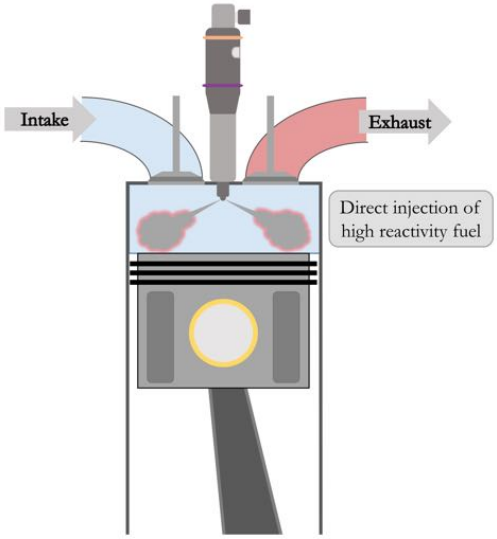

Figure 1.5: Schematic representation of CDC operation. Generally, a mixture of fresh air and recirculated exhaust gas is inducted via the intake valve. Fuel is directly injected into the cylinder.

as the piston moves upwards. Somewhere near TDC, fuel is administered directly into the combustion chamber with extremely high fuel pressure. The low volatility, but highly reactive fuel atomizes, evaporates in the hot environment and rapidly mixes with the available air. A short time period is needed for ignition to occur; this period is called the ignition delay. The ignition delay is followed by autoignition of the pre-mixture and a rather intense first part of the combustion event called the premixed phase. Depending on the duration of injection, the fuel subsequently burns in a quasi-steady, lifted diffusion flame for a certain amount of time. Eventually, injection stops and the flame may retreat back towards the injector in a process called combustion recession. The mixing rates gradually decline and the rate of heat release subsides as the remaining fuel fragments slowly burn out. The described sequence of combustion phases is further elucidated in Figure 1.6 and Figure 1.7. The former plot shows four image stills taken on a heavy-duty optical diesel engine, whereas the latter plot displays a typical rate of heat release in CDC operation.

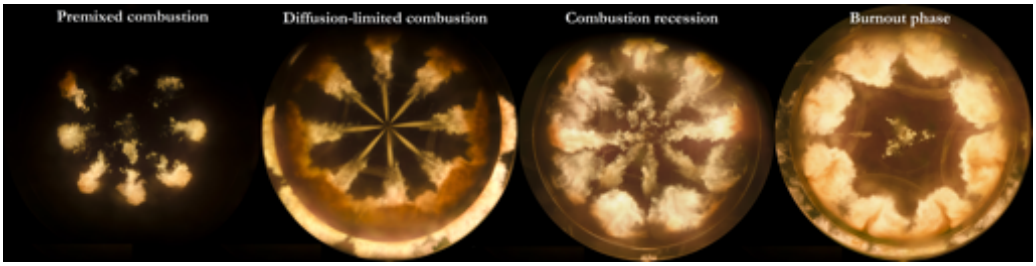

Figure 1.6: True-color recordings of conventional diesel combustion in a heavy-duty optical engine. The pictures are taken with a consumer camera from below a transparent piston using a 45° turning mirror and represent the four distinctive phases detailed in the main text. Images courtesy of Robin Doddema and P.C. Bakker.

Compression ignition operation is in general more efficient than spark ignition operation. This fact is to a large extent due to better satisfying the requirements of the theoretical efficiency as defined in Equation 1.3. Injecting fuel directly in the cylinder around TDC as a means to control the autoignition moment allows to operate at higher compression ratios. Spark ignition (gasoline) engines, on the other hand, run on a well-mixed, stoichiometric air-fuel charge. Autoignition is prevented by lowering the compression ratio, since the combustion process would otherwise be too violent. Unlike gasoline engines, diesel engines are operated with an excess of air. This excess air acts as a heat buffer and readily suppresses the global gas temperature, thereby maintaining a higher ratio of specific heats. The lack of a throttle mitigates gas exchange losses; another favorable aspect of the diesel engine.

In terms of pollutant emissions, the gasoline engine generally performs better compared to the diesel engine. Because of sufficient mixing prior to combustion, very little soot is formed in spark ignition operation. Unburned hydrocarbons (UHC), carbon monoxide (CO) and NO_x are indeed emitted, but these components are effectively reduced via three-way catalytic conversion. The diesel engine, however, produces considerable amounts of soot and NO_x, because an injected fuel parcel resides in both rich (high Φ) and hot conditions [19]. This is visualized in Figure 1.8, where a Φ-T diagram is illustrated including the aforementioned fuel parcel trajectory. The (local) equivalence ratio (Φ) is defined as

$$\Phi = \frac{AFR_{st}}{AFR} \tag{1.7}$$

where AFR is the actual air-to-fuel ratio and AFR_{st} is the associated stoichiometric value.

Soot and NO_x formation zones are displayed in grey and red, respectively. In blue, the trajectory of a fuel parcel is indicated. Although a vast amount of soot is formed in the grey zone, most is oxidized later on in the lean, hot conditions of the NO_x formation region. Still, some of the soot is expelled into the exhaust together with substantial amounts of NO_x. Application of a three-way catalyst requires stoichiometric operation and is thus not effective in CDC, because of its continuous operation with excessive air. In modern diesel engines, combustion temperatures are therefore suppressed by applying (cooled) EGR to mitigate the formation of NO_x. This same method is applied in this dissertation, where the aim is to keep the specific NO_x levels in CDC operation below 7 g/kWh so that a typical aftertreatment system is capable of bringing it down to legislative levels. Unfortunately, measures like EGR to reduce combustion temperatures do also increase the emission of soot. This tradeoff is persistent and is usually referred to as the diesel dilemma. The aim in this dissertation is to keep engine-out soot below 0.01 g/kWh, which is the current legislative standard. To lower the tailpipe emission of soot, a diesel particulate filter (DPF) is now standard equipment,

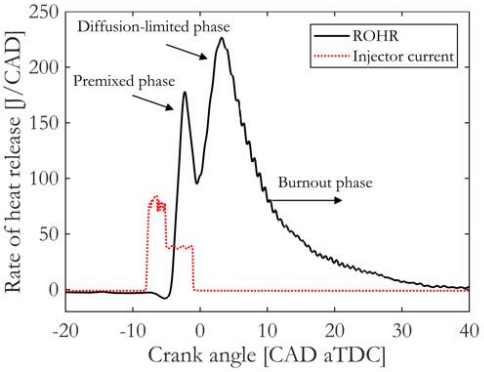

Figure 1.7: Typical aROHR plot for conventional diesel combustion. The actuation current is shown to indicate the injection event.

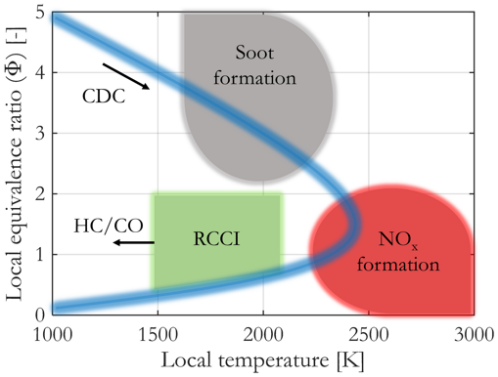

Figure 1.8: Local equivalence ratio versus local temperature representing the combustion space. Soot and NO_x formation zones are shown in grey and red, respectively. The blue line indicates the trajectory of a fuel parcel in CDC operation. The green region displays the ideal operating area of RCCI combustion.

which has to be actively regenerated periodically. Further NO_x reduction has to be accomplished using sophisticated aftertreatment systems. The most common technology is selective catalytic reduction (SCR), for which ammonia or urea is injected into the exhaust stream. Both DPF regeneration and SCR fluid consumption increase the total cost of operation and are hence undesired.

1.5 Reactivity controlled compression ignition

The increasing need for highly efficient and clean engines has moved research towards combustion concepts that provide ample time for mixing of fuel and air before autoignition. Initially, the focus was directed to virtually fully homogeneous, heavily diluted mixtures that are ignited by compression, which is known as homogeneous charge compression ignition (HCCI) [20]. Due to its homogeneous nature, ignition and combustion are largely governed by chemical kinetics making it difficult to control the ignition timing. To prevent premature ignition and extremely violent combustion, considerable EGR rates and boosted intake manifold pressures are used to lower the charge reactivity [21]. Furthermore, higher octane fuels are generally more suitable for HCCI operation, although there exists a tradeoff between extending the high load limit and preventing excessive combustion losses at low load. These issues endow HCCI with a limited operable load range and little control authority on combustion phasing. Moreover, settings of intake manifold pressure and temperature, as well as the EGR rate, do not provide the timely response needed for transient engine operation. Several strategies have been proposed to increase the HCCI controllability and operating range, such as partial stratification of the air-excess ratio ($\lambda = 1/\Phi$) using both direct injection (DI) and port fuel injection (PFI) [22].

The idea of combustion phasing control using a varying degree of λ-stratification led to the emergence of two other combustion concept called premixed charge compression ignition (PCCI) and partially premixed combustion (PPC). Although PCCI and PPC are not that distinctive in practice, it is the actual level of premixing that sets them apart. PCCI, for that matter, is closer related to HCCI than PPC. Still, all three concepts share the properties of long mixing times and low local temperatures, hence these new operating regimes were grouped under the general term low temperature combustion (LTC) [23]. LTC has the potential for very low soot and NO_x emissions, while attaining diesel like efficiency, or higher. The issues of poor controllability unfortunately per-

sisted, which seems to primarily stem from the use of a single fuel. Olssen [24] therefore proposed a dual-fuel HCCI concept by applying two PFI systems. In their work, the difference in reactivity between ethanol and n-heptane was used to control the ignition timing. With increasing load, relatively more low reactivity ethanol was injected to prevent an early onset of combustion. Other groups combined the methods of partial λ-stratification and blending of fuels with different reactivities [25, 26] by a combination of low reactivity fuel injection in the intake manifold and high reactivity fuel injection directly into the combustion chamber. This provided an additional degree of freedom in combustion phasing control, while still attaining low NO_x and soot emissions. Inagaki [27] refined this partially stratified, dual-fuel concept and proposed to use the blend ratio of the two fuels for ignition control, while spatial stratification provides a way to temper the combustion rate. Researchers at the University of Wisconsin-Madison further investigated the potential of this new LTC concept, which was eventually termed reactivity controlled compression ignition (RCCI). That same group reported gross indicated efficiencies (GIE) over 50% [28], while complying with US legislation for soot and NO_x without aftertreatment. RCCI is at present considered a very - if not the most - promising combustion concept for compliance with upcoming CO_2 and pollutant regulations.

A schematic representation of RCCI operation is illustrated in Figure 1.9. A relatively volatile, high octane number (ON) fuel is injected into the intake air stream, which is indicated by the orange color. This fuel has a considerable time to distribute in the combustion chamber, forming a practically homogeneous mixture. The initial charge represents the base reactivity, which can subsequently be adjusted using direct injection of a high reactivity fuel. In case the base reactivity is not sufficiently low, and still causes premature ignition, either the EGR rate can be increased or an even higher ON fuel must be applied. The direct injection of a high reactivity fuel, indicated by the green color, lowers the global ON, thereby increasing the tendency for autoignition. Hence, the balance of the two fuels can be varied according to the requirements of a particular operating point, such that ignition occurs at a thermodynamically favorable moment. Furthermore, the DI timing can be used to create a spatial stratification of Φ and ON to further adjust the local ignitability of the charge. This provides an additional means for controlling combustion phasing, but also allows to reduce the ROHR intensity. In practice, also temperature is unevenly distributed within the cylinder and this too affects the local reactivity. However, there are no direct measures to adjust this temperature distribution. Hence, the term fuel reactivity stratification used throughout this dissertation refers to the stratification of Φ and ON.

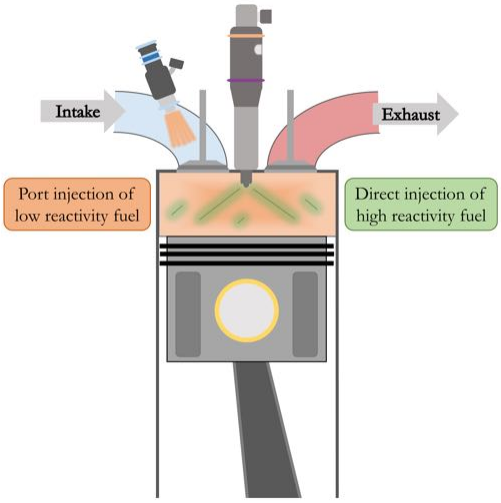

Figure 1.9: Schematic representation of RCCI operation. The blend ratio of PFI to DI fuel controls the global octane rating, whereas the direct injection timing is used to adjust the stratification.

Figure 1.8 displays the optimal combustion space for RCCI operation in green. Allowing the fuel sufficient time to mix creates local conditions that are lean and cool enough to mitigate both soot and NO_x formation. The work in this dissertation aims to keep both of these pollutant emissions in RCCI operation below their legislative levels without any aftertreatment. The ability to operate in the ideal combustion space is crucial, thus

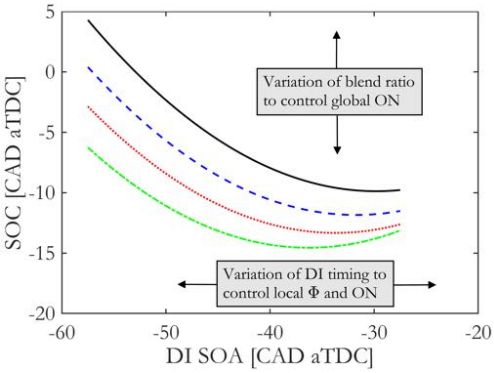

Figure 1.10: Example plot of SOC versus DI timing at four different blend ratios. SOC is used to express the charge reactivity. ON = octane number.

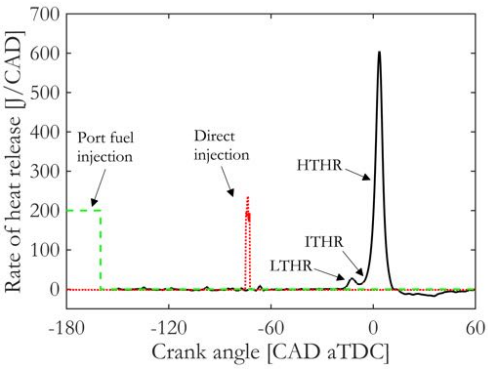

Figure 1.11: Typical aROHR plot in RCCI operation using gasoline and diesel. Both the PFI and DI actuation intervals are displayed in arbitrary units. Low temperature (LTHR), intermediate temperature (ITHR) and high temperature heat release (HTHR) are indicated by arrows.

the selection of appropriate fuels, fuel injection parameters and air path settings are essential. It is especially a low combustion efficiency that is of concern, which occurs at too lean and cold local conditions where the oxidation of HC and CO stagnates. Figure 1.10 shows the start of combustion (SOC) as function of the DI start of actuation (SOA) for four different blend ratios. The SOC is here used as an alternate expression for reactivity, meaning that retarded SOC is the result of lower reactivity, and vice versa. The extent in which the SOC can be adjusted is largely dependent on the difference in octane ratings of the two applied fuels. The larger the difference, the more leeway is created for SOC adjustments. Figure 1.10 furthermore shows an inverse relation of SOC and the DI SOA: an earlier direct injection retards combustion. This behavior is the opposite of that in CDC, where mixing is the limiting factor for ignition. After all, fuel injection occurs around TDC when global temperature has already exceeded the autoignition temperature of the fuel. In RCCI operation, contrarily, the mixing process takes place much earlier in the compression stroke, which makes temperature the limiting factor for ignition. As the local Φ decreases by extending the mixing time, a higher temperature is required to initiate combustion. The range in which such a kinetically controlled ignition event occurs is in this dissertation defined as the RCCI regime.

Since ignition and combustion in RCCI are governed by chemical kinetics, the ROHR is vastly different than in CDC. Figure 1.11 shows a sample plot of the apparent ROHR in a typical RCCI experiment. Generally, the burn duration is much shorter compared to CDC. While this is considered a positive feature from a thermodynamic viewpoint, it can also result in excessive peak pressures and pressure rise rates. In all experiments done within the scope of this dissertation, peak pressures were kept below 200 bar and the maximum pressure rise rates were limited to 20 bar/CAD as a safety constraint. Furthermore, combustion stability in terms of the mean effective pressure and combustion phasing is meticulously monitored in real-time during the RCCI tests. An obvious feature of RCCI combustion is a small "hump" before initiation of the main heat release. This event is called the low temperature heat release (LTHR), which occurs below 850 K. LTHR produces a radical pool through hydrogen abstraction and isomerization reactions [21]. This LTHR phase is followed by a period of insignificant heat release. Above 1000 K, heat release continuous through an increasing formation of hydroxyl (OH) radicals, which further increases temperature. This phase is called the inter-

mediate temperature heat release (ITHR). When the temperature eventually reaches 1200 K, chain branching reactions become dominant, thereby significantly accelerating OH generation. In this high temperature heat release (HTHR), the fuel is rapidly consumed.

1.6 This dissertation

1.6.1 Objective

The main objective of this work is to increase the understanding of the combustion process to enhance the GIE of heavy-duty diesel engines, while attaining acceptable levels of pollutant emissions. This is necessary to facilitate a sustainable future of freight transportation and to comply with upcoming emission legislation. Part of the carbon footprint reduction must come from the use of sustainable fuels, and as such, fuel production is expected to shift from fossil sources to (local) renewable alternatives. A prerequisite of future heavy-duty engines is thus a fuel flexible character, for which both CDC and RCCI show promise through utilization of, e.g., synthetic diesel fuels and bio-alcohols. However, current CO_2 regulations focus on tailpipe emissions, thereby ignoring the potential CO_2 reduction from well-to-tank. This explains the evident focus on increasing brake efficiency, for which both further improvement of CDC or adopting the RCCI concept are viable approaches. Despite significant progress developing and understanding RCCI combustion on a laboratory level by several research groups [29, 30], the concept has not been put into production to date. What is the peak GIE potential of RCCI, and how does this compare to CDC? This needs to be further clarified to make the concept attractive for development towards production. How are these peak values of GIE established with settings of operational parameters, and how are the energy loss channels distributed? This work aims to answers these questions and shed light on the implications towards increasing the brake efficiency of future engines. The use of "practical" fuels is favored for the moment. These include fuel candidates that are compatible with contemporary engine hardware and have an existing production and retail infrastructure. European specification diesel (EN590) is therefore applied in the CDC tests and as high reactivity fuel in the RCCI experiments. Conventional gasoline (EN228) and E85 (a blend of 85% ethanol and 15% gasoline by volume) are studied as low reactivity fuels in RCCI mode.

1.6.2 Outline

This dissertation is organized as follows. Chapter 2 discusses the engine setups and the experimental design. The design of experiments (DOE) methodology is used to arrange the test runs, and statistical techniques are applied to analyze the data. The DOE methodology has the benefit of testing multiple operating parameters and their interactions in a limited number of test runs. In most research, only one parameter is swept at a time, which induces the risk of missing important interactions. To get a comprehensive understanding of the different combustion processes, i.e., RCCI and CDC, these complex interactions need studied in a systematic manner.

Thereafter, Chapter 3 and 4 are dedicated to improving CDC through injection rate shaping. By carefully adjusting the fuel flow, the ROHR can be tuned to a thermodynamically more favorable shape. This fuel rate shaping is done in two ways: multiple injections and continuous fuel rate shaping. Chapter 3 investigates the application of a post injection (i.e., a small quantity fuel pulse after a larger main injection event) with the use of Delphi's DFI21 injector. Particular attention is put on how the efficacy of a post injection changes under various operating conditions. Reductions of fuel consumption, soot and NO_x emissions are sought through optimal scheduling of a post injection. Chapter 4 investigates the potential for increasing GIE by continuous fuel rate adjustment (i.e., without flow interruption) using Delphi's DFI7 injector. Specifically, ramped injection rates are compared to conventional square rates.

In Chapter 5, RCCI is thoroughly optimized for maximal GIE at acceptable emissions using an extensive set of fuel injection and air path parameters. RCCI is compared to CDC operation, which

is necessary to assess the capabilities of the two combustion modes to comply with future legislation. Conventional gasoline and diesel are applied in these tests. The fundamental differences of the two combustion regimes in terms of their peak GIE potentials are revealed and discussed. The balance of separate energy loss channels is determined to pinpoint directions for further GIE optimization. The two chapters thereafter further focus on RCCI combustion using E85 as low reactivity fuel. A detailed rate of heat release analysis is done in Chapter 6 to investigate which heat release shape is most efficient in RCCI operation and how this is established. Chapter 7 extends the RCCI tests to a new single-cylinder engine setup. Direct injector nozzles are tested with different spray included angles to investigate how these affect the diesel distribution and the eventual GIE.

A general discussion finalizes this dissertation, highlighting the advantages of both combustion regimes. Emphasis is put on the magnitude of the energy loss channels in both RCCI and CDC, and how these fit in the scheme of further improving the diesel engine. Points of attention are exhaust gas aftertreatment, waste heat recovery, mode-switching, turbocharger technology, fuel flexibility and injection equipment. Ultimately, an outlook is provided for efficient and sustainable use of diesel engines in the freight transportation sector.

Chapter 2
Experimental setups and design

Introduction

The experiments discussed in this dissertation have been executed using dedicated test engines. Being based on their on-road counterparts, they largely consist of standard components, making them a reasonable representation of the actual engines utilized outside of the lab. But there are crucial differences, one being the feature of having just a single cylinder for measurements. This chapter treats the details of the experimental setups, the measurement equipment, the post-processing routines and (statistical) analyses. The way in which the tests are organized, i.e., the experimental design, is discussed as well. Some examples will be treated to clarify the procedures followed in the upcoming chapters.

The contents of this chapter are in part based on previous descriptions in several publications by the author and colleagues [74, 75, 84].

Table 2.1: XEC single-cylinder engine specifications.

Displaced volume	2.097 L
Bore	130 mm
Stroke	158 mm
Compression ratio	15.85
Piston bowl shape	Double step
Cylinder head	Low swirl
Number of valves	4
Exhaust valve closure	-346 CAD aTDC
Intake valve closure	-153 CAD aTDC
Exhaust valve opening	128 CAD aTDC
Intake valve opening	344 CAD aTDC
Direct injector	Delphi DFI21
Number of holes	7
Hole diameter	0.195 mm
Spray included angle	139°
Port fuel injector	Bosch EV1

2.1 Single-cylinder engine setups

2.1.1 DAF XEC engine

The experiments in Chapters 3 to 6 have been conducted on a single-cylinder test engine adapted from a production variant 12.6 liter DAF XEC. A schematic overview of the setup is shown in Figure 2.1, whereas engine specifications are summarized in Table 2.1. Three out of the six cylinders run on the standard engine control unit to drive the crank shaft, while two cylinders are non-firing. A Schenck W450 eddy-current brake is used to set and maintain stable engine speeds. The test cylinder is, except from the crank and cam shafts, completely isolated from the rest of the engine. It has its own air and fuel path allowing to freely select intake manifold and fueling parameter settings. A common rail system with Delphi DFI21 injector and double-step piston are installed to match

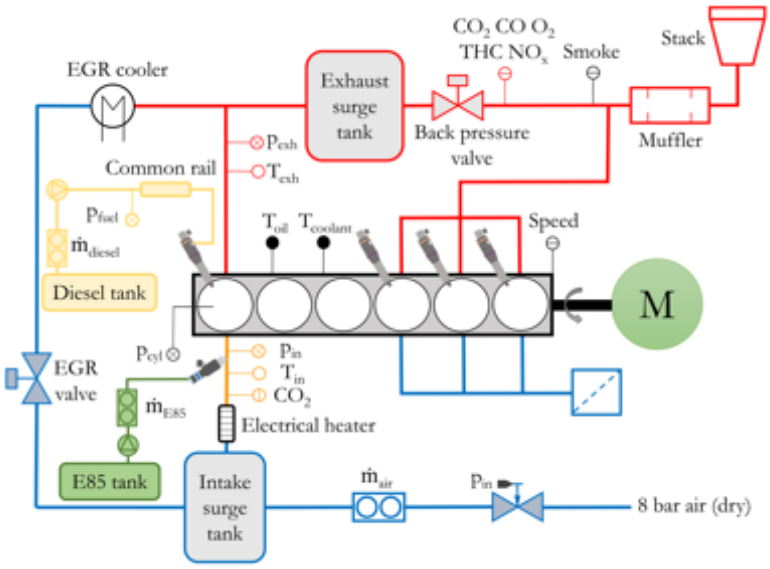

Figure 2.1: Schematic overview of the XEC test setup. Color coding indicates the hot (red) and cold (blue) streams. Most of the features apply to the MX-13 setup as well; details of the differences are given in the main text.

EURO VI specifications, but note that this piston is not optimized for reactivity controlled compression ignition (RCCI). The compression ratio has been lowered to 15.85 to facilitate the contrasting requirements between CDC and RCCI.

Air path system

Boosted dry air is provided by an external compressor and intake manifold pressure is adjusted using a pressure regulator. Mass flow of fresh air is subsequently measured by a Micro Motion CMF200M. An electrical heater element is used to maintain a constant intake charge temperature. Steady pressures and temperatures are furthermore measured in both the intake and exhaust manifolds. A back-pressure valve is fitted in the exhaust to mimic a variable geometry turbocharger and generate exhaust gas recirculation (EGR). Another valve subsequently sets the EGR rate. Recirculated exhaust gas is heavily cooled to approximately room temperature by a cold stream of process water that is connected to a production type EGR cooler. Condensate from the exhaust stream is collected in a vessel and drained in between experimental runs. Surge tanks in both the intake and exhaust paths dampen pressure fluctuations induced by single-cylinder operation. The engine is warmed up to steady oil and coolant temperatures of 90 and 85 °C, respectively, prior to the experiments.

Fueling system

Diesel is delivered to a custom common rail by a Resato HPU200-625-2 pump. Fuel pressure is measured downstream of the pump and a feedback controller maintains the desired setting. For port fuel injection (PFI) of a low reactivity fuel in RCCI operation, a Bosch EV1 injector is fitted in the intake channel at the right-hand side from intake manifold perspective. The PFI injector is driven by a MoTec M400 control unit. Low reactivity fuel is fed to the injector by a low-pressure pump located inside the fuel tank, which is manually set to approximately 5 bar by adjusting its rotational speed. Due to this manual control, slight deviations from the setpoint are possible, but are expected to be of minor influence. Mass flows of the DI and PFI fuel are measured using two identical Micro Motion CMF010M mass flow meters.

Measurement system

In-cylinder pressure is measured using an uncooled AVL GU21C piezoelectric transducer wired to a Kistler 5011B charge amplifier. Crank angle information at 0.1 degree resolution is provided by a Heidenhain ROD 420 3600 encoder. These data are logged on a Smetec COMBI data acquisition system, which logs 70 consecutive raw pressure traces for post-processing. Gaseous emissions (CO, NO_x, THC, CO_2 and O_2) and air-excess ratios (λ) are analyzed with a Horiba MEXA 7100 DEGR system. Aside from measurements in the exhaust, the CO_2 concentration in the intake charge is detected to compute the rate of EGR using

$$EGR = \frac{CO_{2,in}}{CO_{2,exh}} \tag{2.1}$$

Smoke is detected by an AVL 415s smoke meter using the paper filter method. The smoke meter sample volume is set to 2000 ml to attain sufficient measurement accuracy and precision. Furthermore, three samples are taken and averaged for each experimental run. Steady-state pressures, temperatures, mass flows and species concentrations in intake and exhaust manifold are logged on an in-house built data-acquisition system, which collects signals at a 20 Hz sampling frequency over a 40 second interval. Only the time-averaged values are logged for further analysis.

2.1.2 PACCAR MX-13 engine

The experiments presented in Chapter 7 have been performed on a newly commissioned single-cylinder engine setup, which is based on a modern PACCAR MX-13. Engine specifications are given in Table 2.2. Note that injector nozzle details are not given, as those are the topic of Chapter 7 and will be further addressed in that specific chapter. The original piston bowl (i.e., similar to the one installed in the XEC engine) was used, having a compression ratio of 17.2. Many of the design philosophies are similar to those of the XEC setup, hence, the schematic overview from Figure 2.1 again applies, but there are also differences to note. An ABB 75 kW electric motor is used as both dynamometer and means of propulsion when motoring the test cylinder. This excludes the necessity for propelling cylinders, as applied on the XEC. When the test cylinder is fired, the electric motor acts as a generator and supplies electricity back onto the grid via its frequency converter. The remaining five cylinders are non-firing and their pistons have been punctured to prevent compression. To compensate for the weight that was removed from the piston body, extra mass was added in the piston pin using a tungsten-nickel-iron alloy. The cylinder head was cut down from six cylinders to a single-cylinder design and aluminum plates were constructed to seal off the head and the other five cylinders. A metal oil pan was installed wherein a custom aluminum hatch was constructed for easy access to the connecting rod bolts, allowing a relatively quick piston change. The entire frame is placed on air suspension to reduce vibrations. An external coolant pump and heat exchanger including a thermostat were installed to maintain a stable coolant temperature of 87 °C. The secondary side of the heat exchanger is connected to a central cooling system, which provides a cold stream

Table 2.2: MX-13 single-cylinder engine specifications.

Displaced volume	2.15 L
Bore	130 mm
Stroke	162 mm
Compression ratio	17.2
Piston bowl shape	Double step
Cylinder head	Low swirl
Number of valves	4
Exhaust valve closure	-359 CAD aTDC
Intake valve closure	-173 CAD aTDC
Exhaust valve opening	146 CAD aTDC
Intake valve opening	357 CAD aTDC
Direct injector	Delphi DFI21
Port fuel injector	Bosch EV14

of process water. For warming up the engine prior to tests, an additional heater element was mounted that reduces warm-up time and thereby prevents unnecessary wear. The original oil treatment unit, including the oil cooler and a two-stage filter set, is used to reach and maintain an oil temperature of 95 °C. For cooling the stream of recirculated exhaust gas, the standard EGR cooler is employed, which again transfers heat to the central system.

Air path system

Dry, boosted air at 8 bar is provided by the same external compressor as on the XEC setup. An IMI Norgren R18 pressure regulator reduces this initial pressure to the desired level. Downstream of the regulator, mass air flow is measured by a Bronkhorst IN-FLOW F-106BI-AFD-02-V digital mass flow meter. Directly after, the intake air is heated using a Leister LE 5000 DF unit. Surge tanks in both the intake and exhaust manifolds ensure dampening of pressure fluctuations, while two Valbia butterfly valves create a backpressure and set the EGR rate. A condensation tank collects water from the cooled EGR stream, which needs to be emptied regularly in between sets of experimental runs.

Fueling system

The standard common rail is used in conjunction with a Delphi DFI21 injector. One of the two original in-block plunger pumps is reused to provide fuel to the common rail. The high-pressure pump in turn receives high reactivity fuel from a fuel tank via a low-pressure pump. PFI of low reactivity fuel is done using a Bosch EV14, which is fitted in one of the intake channels of the test cylinder at the left-hand side from intake manifold perspective. To inject low reactivity fuel as close to the intake valve as possible, a freeze plug was removed to insert an injector holder. A custom fuel rail ensures a stable supply of fuel to the PFI injector, which is actuated for injection at -320 CAD aTDC and is fed by a second low-pressure pump. DI and PFI fuel consumption are measured using two identical Siemens Sitrans F C Massflo Mass 2100 Coriolis meters coupled with Mass 6000 signal converters.

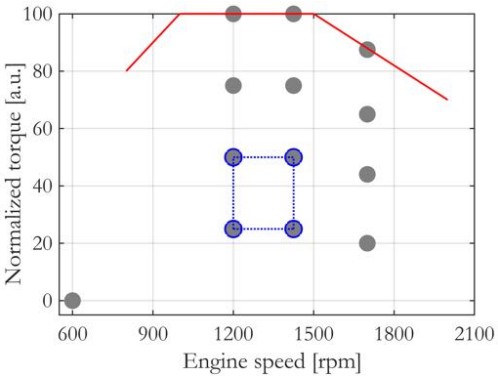

Figure 2.2: Normalized torque as function of engine speed. The red line indicates the full load curve and the grey dots represent the ESC test points. The points encircled in blue are selected for the experiments in this dissertation.

Measurement system

Cylinder pressure is measured by a Kistler 6125C uncooled pressure transducer and amplified with a Kistler 5011B. A Leine Linde RSI 503 encoder provides crank angle information at 0.2 CAD resolution. Actuation currents of both the DI and PFI injectors, as well as the high-pressure fuel pump are measured by a Seneca T201DCH current clamp. Steady-state temperatures and pressures are measured using Type-K thermocouples and pressure sensors at several locations in the intake and exhaust. Signals are collected on a National Instruments CompactRIO equipped with several data-acquisition cards. Setup actuators (injectors, valves) are controlled using the same CompactRIO module. A custom LabVIEW program was written to enable control and data-acquisition on a single host computer. The program records 200 consecutive cylinder pressure traces for post-processing. For each recorded trace of the cylinder pressure, steady-state quantities of all temperatures, pressures and flows are logged as well.

2.2 Load and speed selection

In large parts of Europe, trucks frequently operate on flat roads during highway cruising. The relatively low engine loads and speeds associated

with this routine operation are therefore very common scenarios. Potential improvements to the indicated efficiency, or fuel consumption, and reductions of pollutant emissions can thus have a large impact on the total cost of operation. Figure 2.2 displays an engine map, which shows the normalized engine torque as function of speed. The red line represents the full load curve and the grey dots represent load-speed points of the European Stationary Cycle (ESC). The experiments performed within the scope of this dissertation are all conducted at engine load-speed points in the area framed with blue dotted lines, which is representative of highway cruising of a 40-tonne truck considering its air drag and rolling resistance. Specific details are given in the different chapters. Two common engine speeds are taken into account: the so-called A-speed and B-speed, which equal 1200 rpm and 1425 rpm, respectively.

2.3 Post-processing routines

2.3.1 Pressure and heat release

In-cylinder pressure traces are first averaged and then smoothened with a first-order Savitzky-Golay filter using a frame length of 11 data points. These filter settings allow to reduce high frequency noise with little impact on the actual pressure trace. Subsequently, the apparent rate of heat release (aROHR) is inferred from the pressure [31, 32] using the first law of thermodynamics via

$$aROHR = \frac{\gamma}{\gamma - 1} p \frac{\mathrm{d}V}{\mathrm{d}\Theta} + \frac{1}{\gamma - 1} V \frac{\mathrm{d}p}{\mathrm{d}\Theta} \qquad (2.2)$$

where γ is the temperature and composition-dependent specific heat capacity ratio (C_p/C_v) computed using the NASA polynomials. The global gas temperature is calculated from the pressure trace using the ideal gas law, whereas the composition is taken as an average value at each crank angle (Θ). The latter takes into account the conversion of reactants to products. The combustion chamber volume V is computed using a model and geometry data from Tables 2.1 and 2.2.

2.3.2 Efficiency and loss channels

Engine research relies heavily on combustion pressure indication from which several performance metrics are derived. The gross indicated efficiency (GIE) is a crucial quantity in this dissertation and is expressed by

$$GIE = \frac{P_{gross}}{\dot{m}_{PFI} LHV_{PFI} + \dot{m}_{DI} LHV_{DI}} \qquad (2.3)$$

where $\dot{m}_{PFI}$ and $\dot{m}_{DI}$ are the mass flows of the PFI and DI fuels, respectively. LHV_{PFI} and LHV_{DI} are the corresponding lower heating values. Note that for CDC only $\dot{m}_{DI}$ and LHV_{DI} are applicable. The gross indicated power (P_{gross}) is computed using

$$P_{gross} = \frac{1}{2} W_{gross}\, n \qquad (2.4)$$

where n is the engine speed in revolutions per second and W_{gross} is the gross indicated work, computed by integration of the pressure-volume diagram via

$$W_{gross} = \oint_{\Theta=-180^\circ}^{\Theta=180^\circ} p \,\mathrm{d}V \qquad (2.5)$$

In the following chapters, values of the gross indicated mean effective pressure (IMEP) are reported to indicate the load at which tests were run. IMEP normalizes the indicated work with the displaced volume of the test cylinder (V_d) via

$$IMEP_{gross} = \frac{W_{gross}}{V_d} \qquad (2.6)$$

Aside from the GIE, energy loss channels are quantified to assess where potential improvements can be made. The combustion losses (CL) are inferred from the emissions of carbon monoxide (CO) and total hydrocarbons (THC) using

$$CL = \frac{ISCO\ LHV_{CO} + ISHC\ LHV_f}{ISFC\ LHV_f} \tag{2.7}$$

where ISCO and ISHC are the gross indicated specific emissions of carbon monoxide and hydrocarbons, respectively, in g/kWh. The lower heating value of HC is assumed to be equal to that of the fuel (LHV_f). For RCCI combustion, LHV_f is calculated using the mass fractions of PFI and DI fuel in the blend ($Y_{PFI}\ LHV_{PFI} + Y_{DI}\ LHV_{DI}$), equal to the approach of Pedrozo [33]. Flame ionization detectors (FID) are known to be less sensitive to oxygenated compounds in the exhaust sample [34]. The HC readings are hence, where applicable, corrected for the use of ethanol using the correlation provided by Kar and Cheng [35].

The PFI mass fraction or PFI rate (Y_{PFI}), associated only with RCCI operation, is reported on several occasions in this dissertation to characterize the fuel blend and is computed by

$$Y_{PFI} = \frac{\dot{m}_{PFI}}{\dot{m}_{PFI} + \dot{m}_{DI}} \tag{2.8}$$

The gross indicated specific fuel consumption in g/kWh is computed using

$$ISFC_{gross} = \frac{\dot{m}_{PFI} + \dot{m}_{DI}}{P_{gross}} \tag{2.9}$$

Determining the in-cylinder heat losses is generally difficult. The total amount of heat transfer to the surfaces of piston, liner and cylinder head is often used as a closing term after calculation of the previously defined efficiencies and the sensible heat in the exhaust stream. Temperature measurements can in principle be used to determine the latter, but typical measurements are done somewhere downstream of the cylinder head. While this does provide insight in the amount of sensible heat that can be used to drive a turbine or light-off a catalyst, the residual energy cannot simply be ascribed to heat transfer inside the combustion chamber, as additional heat is lost to exhaust valves, cylinder head and exhaust manifold. Another prevailing method is the use of empirical correlations, like the original correlations by Woschni [36] and Hohenberg [37]. An adapted version of the original Woschni model has been suggested by Chang [38] for premixed combustion concepts. However, as with the original model, certain constants need to be tuned between different engines and operating conditions. This limits the usefulness of such correlations and leads to uncertainties that are hard to eliminate.

In this dissertation, aROHR information derived from the pressure trace is used to compute heat transfer losses. The aROHR was formerly introduced in Equation 2.2, and is subsequently integrated as function of crank angle, as shown in Figure 2.3. This provides the net amount of energy by the release of combustion heat and the heat transferred between gas and combustion chamber surfaces. The total heat transfer loss (Q_{hl}) is then estimated by the difference in the energy level upon exhaust valve opening (EVO) and the total amount of heat released (Q_{tot}). The latter is computed by multiplication of the total fuel mass, the lower heating value of the fuel (blend) and the combustion efficiency. The heat transfer loss fraction (HL) is eventually computed using

$$HL = \frac{Q_{hl}}{m_f\ LHV_f} \tag{2.10}$$

The described method does not provide information at crank angle resolution, but rather a single quantity, which is deemed sufficient for this research. The exhaust loss fraction (EL) is finally used as a closing term in the energy balance as

$$EL = 1 - CL - HL - GIE \tag{2.11}$$

Note that EL does not necessarily yield the useable energy in the exhaust stream, as some of it still ends up in the cooling circuit. This procedure of determining the energy budgets is the same for all experiments discussed in the following chapters.

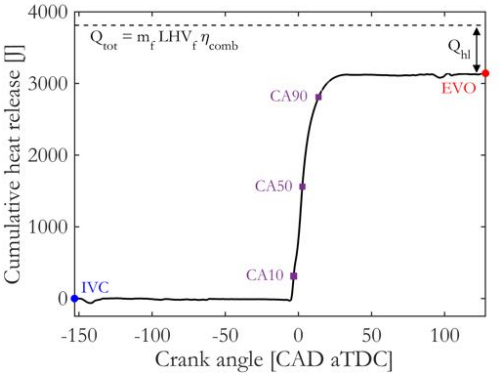

Figure 2.3: Cumulative heat release in a typical CDC experiment. Intake valve closure (IVC) and exhaust valve opening (EVO) are indicated with markers, as well as three typical combustion phasing metrics.

2.3.3 Combustion metrics

Figure 2.3 also illustrates how combustion phasing metrics are determined. The crank angles at which 10%, 50% and 90% of the total heat is released are termed CA10, CA50 and CA90, respectively. CA10 is used as an indicator for the start of combustion (SOC), whereas CA90 marks the end of combustion (EOC). The burn duration is determined with

$$BD = CA90 - CA10 \tag{2.12}$$

In CDC, the ignition delay (ID) indicates the short time interval in which fuel injection has started, but combustion has yet to commence. It is an important characteristic that influences the ensuing aROHR behavior, especially the so-called premixed peak, and is defined as

$$ID = CA10 - SOI \tag{2.13}$$

where SOI is equal to the start of actuation (SOA) of the solenoid injector plus a constant time delay of 200 µs, which is determined from an initial decline in the apparent rate of heat release due to the evaporation of fuel before combustion starts. The delay proved to be roughly constant for various fuel pressure settings. SOA is frequently mentioned in this dissertation as one of the independent parameters in an experiment. For RCCI, the ID is less useful, since ignition is not initialized directly by the injection event. Instead of being mixing controlled, RCCI is governed by chemical kinetics and thus relies on local equivalence ratios and temperatures. The available time for mixing of high reactivity fuel with the already present low reactivity charge is determined by the ignition dwell, defined as

$$IDw = CA10 - EOI \tag{2.14}$$

To study the impact of the heat release profile on GIE, a metric that relates the heat release durations before and after CA50 is introduced as

$$R_b = \frac{CA90 - CA50}{CA50 - CA10} \tag{2.15}$$

This burn ratio (R_b) was formerly used to study the late phase in CDC with respect to the premixed and diffusion-limited phases [39]. In Chapter 6, R_b will be used to characterize the aROHR in RCCI and investigate its relation to GIE.

2.3.4 Indicated specific emissions

Volumetric concentrations of exhaust gas species, as measured by the Horiba MEXA 7100 DEGR system, are converted to gross indicated specific emissions via

$$IS_i = X_i \frac{M_i}{M_{exh}} \frac{\dot{m}_{exh}}{P_{gross}} \tag{2.16}$$

where X_i is the species concentration in ppm, M_i and M_{exh} are the molar masses of the species and exhaust gas, respectively, and $\dot{m}_{exh}$ is the exhaust mass flow. The molar mass of NO_x is treated as NO_2, according to European legislation [40].

Soot emissions are calculated from samples taken by the AVL 415s smoke meter. Filter smoke numbers (FSN) are converted to soot mass density

(C_{PM}) in mg/m^3 using the correlation by Christian et al. [41],

$$C_{PM} = \frac{4.95}{0.405} FSN\, e^{0.38\, FSN} \tag{2.17}$$

Northrop [42] has quite recently re-evaluated several empirical expressions available in literature. It was found that the expression in Equation 2.17 provides the most accurate estimate of soot mass, and is valid even for the extremely low FSN values seen in modern engines. Do note that the particulate composition can deviate from pure carbonaceous particles and could thus lead to an underestimation of the particulate emissions.

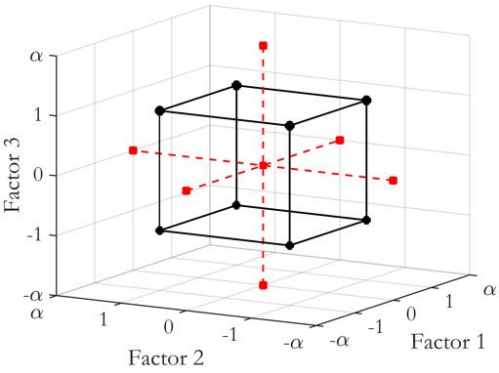

Figure 2.4: A three-factor central composite design. The black cube comprises the full-factorial design. The red dots represent the center and axial points.

2.4 Design of experiments

The design of experiments (DOE) methodology is applied in the experiments described throughout this dissertation. This method allows to study multiple engine and combustion related parameters and their associated interactions without needing to run all permutations. As many input factors (e.g., injection timing, intake manifold pressure, EGR rate) and their interactions can have a strong influence on a response (e.g. GIE), the DOE method becomes a very time-efficient approach. It also provides the means of analyzing the resulting data with statistical methods, such as linear regression and significance tests. A limited number of publications on the use of DOE in engine research can be found [43, 44, 45], regarding both experimental and simulation work. Its application to RCCI is rather occasional. In [46], for example, a fractional factorial design is used for conducting simulations to optimize fueling strategies in a natural gas and diesel fueled RCCI engine. In this dissertation, a central composite design (CCD) is used following the theory of Box and Wilson [47]. This design is useful for detecting curvature in a response, e.g. GIE, and can be used to subsequently construct response surface plots from regression polynomials [49].

A graphical example of a CCD with three factors is shown in Figure 2.4. The values on all axes are in coded units, which is generally done to ease the construction procedure. The base of a CCD matrix is a so-called two-level, full-factorial design (the black cube in Figure 2.4), which means that all possible combinations between the factors at these two levels (-1 and 1) are run. This full-factorial design consists of vectors that are orthogonal to each other in the parameter space. In this way, a set of linearly independent vectors is constructed that allows to separate effects of different factors and interactions on the response. Fractional factorial designs can also be employed, which can be useful when a large number of independent factors are tested. Here, this is deliberately not done, since using fractional matrices also endows the design with the property of having confounded effects (i.e., two or more variables have a mixed effect on the output that cannot be separated). A unique center point (0) is added to the design, which is repeated at a number of random instances to assess experimental drift and repeatability. To complete the CCD, axial points ($-\alpha$ and α) are included in the matrix, in which each operating parameter is set to an extremum while the others are kept in their center point value. The relative distances of axial points to the center point are determined by

$$\pm\alpha = \sqrt[4]{2^k} \tag{2.18}$$

where k is the number of factors in the CCD.

These coded positions are eventually converted into physical quantities relevant for the operating parameters employed in the tests. The total number of runs in a CCD equals $2^k + 2k + C$, where C is the selected amount of center points. Note that a total of five levels is used for each factor to assess response curvature. It now becomes clear why a CCD is a very time-efficient design from an experimental viewpoint. For a four-factor experiment where a single center point is included, the total number of runs equals 25. If those same four factors where tested at five levels including each possible combination, the total number of runs increases to 625 (5^4). The order of experiment runs is randomized before testing to ascertain that the specific order does not affect the outcome. The CCD matrices in this dissertation are practically constructed using the *ccdesign* function in Matlab. A circumscribed design is used, which means that, for the three factor example in Figure 2.4, the design points circumscribe a sphere around the full factorial cube. In this manner, the design is bestowed with the feature of rotatability, which ensures a uniform prediction variance for any point at a particular distance from the center point. This is a useful property for response surface analysis, because the position of an optimum is not known upfront. Thus, a rotatable design permits to move in any direction within the response space, while maintaining the same magnitude of prediction error as in the other directions.

2.5 Multiple linear regression

Regression polynomials are fitted to the experimental data for further analysis. Ordinary least squares fitting is applied by using the Matlab function *fitlm*. An example regression polynomial for a given response variable (y) with two predictor variables (x_1 and x_2) is written as

$$y = \beta_0 + \beta_1 x_1 + \beta_2 x_2 + \beta_3 x_1 x_2 + \beta_4 x_1^2 + \beta_5 x_2^2 + \varepsilon \tag{2.19}$$

where β_i are the regression coefficients, x_i are the predictor variables and ε is the error or residual term. This general form is used for all regression polynomials and is extended with more factors according to each particular set of experiments. Note that not necessarily all terms are used, as their individual statistical significance might be low, in which case a term is excluded.

A forward selection scheme (i.e., a stepwise procedure in which terms are added one by one) is used. Single factor terms, two-factor interaction terms, and quadratic terms are each evaluated for significance based on individual t-test p-values. A p-value below 0.05 is generally considered significant, although caution is advised when assigning significance to terms using a single - somewhat arbitrary - criterion. These p-values make a statement about the effect of a factor with respect to the uncertainty in the data. When a sample is small, or the measurement error is high, the p-values tend to be high too. This is not necessarily because an effect is absent, but can just as well be a consequence of an overly insensitive experiment. To further support the claim of significance, terms are only added if they increase the adjusted coefficient of determination (R^2_{adj}) of the model defined as

$$R^2_{adj} = 1 - \left(\frac{n-1}{n-p}\right)\frac{SS_R}{SS_T} \tag{2.20}$$

where n is the number of observations, p is the number of regression coefficients and SS_R is the sum of squared residuals defined as

$$SS_R = \sum_{i=1}^{n} \left(y_{i,obs} - y_{i,pred}\right)^2 \tag{2.21}$$

where $y_{i,obs}$ and $y_{i,pred}$ are each of the measured and predicted values, respectively. SS_T is the total sum of squares expressed by

$$SS_T = SS_M + SS_R \tag{2.22}$$

where SS_M is the model sum of squares, which is in turn computed using

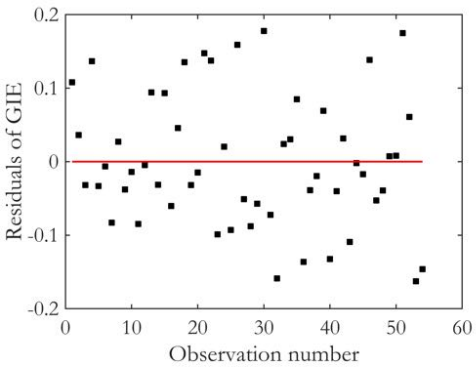

Figure 2.5: An example plot of residuals versus the observation number for a typical GIE regression model based on CDC experiments.

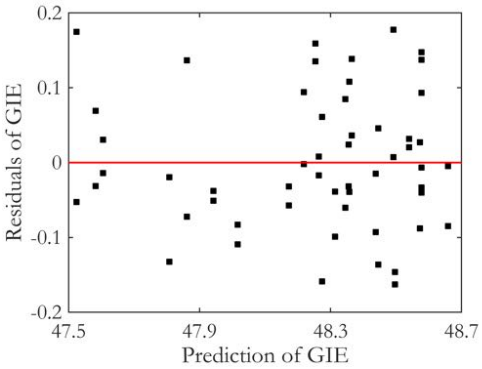

Figure 2.6: An example plot of residuals versus predicted values for a typical GIE regression model based on CDC experiments.

$$SS_M = \sum_{i=1}^{n} \left(y_{i,pred} - \bar{y}_{pred}\right)^2 \qquad (2.23)$$

where $\bar{y}_{pred}$ is the mean predicted value of the response variable. Because R^2_{adj} corrects for the number of predictors, its value does not automatically increase when more terms are added to the equation. This is in fact the case for the ordinary variant; $R^2 = 1$ can in principle always be obtained when the number of predictors equals the number of observations. Clearly, this is not a desired outcome and the R^2_{adj} provides a better reason to select a certain number of predictors. After all, the regression equation of a response variable should be as simple as possible, for ease of interpretation and optimization, but should also sufficiently describe response behavior to enable a meaningful analysis.

The resulting polynomials are tested for validity prior to further analysis. Residuals $(y_{i,obs} - y_{i,pred})$ are plotted to find possible flaws in the experiments and fitting procedure. Two types of residual plots are created for each data set. First, the residuals are plotted versus the measurement number in chronological order. This is shown in Figure 2.5, where an example is shown for a typical GIE regression. If any unanticipated drift has occurred during experiments a trend will be visible. As can be seen the residuals nicely scatter around the zero line, confirming the lack of drift during the experiments. Second, residuals are plotted as function of predicted data to assess whether an appropriate polynomial is selected. Again, a trend will show when the fit does not describe the observed behavior. Another example for the same GIE model is shown in Figure 2.6. Here, the residuals again scatter around zero, which serves as confirmation that a proper polynomial degree is chosen.

An assumption involved with the described procedure is that measurement samples are presumed to be taken from a normal distribution. To check whether this is the case, normal probability plots are created for each data set. It was found that for the ranges in which operational inputs were varied, the emissions of soot and NO_x sometimes deviated from normality. Their distributions were in some cases strongly skewed and a log-normal distribution proved more suitable. For this reason, a logarithmic transformation of the entire response vector, i.e., $\ln(y_{obs})$, was done prior to the described fitting procedure. A presumption of using a CCD is that if curvature in the response exists, it will be detected due to the inclusion of center and axial points. This is not necessarily the case. It might well be that curvature is not present around the center point, but does exist in the outer bounds of the parameter space. If several factors are set to an extreme value to reach the projected optimum, it is essentially an extrapolation and additional mea-

surements were performed for confirmation. In cases where the optimum was predicted outside of the initial domain, an extra CCD was run.

2.6 Analysis of variance

The use of DOE often yields multi-dimensional data sets with many interactions among the tested factors. To ease the search for the most dominant effects, a multi-factor analysis of variance (ANOVA) is first done on the full-factorial data points, analogous to the approach of De Cuyper et al. [50]. It is a statistical technique for breaking up the variation in the data and ascribing it to separate factors and interactions. This procedure immediately reveals the most influential factors and interactions in a large experimental design, so that later on the response surface analysis can be narrowed down to certain areas in an effective manner. The technique moreover quantifies the experimental error and incites to contemplate about the various effects before actually observing response surface plots. In this dissertation, use is made of the *anovan* function in Matlab, but a manual - and strongly simplified - example following the approach of Andersson [49] is treated here to elucidate the procedure.

Consider a CDC experiment, in which two factors are varied according to a two-level, full-factorial design. Each factor has a low (-1) and a high (1) setting; the physical values are irrelevant. Table 2.3 displays the experiment matrix with SOA and fuel pressure as the independent factors and $ISNO_x$ as the dependent response variable in g/kWh. An interaction effect between SOA and fuel pressure is included by multiplication of the coded values of each run. There are four combinations possible between the two factors at these two levels and each setting is repeated once. Therefore, a total of eight experiment runs is shown. The grand mean of $ISNO_x$ is also given, which plays a key role in the following steps. Mean values of every factor at each level are calculated as shown in Table 2.4.

The data has now been divided into a total of seven mean values, which are used in the next step of computing the actual of variation in the data set.

Table 2.3: An example of a full-factorial matrix with SOA and fuel pressure as factors, including their interaction and the response of $ISNO_x$ in g/kWh.

Run	SOA	pFuel	SOA·pFuel	$ISNO_x$
1.	-1	-1	1	7.04
2.	1	-1	-1	4.56
3.	-1	1	-1	8.56
4.	1	1	1	6.02
5.	-1	-1	1	6.82
6.	1	-1	-1	4.84
7.	-1	1	-1	8.75
8.	1	1	1	5.76
			Grand mean	6.54

Table 2.4: Mean values of $ISNO_x$ in g/kWh of the two factors and their associated interaction at both the low (-1) and high (1) setting.

Mean	SOA	pFuel	SOA·pFuel
Low (-1)	7.79	5.82	6.68
High (1)	5.30	7.27	6.41

Table 2.5 shows the data variance split up into several parts, including a sum of squares at the end of each column. Starting from the left, the first column displays the total variation determined by subtracting every $ISNO_x$ value in Table 2.3 with the grand mean. The second, third and fourth columns are assigned to the variation due to the two factors and their interaction. The value in each element of these columns is computed by subtracting the grand mean from the mean of each factor at a particular level as shown in Table 2.4. The rightmost column depicts the residuals, obtained by subtracting the values of SOA, pFuel and SOA·pFuel from the total variation.

With all the variation arranged in Table 2.5, the ANOVA table is constructed and displayed in Table 2.6. The first column shows the factors and interactions that are tested, as well as an entry

Table 2.5: Variation in the $ISNO_x$ data divided into several parts.

Run	Total	SOA	pFuel	SOA·pFuel	ε
1.	0.50	1.25	-0.72	-0.13	0.10
2.	-1.98	-1.24	-0.72	0.14	-0.16
3.	2.02	1.25	0.73	0.14	-0.10
4.	-0.52	-1.24	0.73	-0.13	0.12
5.	0.28	1.25	-0.72	-0.13	-0.12
6.	-1.70	-1.24	-0.72	0.14	0.12
7.	2.21	1.25	0.73	0.14	0.09
8.	-0.78	-1.24	0.73	-0.13	-0.14
	SS_T = 16.44	SS_{SOA} = 12.40	SS_{pFuel} = 4.21	$SS_{SOA \cdot pFuel}$ = 0.15	SS_E = 0.12

Table 2.6: Resulting ANOVA table of $ISNO_x$ data.

Source	SS	d.f.	MS	F-stat	p-value
SOA	12.40	1	12.40	413.33	3.45e-5
pFuel	4.21	1	4.21	140.33	2.91e-4
SOA·pFuel	0.15	1	0.15	5.00	0.089
Error	0.12	4	0.03		
Total	16.44	7			

for the error and total variation. The second column depicts previously computed sum of squares (SS). The third column contains the corresponding degrees of freedom (d.f.) of each source. The mean squared (MS) terms in the fourth column are subsequently computed by dividing the sum of squares by the d.f. value. The F-statistic in the fifth column is the ratio of the explained and unexplained variances. In other words, the values in this column are obtained by dividing each mean squared term with the mean squared error. Finally, an F-test is done at a 95% confidence level [48]. This test, as well as other statistical tests, examines the *null hypothesis*, which postulates that the independent factors have no influence on the response. The corresponding p-values are displayed in the last column. A higher F-statistic yields a lower p-value, indicating that more variation in the data is explained by that particular variable. Table 2.5 shows that SOA is the most influential factor in this experiment, followed by fuel pressure. Both of these factors influence local gas temperatures to an extent, which links to NO_x formation. Their interaction has a noticeable effect as well, since its mean squared value stands out from the mean squared error. However, it is not statistically significant at the specified confidence level. There is apparently less need to emphasize the analysis on this interaction, although some more insight might be required before completely ignoring this interaction. There can be a causal effect that still makes it worthwhile to include it in the regression procedure. This approach of attributing variance to factors and interactions, and ranking them in terms of importance, is used in this dissertation to select focus areas in the analyses.

Chapter 3

Assessing post-injection efficacy

Introduction

Literature indicates that post injections are effective for reducing soot emission, which is thought to stem from enhanced mixing and an increased temperature in the burnout phase. Yet, results differ a lot between publications, which is likely caused by the selected operating conditions in separate studies. Efforts to reduce not only soot, but also fuel consumption and emissions of nitrogen oxides complicate the understanding even more. The current chapter presents dedicated experiments to shed light on the detailed interactions between post injections and additional operational settings, like the amount of excess air and combustion phasing. Figure 3.1 shows a visual impression of a post injection (images courtesy of P.C. Bakker). The top image displays combusting fuel remnants from the main injection event, whereas the actual post injection is seen in the middle still. In the bottom still, considerably more structure is observed in the luminous clouds, hinting at better mixing of air and remaining fuel.

The contents of this chapter are based on Robbert Dreezen's master thesis and have been published as Willems, R., et al., "The Impact of Operating Conditions on Post-Injection Efficacy; a Study Using Design-of-Experiments," SAE Technical Paper 2018-01-0229, 2018, doi:10.4271/2018-01-0229 [74].

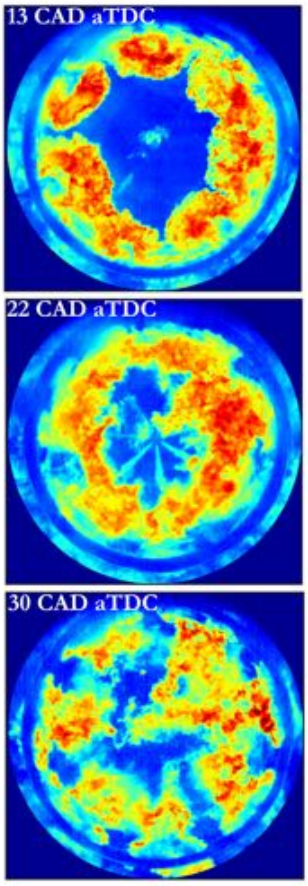

Figure 3.1: High-speed luminosity recording of a post injection in an optical engine. Images are taken from below a transparent piston using a turning mirror. The stills represent the moments before, during and some time after the post injection. Corresponding crank angles are shown in the top left corner of each image.

3.1 Literature review

The use of post injections in diesel engine combustion has been widely studied throughout recent years, primarily driven by advancements in the capabilities of fuel injection equipment. It is mainly the ability of post injections to reduce soot emissions that is reported in both light-duty [51, 52, 53, 54] and heavy-duty [55, 56, 57] engines. Although these merits to soot reduction are frequently reported, responses to the applied fuel injection strategy often differ, which is likely related to the selected operating conditions and engine hardware in separate studies. Common explanations for the efficacy of soot reduction by post injections are enhanced mixing of fuel and oxidizer and an increased temperature late in the combustion cycle, as discussed in a review paper by O'Connor and Musculus [58]. The post-injected reacting jet pushes fresh oxygen and combustion radicals (e.g., hydroxyl) into the main soot clouds resulting in better utilization of the available air and thereby promoting late-cycle oxidation reactions. This mixing improvement is probably complemented by an increased temperature, although it is difficult to isolate separate effects.

If timed and quantified correctly, the aforementioned benefits in engine-out soot are generally accompanied by marginal or even negligible increases in nitrogen oxides (NO_x) emissions and fuel consumption. In some cases, even favorable shifts of the common soot and NO_x tradeoff have been established [51, 59, 60, 61], but not without optimizing other operating parameter settings as well. The rate of exhaust gas recirculation (EGR) has proven to be a valuable control parameter in most of these studies. Improvements of indicated efficiency by use of a post injection, compared to a single main injection, have been reported as well [57, 58, 59]. An acceleration of the burnout phase with a consequent enhancement of the thermodynamic cycle efficiency is a plausible explanation for this, as was for example hypothesized by Desantes et al. [53]. To what extent reduced heat losses play a role in such efficiency gains are, to the author's knowledge, never been charted. Splitting the heat release by using multiple injections could be beneficial. The heat loss reduction is either caused by lower peak values of the local gas temperature or a shorter interaction duration between spray and piston bowl. The formerly mentioned discrepancies between published results are even further complicated when NO_x emissions and indicated efficiency are incorporated in the analysis.

Engine hardware plays a significant role in the efficacy of post injections as well. The eventual positions of remaining fuel fragments and soot pockets depend on the geometrical designs of the piston bowl and injector nozzle, as these determine the diffusion flame direction upon flame-bowl contact. The extent of this interaction between a post injection and the main combustion remnants will thus also depend on these designs. Horibe [62] has investigated injection strategies using several combinations of piston bowl and injector nozzle geometry. It was found that the soot reduction response to the post-injection timing flattens as the number of nozzle holes is increased. A similar trend was found when a re-entrant piston bowl was replaced by a straight-sided variant [63]. Above all, these studies of Horibe and co-workers stress the importance of careful engine hardware selection when employing multiple-injection strategies.

To deal with the complexity of optimizing multiple-injection strategies, some groups have adopted the design of experiments (DOE) methodology, although approaches somewhat vary. Montgomery and Reitz [64] studied double injections while varying several operating conditions, such as injection pressure, intake manifold pressure and EGR rate. They used fractional factorial experiments to generate a first-order polynomial of a predefined objective function. The gradient of this polynomial was determined and more experiments were conducted in the direction of the projected optimum. If necessary, the procedure was iteratively repeated with smaller intervals between factor values to find the actual optimum. Despite the efficient tracking of extrema, the method is inherently superficial from a fundamental standpoint (i.e., physicochemical reasons why an optimum is found). D'Ambrosio

and Ferrari [65] have instead complemented their DOE efforts with a three-zone combustion model to back up their experiments, which proved useful for clarifying observed trends.

In pursuit of a more generic approach, Martin and co-workers [66] published a comprehensive study with general guidelines for timing and quantifying post injections for soot reduction. Their work showed that in the closed-coupled regime (i.e., with a short separation between the main and post injection), timing of the post injection is the crucial factor for reducing soot, whereas in the long-dwell regime the quantity proved more influential. It was concluded that close-coupled post injections resulted in minor reductions of soot with slight enhancements to fuel economy, but at the expense of higher NO_x emissions. Post injections with a long dwell, on the other hand, resulted in a large reduction of soot with little impact on fuel consumption. Other operating parameters were kept constant in their work; hence, conclusive remarks on how these settings would influence the results cannot be made. This chapter aims to bridge that gap by studying the interaction of post injections with other operational parameters.

Table 3.1: Nominal operating conditions.

Intake manifold T	40 °C
Exhaust manifold Δp	0.5 bar
A25 net IMEP and speed	7 bar at 1200 rpm
A50 net IMEP and speed	13 bar at 1200 rpm
B50 net IMEP and speed	13 bar at 1425 rpm
Fuel specification	EN590 diesel

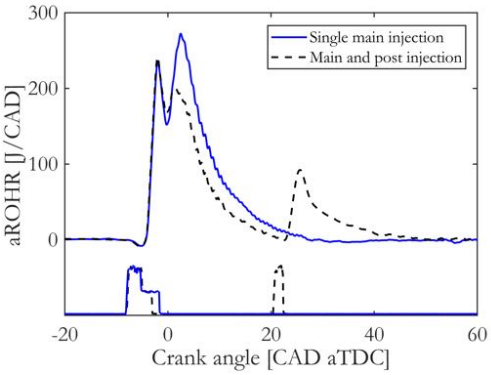

Figure 3.2: Typical injector actuation currents with corresponding heat release rates for a single main injection event and a post-injection strategy.

3.2 Experimental approach

Three European Stationary Cycle (ESC) points (A25, A50, B50) are selected for the tests, which are executed on the XEC platform. Target fuel quantities are 83 mg per cycle for A25 and 140 mg per cycle for A50 and B50. Nominal operating conditions are depicted in Table 4.1. The total injected fuel mass is the same for all experiments. Hence, the fuel to be supplied in the post injection is subtracted from the main injection. The actuation of the main injection is first set to obtain the desired main fuel quantity based on the current split value. Then, a post injection is added and its energizing time is increased until the total target fuel quantity is reached. This will advance the EOA of the main injection, while its SOA remains unaffected; this is illustrated in Figure 3.2. Injector currents are plotted in arbitrary units along with typical apparent rates of heat release (aROHR).

DOE is utilized to cover a large variety of operating conditions and post-injection schedules. Two central composite design (CCD) matrices are created for each load-speed combination: one for the single injections and one for the post injections. Quadratic regression polynomials are subsequently fitted to the experimental data obtained from the DOE matrices. Net indicated specific NO_x and PM emissions, as well as fuel consumption are selected as response variables. An overview of the adjusted R^2 values of their regression equations are shown in Table 3.2. The reader is referred to Chapter 2 for more details about DOE and the regression procedure.

The factors and levels used in the tests are depicted in Table 3.3 (A25), Table 3.4 (A50) and Table 3.5 (B50). Double horizontal lines separate the factors and levels used only in post-injection experiments,

Table 3.2: Adjusted R^2 values of the regression equations of ISFC, $ISNO_x$ and ISPM.

	Single injection			**With post injection**		
	A25	*A50*	*B50*	*A25*	*A50*	*B50*
ISFC	0.803	0.813	0.891	0.909	0.933	0.831
$ISNO_x$	0.969	0.947	0.988	0.990	0.959	0.982
ISPM	0.965	0.954	0.960	0.962	0.958	0.922

for dwell and split are not applicable to single injections. Dwell is defined here as the crank angle interval between the EOA of the main injection and SOA of the post injection,

$$Dwell = SOA_{post} - EOA_{main} \tag{3.1}$$

Note that this dwell demand is not necessarily equal to the physical separation, as the actual values also depend on the applied actuation duration and can besides differ between injectors. Split is the mass percentage of the total fuel amount (m_{tot}) that is supplied in the post injection (m_{post}),

$$Split = \frac{m_{post}}{m_{tot}} \tag{3.2}$$

Fuel pressure levels for A50 and B50 have been increased in comparison to A25, as to prevent excessive injection durations at higher load. Moreover, the intake pressure is elevated to attain acceptable air-excess ratios. All measurements are used in the regression procedure with an exception at mode A25, which was run with a rather broad dwell range from 7 to 39 CAD. The rationale behind this was to be sure to capture the relevant response behavior. However, after assessment of the results it was found that dwell values above 29 CAD had excessive negative impact on engine efficiency. Both combustion efficiency (high THC and CO) and thermal efficiency deteriorated, rendering these operational conditions undesired. It was decided to exclude these long dwells from the regression procedure and further analysis. The dwell range was scaled down accordingly in the remaining two load-speed points.

The center point values in this chapter are based on a contemporary calibration of a similar engine, which utilizes single injections. That calibration will act as a reference and each factor is varied around this baseline. The center point is repeated multiple times on random occasions during the experiments to quantify measurement error and to detect possible drift. The axial points for single injection experiments are displayed within parentheses; the full factorial and center point settings are equal for all runs. The axial points are all run twice to check measurement repeatability in the outer bounds of the experiment matrix. The total number of experimental runs per load-speed combination equals 39 for the single injection matrices (16 factorial points + 16 axial points + 7 center points) and 103 for the post-injection matrices (64 factorial points + 24 axial points + 15 center points).

3.3 Results and discussion

To assess the impact of operating conditions on post-injection efficacy, tradeoffs of net ISFC, ISPM and $ISNO_x$ are presented. Particular attention is given to the effects of air-excess ratio (i.e., EGR rates and intake pressures), combustion phasing and fuel pressure. Single injections are incorporated in the analysis for comparison. Response surfaces of net ISFC, $ISNO_x$ and ISPM are treated to address the interaction of dwell and split while keeping other operational parameters fixed in their center point values. This gives an idea how quantity and timing of the post injection interact, and eventually determine its efficacy. The analysis is first directed to the low load case (A25). Then, an investigation is done to assess how the efficacy

Table 3.3: Selected factors and levels for mode A25. Axial points for the single injection experiments are shown within parentheses. The double horizontal line separates the post-injection parameters from the other settings.

A25	$-\alpha$	-1	0	1	α	Unit
SOA main	-15 (-13)	-10.5	-8	-5.5	-1 (-3)	CAD aTDC
Fuel pressure	1025 (1125)	1250	1375	1500	1725 (1625)	bar
EGR rate	15 (17)	20	23	26	31 (29)	%
Intake pressure	1.4 (1.45)	1.5	1.55	1.6	1.7 (1.65)	bar (a)
Dwell	7	17	23	29	39	CAD
Split	3.5	10	13.5	17	23.5	%

Table 3.4: Selected factors and levels for mode A50. The advance of main injection timing is limited to prevent excessive peak firing pressures. Dwell values are significantly reduced with respect to the lower load case.

A50	$-\alpha$	-1	0	1	α	Unit
SOA main	-13.5 (-12)	-10	-8	-6	-2.5 (-4)	CAD aTDC
Fuel pressure	1225 (1325)	1450	1575	1700	1925 (1825)	bar
EGR rate	14 (16)	19	22	25	30 (28)	%
Intake pressure	1.9 (2.0)	2.1	2.2	2.3	2.5 (2.4)	bar (a)
Dwell	3	7.5	10	12.5	17	CAD
Split	3.5	10	13.5	17	23.5	%

Table 3.5: Selected factors and levels for mode B50. The start of actuation of the main injection is slightly advanced to account for the increase in engine speed.

B50	$-\alpha$	-1	0	1	α	Unit
SOA main	-14.75 (-13.5)	-12	-10.5	-9	-6.25 (-7.5)	CAD aTDC
Fuel pressure	1225 (1325)	1450	1575	1700	1925 (1825)	bar
EGR rate	14 (16)	19	22	25	30 (28)	%
Intake pressure	1.9 (2.0)	2.1	2.2	2.3	2.5 (2.4)	bar (a)
Dwell	3	7.5	10	12.5	17	CAD
Split	5.5	10	12.5	15	19.5	%

and injection scheduling requirements change at higher load (A50). That same method is applied for increased engine speed (B50).

3.3.1 A25 - Impact on common tradeoffs

Figure 3.3 shows predicted tradeoffs of net ISFC and ISNO$_x$ emissions at 20% and 26% EGR rate. The main injection timing is varied equally along each curve from -3 to -13 CAD aTDC (left to right), while dwell (17 CAD) and split (17%) are fixed. Several observations can be noted from these plots. At 20% EGR, the post-injection strategy reduces NO$_x$ levels over the entire range of main injection timings. Intuitively, this reduction would be a consequence of the fact that post-injected fuel is supplied during the expansion stroke, effectively suppressing NO$_x$ formation rates. Still, in-cylinder temperature is far from homogeneous in diffusion-limited combustion and NO$_x$ formation is largely dictated by local conditions. It is plausible that a post-injection will produce NO$_x$ when it transports fresh air and combustion radicals into hot (partially) burnt gases from the main injection. As residence time at a global high temperature will be reduced when a post-injection is applied, an increase in NO$_x$ can be ascribed to a higher momentary local temperature. Some evidence of this is found in the bottom graph of Figure 3.3, where EGR is increased to 26%. It can be seen that for retarded main injection timing, NO$_x$ emissions are higher in the post-injection scheme compared to single injection operation. Despite that the SOA of the post injection is surpassing 20 CAD aTDC, NO$_x$ formation is promoted.

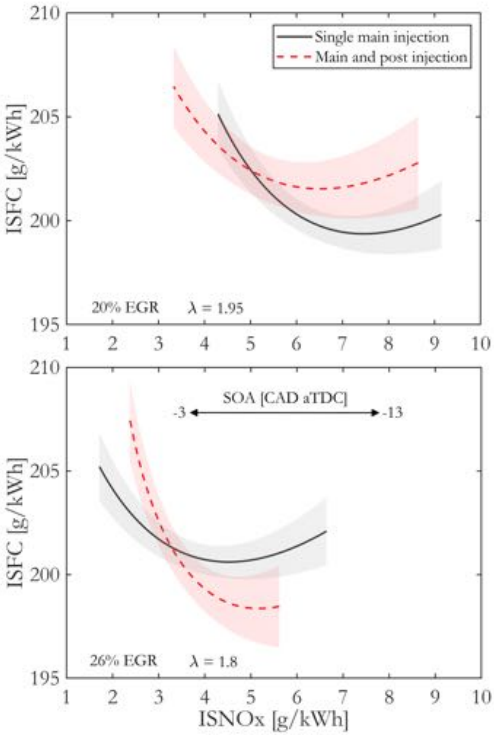

Figure 3.3: Regressed tradeoffs of ISFC and ISNO$_x$ for two EGR rates under varying main injection timings. Air-excess ratios (λ) are shown for reference. Intake pressure and fuel pressure are equal for each curve at 1.6 bar and 1250 bar, respectively.

The top graph in Figure 3.3 illustrates that net ISFC is generally lower at constant NO$_x$ when using a single injection strategy at 20% EGR. The reason for a single injection scheme to perform better is revealed by heat release analysis indicating overall shorter burn durations. However, a remarkable shift is seen when EGR is increased to 26%. The elevated EGR rate allows considerable advancement of combustion phasing when applying a post-injection strategy, which is reflected by the position of the fuel consumption optimum. Contrarily, the optimal SOA of the single injection scheme seems hardly affected. Despite that burn durations are still mostly shorter for the single injection scheme, the post-injection strategy performs significantly better. This can partly be accounted for by a shift of CA50 towards TDC. Reduced heat loss rates to the piston bowl or cylinder wall are expected to play a role here. As mentioned earlier, this reduced heat loss is either caused by reduced peak values of the heat release rate (revisit Figure 3.2) with evident impact on the global gas temperature history, or a shorter duration of diffusion flame-bowl interaction (lower convective heat losses). The question is how competing mechanisms of heat loss, combustion phasing and burn duration contribute to the eventual efficiency, and how this balance changes when EGR rate or injection strategy is adapted. These

answers are likely ambiguous, but the presented results do show considerable differences in these tradeoffs, which can be used as an advantage for particular settings.

In Figure 3.4, PM-NO_x tradeoffs are shown for the same operating conditions. For both EGR rates, the sooting tendency when changing combustion phasing is lower with the post-injection strategy, which is displayed by more moderate slopes. Especially at retarded main injection timing, a post injection can greatly reduce PM emissions. As the burnout phase is shifted further into the expansion stroke, soot oxidation rates decline, giving rise to relatively high engine-out PM levels. A post injection can be of aid at this point by locally increasing temperature and supplying fresh air to oxygen-depleted regions, as ofttimes proposed in work by other research groups [59, 60, 65]. When advancing the main injection, this soot reduction is gradually declining and eventually turns into an increase for both EGR rates. At such an early combustion phasing, burnout takes place closer to TDC when density and temperature are still high, resulting in more effective oxidation of soot. Supplying a part of the fuel later in the cycle with a post-injection does not serve the intended purpose of improved oxidation then.

To summarize, the graphs presented in Figure 3.3 and Figure 3.4 show distinct impact of EGR rate (i.e., air-excess ratio) and main injection timing on post-injection efficacy at low load and nominal engine speed. Increasing the EGR rate and advancing the main injection timing simultaneously shows potential to lower both fuel consumption and NO_x emissions. Contrarily, soot emissions increase at early combustion phasing in these particular conditions, revealing that existing tradeoffs are not easily broken. Still, at 26% EGR and roughly 5 g/kWh $ISNO_x$ a significant fuel consumption benefit is seen without much impact on PM emissions. Moreover, for conditions where increasing the EGR rate or retarding the main injection timing is limited by soot emissions, appropriate scheduling of the post injection is a valuable tool to increase the tolerance to dilution or combustion phasing.

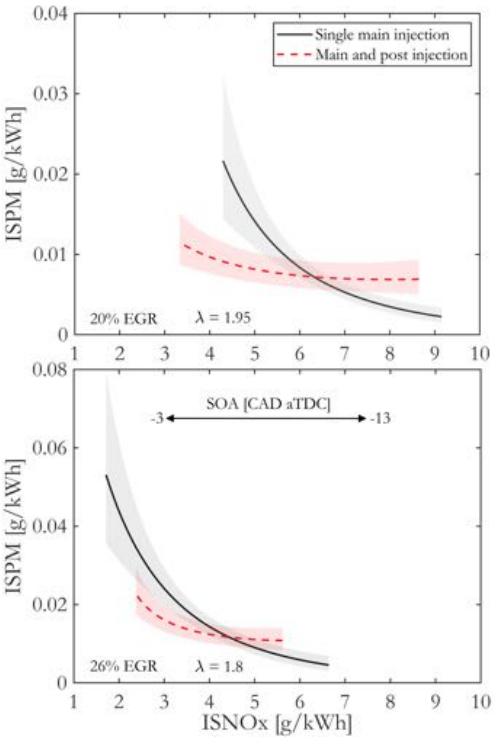

Figure 3.4: Regressed tradeoffs of ISPM and $ISNO_x$ for two EGR rates. Corresponding operational settings are equal to the results presented in Figure 3.3.

3.3.2 A25 - Soot reduction capabilities

The influence of excess air on soot reduction by post injections is assessed and optimal injection dwell values are sought under varying oxygen availabilities. Lowering the air-excess ratio is readily achieved by increasing the EGR rate. Alternatively, one can reduce the intake pressure while keeping the EGR rate constant to obtain a similar variation. In Figure 3.5, the response of net ISPM to dwell is shown for three intake pressures and EGR rates. All other operating parameters are set to their center point values. Predicted single pulse ISPM levels from the regression equations are shown with horizontal lines in corresponding colors.

At first glance, the striking resemblance between the two graphs is noticed. Imposed variations in air-excess ratio are nearly identical for shown in-

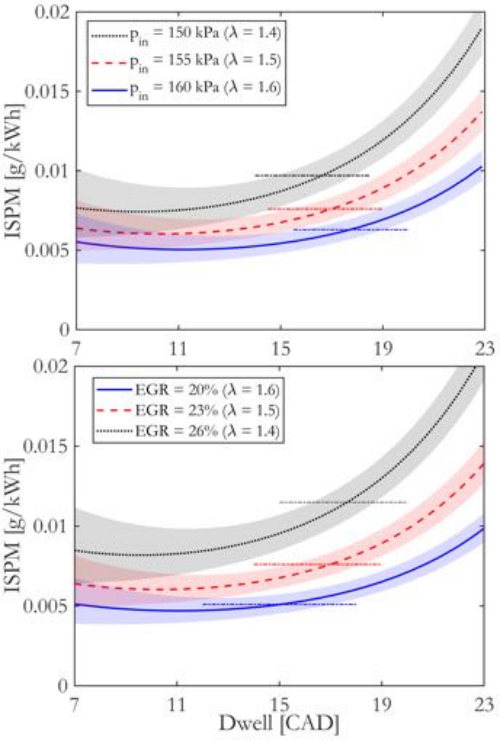

Figure 3.5: ISPM as function of dwell for three different intake pressures (top) and EGR rates (bottom). Other operating parameters are set to their center point values. Single injection levels are shown by horizontal lines in corresponding colors.

crements in EGR rate and decrements in intake pressure, and range roughly from 1.4 to 1.6. The resulting responses to injection dwell are similar as well, as can be clearly seen. The lower the air-excess ratio, the shorter the optimal dwell. It is thought that depletion of oxygen in the soot clouds originating from the main combustion event occurs earlier in the cycle, hence the need for reduced dwell times. This hypothesis suggests that indeed enhanced late-cycle mixing of combustible gases and particles with oxidizer plays an important role in the soot reduction capabilities of post injections. Moreover, both graphs show that the eventual relative soot reduction increases when the air-excess ratios are lowered, which further substantiates the idea of enhanced mixing as primary mechanism in soot oxidation improvements. This finding is in accordance with results from previous work of, for example, Pandurangi et al. [67]. Their modeling efforts indicated that soot oxidation by molecular oxygen is strongly enhanced when employing a post injection, particularly at elevated EGR rates.

Despite strong similarities between the two graphs in Figure 3.5, there are also differences to note. First, the absolute levels of ISPM are slightly higher for varying EGR rates compared to intake pressure variations. Increasing the EGR rate has a reducing effect on temperature, thereby posing a penalty on soot oxidation. Although changing the intake pressure also has its impact on temperature, the effect is different compared to varying EGR, and local temperature changes do not necessarily follow global trends. Furthermore, altering the intake pressure consequently affects density, thereby changing relevant mixing processes. It is especially the entrainment rate that is proportional to the gas density [68]; this relation is not applicable to EGR rate variations. Second, when looking at the soot reduction window (i.e., the dwell range resulting in lower ISPM), it can be observed that for increasing EGR the window widens. On the contrary, for decreasing intake pressure (thus a similar change in air-excess ratio) the window narrows. Distinctive impact of both parameters on in-cylinder bulk temperature are of importance here. Although governing mechanisms are difficult to distill from these results alone - nor is it in the scope of this work to identify them - the presented graphs hint at more effects playing a role; temperature influences are to be considered as well.

3.3.3 A25 - Response to dwell and split

In the previous sections, the impact of excess air and combustion phasing on post-injection efficacy was discussed. The response to variations in dwell has been charted for different air-excess ratios, showing the importance of careful selection of both post-injection timing and settings of other operating parameters. However, post-injection timing is not the only crucial parameter to be considered. The interplay of dwell and split will determine its eventual efficacy. In this sec-

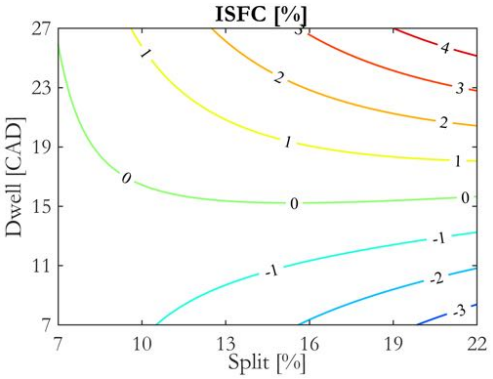

Figure 3.6: A25 - Response surface of ISFC change as function of dwell and split. Other operating parameters are set to their center point values.

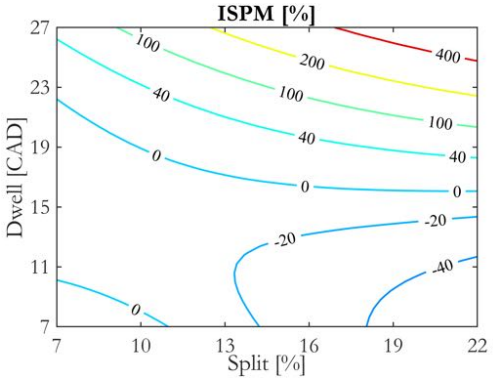

Figure 3.7: A25 - Response surface of ISPM change as function of dwell and split. Operating parameter settings correspond to those in Figure 3.6.

tion, so-called response surfaces are presented for net ISFC, ISNO$_x$ and ISPM. Other operating conditions are kept constant in their corresponding center point value. Results are presented as percentual differences with respect to the predictions of single injections. Negative values hence represent a reduction, whereas positive values denote an increase.

The response surface of the net ISFC change is shown in Figure 3.6. Notable improvements of fuel consumption are seen in a considerable area. There is also a sizeable range at an injection dwell value of about 15 CAD where fuel consumption is almost not responsive at all to split. This observations implies that several mechanisms impact on the thermodynamic efficiency that seemingly cancel each other out. By carefully choosing a proper combination of dwell and split, the balance of these processes can be adjusted to obtain a reduction in fuel consumption. Especially short dwells together with large splits add up to more than three percent improvement, but smaller splits also result in more moderate efficiency gains. For dwells longer than circa 15 CAD the benefits of a post injection disappear regardless of the split value. This increase in ISFC is expected, for fuel is introduced too late in the cycle, which effectively reduces the expansion ratio. As split is enlarged for these long dwells the predicted fuel consumption is obviously further increasing.

Figure 3.7 depicts the response surface plot of net ISPM change corresponding to the ISFC results. Here, a substantial region is found where soot emissions are reduced compared to single injection operation. Interestingly, the soot reduction area spans approximately the same range of dwell and split values as the fuel consumption reductions seen in Figure 3.6. This overlap could be an indication that improved burnout, and a subsequent advance of the end of combustion, plays a role in the projected efficiency gains. No soot reduction is observed when the dwell is increased beyond 23 CAD; a trend that becomes stronger when larger splits are applied. The interaction between the main injection soot pockets and the post-injected reacting spray is expected to be minimal, if not absent, in those cases. In the long-dwell regime, soot emissions are relatively insensitive to fuel split variations, whereas in the close-coupled regime these variations make the difference between an almost negligible effect and relative soot reductions up to 40%. This is another implication that physical interaction between main combustion fuel residues and the post injection is essential for its effectiveness.

A response surface plot of net ISNO$_x$ change is presented in Figure 3.8. For the selected operating conditions, virtually all combinations of dwell and split result in a reduction of NO$_x$ levels. Although it was shown in Figure 3.3 that burning a

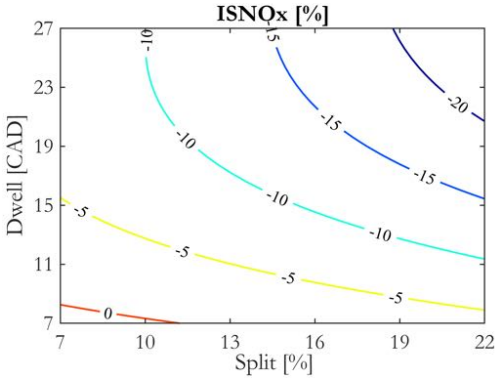

Figure 3.8: A25 - Response surface of $ISNO_x$ change as function of dwell and split under equal operating parameter settings as in the previous plots.

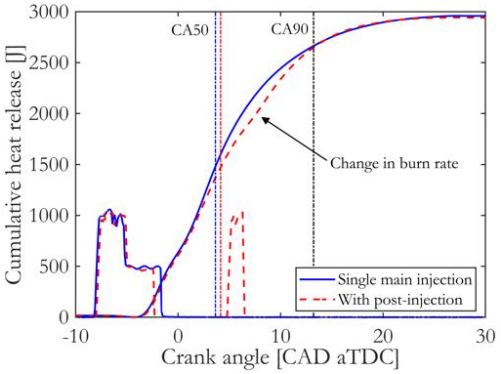

Figure 3.9: Comparison of cumulative heat release traces for a single main injection and a close-coupled post-injection strategy.

portion of the fuel later in the cycle does not always result in lower NO_x, it does hold for the conditions treated here. The largest reduction in NO_x is consequently reached for the longest dwell and largest split under consideration. Looking at Figures 3.6, 3.7 and 3.8 learns that there is a region of simultaneous reduction in ISPM, $ISNO_x$ and ISFC for short dwells and relatively large splits. Despite that soot reduction mechanisms are usually extensively discussed in available literature, the same cannot be said for NO_x reduction and efficiency gains. The governing processes affecting the latter two are vague at best, and are in need of more research on, for example, optical engine rigs.

Figure 3.9 shows two cumulative heat releases from a single injection and a post-injection experiment. Injection dwell and fuel split of the post-injection scheme are set to 7 °CA and 13.5%, respectively. As all other operational parameters are equal for the two injection strategies, the combustion processes are identical up to just after TDC. Thereafter, the heat release trace of the post-injection strategy starts to level off, as burn rates decline. This is expected, for the main injection ends earlier compared to single injection operation. As a consequence, CA50 is retarded by about 0.5 CAD for the post-injection scheme. This slightly later combustion event can partly explain lower NO_x levels and reduced heat losses to the cylinder walls. However, a shift of CA50 further into the expansion stroke is typically associated with a deterioration of the thermodynamic efficiency. When the post injection is introduced, however, the cumulative heat release slope steepens again and the post-injection strategy catches up with the single injection case. CA90 of the two strategies ultimately coincide, equalizing the total burn durations.

3.3.4 A50 - Response to dwell and split

The interaction of dwell and split at higher load will be assessed similar to the low load case. Figure 3.10 shows the response surface of the net ISPM change. The soot reduction capabilities seen at low load are preserved at higher load, albeit with a somewhat smaller maximum reduction. Increased fuel pressures can partly account for the apparent lower efficacy of the post injection as regards to engine-out soot. Furthermore, it is argued that burnout is more effective at higher load due to elevated global gas temperatures. The area in which soot reduction is observed is considerably smaller compared to lower load. However, contemporary fuel injection equipment is more than capable to provide sufficiently accurate timing and quantity for even very short fuel pulses to target these areas. Especially split values need to be lowered with respect to low load (revisit Figure 3.7) as to diminish ISPM, whereas shorter dwells again show the

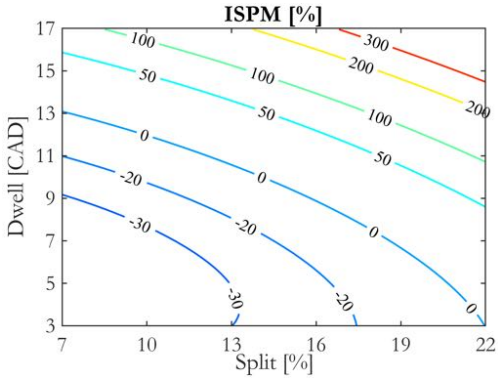

Figure 3.10: A50 - Response surface of ISPM change as function of dwell and split. Remaining operating parameters are set to their center point values.

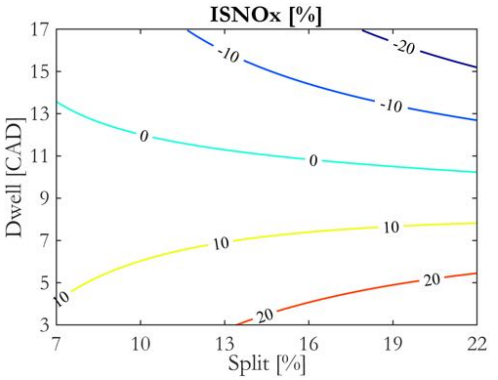

Figure 3.11: A50 - Response surface of $ISNO_x$ change as function of dwell and split. Operational settings corresponds to those in Figure 3.10.

highest efficacy. As the post injection is mainly employed to improve oxidation of fuel residues, a substantially longer post injection event will not be beneficial.

The response surface of the net $ISNO_x$ change is depicted in Figure 3.11. A decrease of NO_x is clearly not as easily obtained at higher load. Increments in excess of 20% are seen for very short dwells in combination with large splits. The tradeoff with ISPM as seen in Figure 3.10 is evident, since regions with soot reduction are in line with areas of NO_x increase, and vice versa. But when the dwell is amply extended, a reduced temperature in which the post fuel is burned proves to be effective in diminishing the formation of NO_x. Again, the longest dwell and largest split combination results in the most prominent reduction. Still, this reduction of $ISNO_x$ for long dwells is accompanied with considerable increments in ISPM and ISFC, making these areas highly undesired. ISFC improvements by addition of a post injection have not been established at all in this specific load-speed point.

3.3.5 B50 - Effects of fuel pressure

Increasing fuel pressure is a common measure to achieve a high thermodynamic efficiency. As burn rates in diffusion-limited combustion are dependent on the rate of fuel injection, the total burn duration can be reduced by increasing the fuel pressure. This is especially useful when engine speed is increased, since the residence time at high pressure and temperature is shorter and thus less time is available to complete chemical reactions. Here, an assessment is done on the possibility to further improve engine efficiency using fuel pressure in a post-injection strategy. Figure 3.12 shows a predicted tradeoff between net ISFC and net $ISNO_x$ at mode B50. A single main injection is again compared to a post-injection scheme with a fixed dwell (12.5 CAD) and split (10%). Fuel pressure is equally varied from 1325 to 1825 bar for both strategies. Increasing the fuel pressure certainly has benefits in terms of fuel consumption for both injection schemes. This comes at a cost of increased engine-out NO_x, for the corresponding increase in burn rate results in elevated peak temperatures. Eventually, the positive impact on fuel consumption might even reverse as the increasing peak temperatures lead to a dominance of total heat loss over reduced exhaust loss. Furthermore, when brake specific fuel consumption is considered, this extremum is possibly reached at an even lower fuel pressure. The latter is a consequence of parasitic losses associated with pressurizing the common rail, which are absent for the engine used in this work since an external high-pressure pump is applied. Nevertheless, the projected tradeoffs shown in Figure 3.12 display a decreasing trend in fuel consumption over the entire range, while

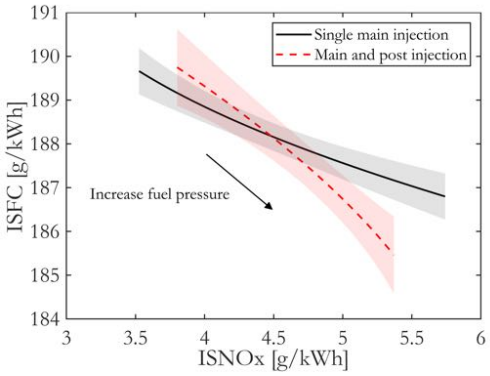

Figure 3.12: ISFC and $ISNO_x$ tradeoff with varying fuel pressure. Dwell and split of the post injection are fixed at 7.5 CAD and 10%, respectively. Intake pressure is set to 2.1 bar, whereas the other operating parameters are set to their center point values.

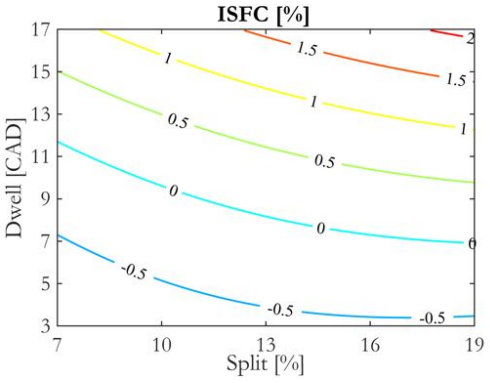

Figure 3.13: B50 - Response surface of ISFC change as function of dwell and split. Remaining operating parameters are set to their center point values.

$ISNO_x$ steadily increases. However, the post injection outperforms the single main injection. As fuel pressure is increased, the predicted downward slope is steeper when utilizing a post injection. The aforementioned compromise between an increased burn rate and higher heat loss rate at elevated fuel pressure seems to favor a post-injection scheme. Splitting the heat release results in a reduction of peak temperature, while the elevated fuel pressure is able to attain a sufficiently short combustion duration needed for efficient conversion of heat to mechanical work.

3.3.6 B50 - Response to dwell and split

A reduction in fuel consumption at B50 was already shown to be feasible in the previous section. The interaction of split and dwell will again be assessed here using response surfaces. The result of ISFC at mode B50 is shown in Figure 3.13. A large region with only moderate fuel consumption improvements is seen for dwell values below 10 CAD. Operating at the A-speed showed that an earlier completion of combustion by applying a post-injection is difficult to achieve. Measurements shown in Figure 3.9 do reveal that an increased burn rate of the post-injected fuel is possible, although this ultimately did not advance CA90. The efficiency gains were rather hypothesized to stem from a reduction in total heat loss, which allows phasing closer to TDC. At higher engine speed the mechanisms leading to reduced fuel consumption are not necessarily the same as at the A-speed. Since combustion generally spans a larger amount of crank angles at elevated engine speed, due to the fact that combustion reactions need a certain time to complete, there is more opportunity to accelerate the late phase of combustion.

The response surface of the net ISPM change at B50 is shown in Figure 3.14. It is again found that the soot reduction capabilities are preserved. The area in which soot reductions are obtained is enlarged with respect to mode A50. Similar to the ISFC response in Figure 3.13, the generally longer burn duration at higher engine speed appears to benefit more from the enhanced oxidation effect that a post injection has on the burnout phase. Moreover, the maximal soot reduction is slightly shifted to larger splits. Although this engine has a low-swirl design, bulk flow velocities somewhat increase with engine speed. Thus, a post injection profits from an increased duration of the imposed post-jet momentum to penetrate the bulk flow and interact with the soot clouds originating from the main combustion event. This is achieved by extending the actuation of the post injection.

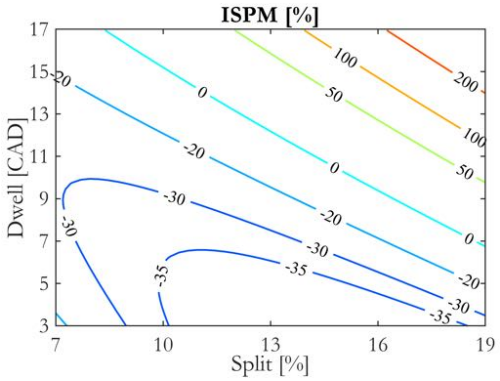

Figure 3.14: B50 - Response surface of ISPM change as function of dwell and split. Other operational settings correspond to those in Figure 3.13.

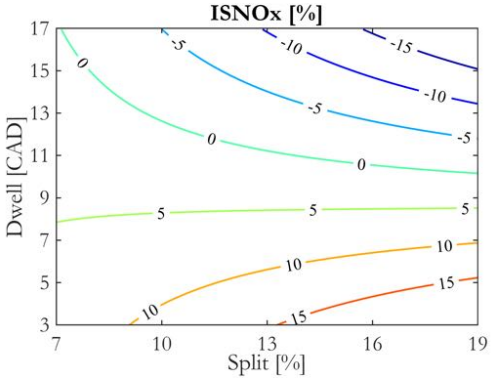

Figure 3.15: B50 - Response surface of $ISNO_x$ change as function of dwell and split. Operating parameters are set equal to the soot and fuel consumption plots.

Figure 3.15 lastly depicts the net $ISNO_x$ response surface for mode B50. Reductions of engine-out NO_x are obtained in the long-dwell regime, and large splits further amplify these reductions. Although this trend is seen for all three load-speed combinations under investigation, only A50 and B50 show considerable rises of $ISNO_x$ in the close-coupled regime. Introducing fresh air into hot combustion products, and thereby changing the stoichiometry towards conditions of enhanced NO_x formation rates seems to mainly occur at higher load, which is possibly linked to the longer residence time at higher global temperature. The post injection therefore needs to be delayed significantly longer compared to low load in order to mitigate NO_x formation rates. The tradeoff with ISPM is again evident, and reduces the usefulness of post injections at higher load, although a broader optimization is needed to investigate the potential of post-injection strategies in the entire load-speed map.

3.4 Conclusions

This chapter discussed experiments to investigate the impact of operating conditions on the efficacy of post injections. The investigations were done at three common load-speed points, each of which showed particular characteristics. Depending on the settings of fuel and air path, a post injection can either be very effective in reducing emissions and fuel consumption, or deteriorate these aspects in varying degrees of severity. The most important findings are summarized in the following.

A25

Low load was found to be most suitable for the application of post injections. The response surface analysis revealed that appropriate selection of dwell and split can simultaneously reduce soot, fuel consumption and NO_x, although the latter with only marginal percentages. A relatively large, close-coupled post injection proved most effective. Furthermore, an important interaction with air path parameters was also observed. The interplay of EGR and the main injection timing showed potential for simultaneous reduction of fuel consumption and NO_x with only a marginal penalty on soot. This is achieved by utilizing a post injection at elevated EGR rates, which allows a considerable advance of the combustion event. Effects of changes in excess air was further explored by varying dwell under various intake pressures and EGR rates. The air-excess ratio (λ) was found to have a strong impact on the soot reduction efficacy of a post injection. Lower values of λ increase the total reduction of soot. Further, the optimal dwell is shortened at lower values of λ. These observations suggest that indeed improved mixing of fuel rem-

nants and oxidizer play an important role in the efficacy of post injections, but the role of increased temperature needs consideration too.

A50

The soot reduction was found to be preserved at higher load. Yet, the soot reduction area as function of dwell and split is smaller as compared to low load, and also shows a lower percentual reduction. These modest abatements of soot emissions come at the expense of higher NO_x and fuel consumption. A reduction in fuel consumption was not established altogether, which considerably curtails the usefulness of a post-injection strategy for this particular load-speed point.

B50

At higher engine speed, the soot reduction is again retained. The tradeoff with NO_x, however, also firmly stands. Regions of lower engine-out soot display higher NO_x emissions, and vice versa. Minor reductions in fuel consumption coincide with a soot reduction in the short dwell regime, rendering post injections moderately suitable. The use of a post injection at elevated fuel pressure demonstrated lower fuel consumption than single injection operation, while NO_x formation is mitigated.

Chapter 4

Ramped versus square injection rates

Introduction

Multiple injections can be used to adjust the heat release rate to a more favorable shape, as the results in the preceding chapter pointed out. Still, post injections almost exclusively affect the burnout phase, but there is potentially something to gain in the first combustion stages as well. One or more pilot injections could be added to the scheme, but that has the disadvantage of having to lift and drop the injector needle several times within the same cycle. Rate shaping without flow interruption is possible with a specialized injector, which is the topic of this chapter. It provides a more direct way of controlling the fueling rate with respect to its digitized counterpart. A novel twin solenoid valve injector, Delphi's DFI7, is put to the test by comparing ramped injection rates to the traditional square profiles. Ramped rates are thought to lower the initial temperature and pressure rise, thereby reducing NO_x formation, compression work and heat transfer. The eventual goal is to find a better compromise between the gross indicated efficiency and the NO_x emissions.

The contents of this chapter have been published as Willems, R., et al., "Ramped Versus Square Injection Rate Experiments in a Heavy-Duty Diesel Engine," SAE Int. J. Adv. & Curr. Prac. in Mobility 2(3):1322-1336, 2020, doi:10.4271/2020-01-0300 [75].

4.1 Literature review

Among several pathways to reduce emissions of CO_2 and pollutants, the ongoing development of fuel injection equipment is opening up additional degrees of freedom for further improvements [69]. One promising approach to gain valuable efficiency points is shaping the rate of heat release, which can be done by adjusting the rate at which fuel is injected into the cylinder. Methods to do this can be roughly divided into two categories: multiple injections and continuous rate shaping. The former employs two or more injections with a basically square fueling profile to regulate the flow rate. These discrete (or "digital") injection patterns subsequently affect the burn rate and open up extra possibilities for combustion control [70]. Shaping the fuel injection rate without flow interruption is possible with specialized equipment. In general, a distinction is made between ramp and boot rates, which are schematically shown in Figure 4.1, alongside an example of digital rate shaping. Each rate shape is characterized by several unique settings that allow tuning of the injection profile. Note that the total amount of pulses for digital rate shaping is not necessarily four, as in this example.

The effects of multiple injections on efficiency and emissions of a diesel engine have been widely researched, especially since the appearance of electronically controlled injectors [51, 54, 71, 72]. Pilot and post injections (i.e. low quantity injections before or after a main injection event) received significant attention, which led to some consensus of their effects. Pilot injections have been found to generally decrease combustion noise [59,

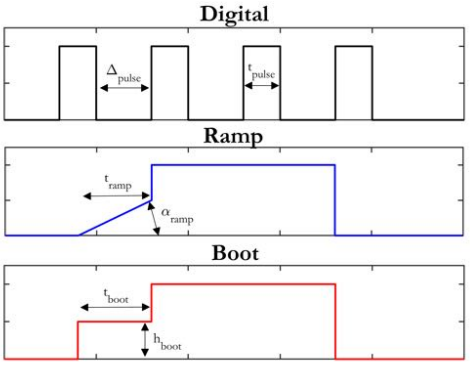

Figure 4.1: Schematic overview of digital, ramp and boot rate shapes. Δ_{pulse} = pulse separation, t_{pulse} = pulse duration, t_{ramp} = ramp duration, α_{ramp} = ramp slope, t_{boot} = boot duration, h_{boot} = boot height.

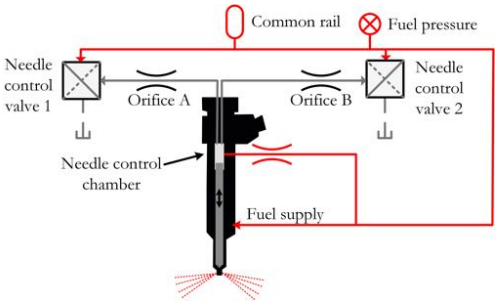

Figure 4.2: Schematic overview of the Delphi DFI7. Pressure in the control chamber can be modulated by specific actuation intervals of both valves.

73], whereas post injections are particularly useful for lowering engine-out soot [58]. Some reports mention efficiency gains by carefully scheduling a close-coupled post injection [53, 66, 74], although the governing mechanisms remain ambiguous. Enhanced mixing late in the cycle, and an ensuing acceleration of the burnout phase, partially explains observed trends.

Injection strategies utilizing a form of continuous rate shaping emerged about two decades ago, when specialized equipment first became available [76]. It is mainly the NO_x reducing capability of ramped and boot-shaped injection rates that is often demonstrated in literature. The initial temperature rise can be suppressed by reducing the intensity of the premixed combustion phase using these injection rates, thereby lowering peak temperatures and mitigating formation of NO_x [77]. Desantes [79] reported such NO_x reductions when applying a ramped or boot-shaped injection pattern, but did not observe major changes in the premixed combustion phase. It was instead the diffusion-limited phase that showed the most significant change in behavior [80]. Two prevailing methods to control the fuel injection rate are found in literature. Firstly, the fuel pressure can be varied to adjust the fuel flow by, for example, a dual common rail application employing a switching valve to change between a low and high pressure rail [81]. An alternate approach is to amplify the fuel pressure within the injector body using an extra actuator [82]. Secondly, the injector needle position can be controlled to throttle the fuel flow into the cylinder [69]. The Delphi DFI7 is a twin solenoid valve injector, which allows such control over the needle motion. An overview is given in Figure 4.2. In idle position, the needle control chamber is pressurized to rail pressure and the needle is kept in its seat. Pressure in the control chamber can be modulated by individually actuating the two needle control valves (NCVs) at certain intervals, thereby controlling the needle lift. This allows for various fueling rates to be produced.

Energizing either NCV individually produces a ramp profile, as fuel gradually flows out of the needle control chamber via either orifice A or B, lifting the needle relatively slowly. This is shown in Figure 4.3. After the initial ramp a plateau is established, as the injector needle enters a hover position, upon reaching a dynamic pressure equilibrium. The orifice diameters are selected such that certain percentages of the maximum flow can be reached. More specifically, for the injector in these experiments, actuating NCV1 or NCV2 alone will produce flow rates at 25% or 50% of the maximum fuel flow, respectively. This also means that a specific NCV, associated with its own orifice, produces a certain ramp slope (α_{ramp}). This is visible in Figure 4.3. Two ramp slopes are possible with the configuration of this injector; NCV1 generates a

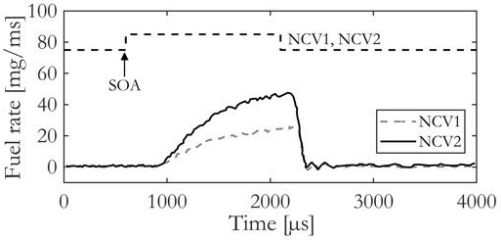

Figure 4.3: Separate responses to actuating either NCV1 or NCV2 alone. The energizing interval of 1500 µs is equal for both rate traces. Fuel pressure is 1600 bar. Note that both rates ultimately start to plateau.

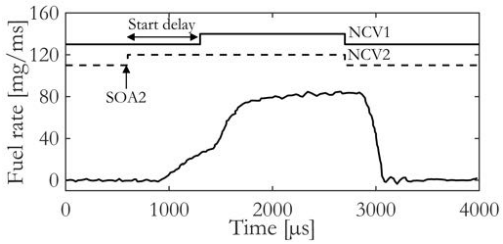

Figure 4.4: Sample ramped rate profile. Actuation of NCV1 is delayed by 700 µs with respect to NCV2. Fuel pressure equals 1600 bar. Note that a shallower initial slope can be obtained by delaying NCV2.

shallower slope than NCV2. When the start of actuation (SOA) of one NCV is scheduled later than the other, an initial ramp followed by a period of maximal flow is obtained. Maximum flow rate is only reached when both NCVs are energized together. Figure 4.4 shows a sample of a ramped injection rate, where actuation of NCV1 is delayed by 700 µs with respect to NCV2. This start delay determines the ramp duration (t_{ramp}). When both solenoid valves are actuated identically, the DFI7 can be used to replicate single valve performance. Such a sample square rate is shown in Figure 4.5, and will be used as a baseline case.

4.2 Experimental approach

The effects of ramped injection rates on the gross indicated efficiency (GIE) and specific emissions are compared to those of square rate fueling profiles. The concepts were already introduced in Figure 4.4 and Figure 4.5. Both types of rate shapes are created using the DFI7 injector and experiments are performed on the XEC platform. Load is kept relatively low at 30% of the rated power by injecting a total of 90 mg of fuel per cycle in all experiments. This corresponds to the requirement per cylinder of a fully loaded truck-trailer combination cruising at 80 km/h on a flat road; a common scenario in large parts of Europe. In addition, two typical engine speeds are selected: 1200 and 1425 rpm. These values correspond to the A and B-speed of this engine in the European Stationary Cycle (ESC). Although ESC tests are usually performed at a fixed torque, here the fuel quantity is kept constant for ease of experimenting, and thus the actual load may vary slightly according to the efficiency. The intake pressure is set to 1.6 bar (absolute) for both load-speed points, which is a typical boost level for the load targeted in this work. The exhaust back pressure is set above the intake boost pressure to drive the EGR flow. Nominal operating conditions are summarized in Table 4.1.

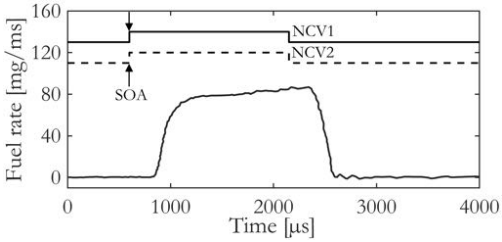

Figure 4.5: Sample square rate profile, analogous to single valve operation. Fuel pressure is 1600 bar and both valves are simultaneously energized for 1550 µs.

The design of experiments (DOE) methodology is applied to study multiple fuel and air path settings and their corresponding interactions, without needing to run all permutations. The examined parameters are organized into central composite design (CCD) matrices, which are shown in the Tables 4.2 to 4.5. CCDs are particularly useful for creating response surface plots, which will be presented and discussed later on. More details of DOE and the regression procedure are given in Chapter 2. For ramped rate operation, start of actuation (SOA) is set separately for each

Table 4.1: Nominal operating conditions.

Intake manifold T	40 °C
Boost pressure	1.6 bar
Fuel quantity	90 mg per cycle
A30 exhaust pressure	1.75 bar
B30 exhaust pressure	1.9 bar
A-speed	1200 rpm
B-speed	1425 rpm
Fuel specification	EN590 diesel

NCV. However, actuation of NCV1 is defined by a start delay with respect to the SOA of NCV2, as previously illustrated in Figure 4.4. Note that for square rates a single SOA value is shown in Tables 4.2 and 4.4, as both solenoid valves are energized identically. Fuel pressure is also incorporated in each matrix for further optimization. The EGR rate is lastly used to target certain NO_x levels, which can be brought below legislative levels using selective catalytic reduction. A two-level full factorial design is the core of a CCD; all possible combinations between the factors at these two levels (-1 and 1) are run. A unique center point (0) is added to the design, which is repeated at a number of random instances to assess experimental drift and repeatability. To complete the CCD, axial points ($-\alpha$ and α) are included in the matrix.

The total number of runs in a CCD equals $2^k + 2k + C$, where C and k are the amount of center points and factors, respectively. Square and ramped rate matrices are tested with $C = 6$ and $C = 8$, respectively. All other test points are repeated once. Hence, the total amount of runs equals 34 (Tables 4.2 and 4.4) and 56 (Tables 4.3 and 4.5). Experiment runs are lastly randomized before testing. All injection rate shapes have been measured on a hydraulic test rig following the engine experiments. The results of these injection rate measurements are included in Appendix 4.A. The adjusted R^2 values of the regression equations for GIE and $ISNO_x$ are shown in Table 4.6.

4.3 Results and discussion

4.3.1 Square rate optimization

Optimization of diesel engine combustion involves not only finding maximum efficiency, but also requires emissions of pollutants to remain within acceptable margins. With contemporary fuel pressures reaching - and often surpassing - 2000 bar, the main challenge is to find the best possible compromise between specific NO_x emissions and efficiency. Figure 4.6 visualizes regressed tradeoffs of gross $ISNO_x$ and GIE for both load-speed points under evaluation. Results for square rates, as well as ramped rates are shown, although the latter will be treated in the next section.

Shaded regions around the predictions depict 95% confidence intervals. Energy distributions at the maxima (indicated by markers) are included within frames for each curve. The curves themselves represent combustion phasing variations, although these are established in different ways for each rate shape. For the square rates discussed here, SOA is varied according to the values depicted in Tables 4.2 and 4.4; associated fuel pressures and EGR rates have been selected in advance for best performance. The aim was to keep NO_x levels below 7 g/kWh, by reasoning that contemporary aftertreatment is capable of bringing these levels down to EURO VI levels. To mitigate in-cylinder NO_x formation, 24% of EGR is added to the intake charge in both modes. Fuel pressures equal 1800 and 1900 bar, while the GIE maxima are ultimately found with SOA values of -9 and -12 CAD aTDC at A30 and B30, respectively. Note that a reduction of heat transfer losses is the main reason for higher peak GIE at B30. The marginal increase of exhaust losses is clearly well compensated. The latter loss channel is also partly neutralized by increasing the fuel pressure and advancing the injection event. Heat transfer losses are readily suppressed by shorter residence times at high temperature, due to the elevated engine speed. This same argument applies to the fact that peak GIE is reached at lower NO_x despite equal EGR rates; the effect of an efficiency increase on lower specific NO_x values is only small.

Table 4.2: Selected factors and levels for square rate experiments in mode A30. Start of actuation (SOA) is applicable to both NCVs, since their energizing schemes are exactly the same.

A30 square	$-\alpha$	-1	0	1	α	Unit
SOA	-11.5	-10	-8	-6	-4.5	CAD aTDC
Fuel pressure	1350	1500	1700	1900	2050	bar
EGR rate	17	20	24	28	31	%

Table 4.3: Selected factors and levels for ramped rate experiments in mode A30. The SOA of NCV2 is considerably advanced to account for the ramp up time.

A30 ramped	$-\alpha$	-1	0	1	α	Unit
Start delay NCV1	600	800	1000	1200	1400	µs
SOA NCV2	-18	-16	-14	-12	-10	CAD aTDC
Fuel pressure	1300	1500	1700	1900	2100	bar
EGR rate	16	20	24	28	32	%

Table 4.4: Selected factors and levels for square rate experiments in mode B30. The SOA has been advanced compared to compensate for the increase in engine speed.

B30 square	$-\alpha$	-1	0	1	α	Unit
SOA	-13.5	-12	-10	-8	-6.5	CAD aTDC
Fuel pressure	1250	1400	1600	1800	1950	bar
EGR rate	17	20	24	28	31	%

Table 4.5: Selected factors and levels for ramped rate experiments in mode B30. The time-based start delay of NCV1 is reduced with respect to the lower engine speed case to target the same crank angle delay.

B30 ramped	$-\alpha$	-1	0	1	α	Unit
Start delay NCV1	500	700	900	1100	1300	µs
SOA NCV2	-20	-18	-16	-14	-12	CAD aTDC
Fuel pressure	1200	1400	1600	1800	2000	bar
EGR rate	16	20	24	28	32	%

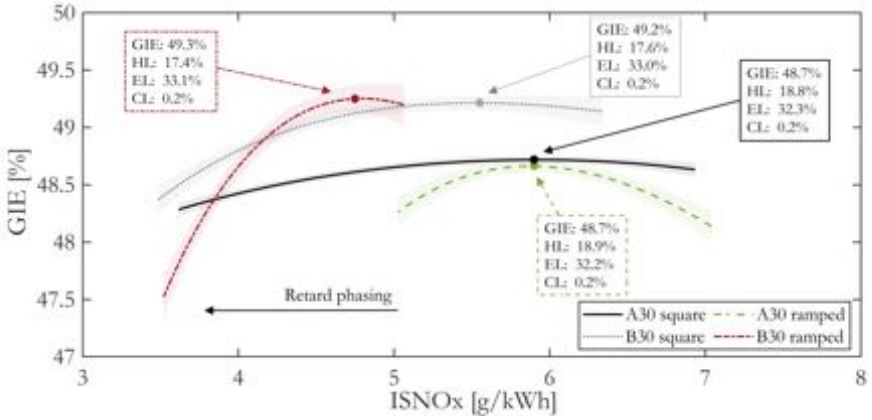

Figure 4.6: Regressed tradeoffs of GIE and ISNOx for both square and ramped injection profiles. Shaded regions around the predictions depict 95% confidence intervals. HL = heat loss, EL = exhaust loss, CL = combustion loss.

Table 4.6: Adjusted R^2 values of the regression equations of GIE and $ISNO_x$.

	Square rate		**Ramped rate**	
	A30	*B30*	*A30*	*B30*
GIE	0.908	0.927	0.913	0.955
$ISNO_x$	0.989	0.987	0.991	0.995

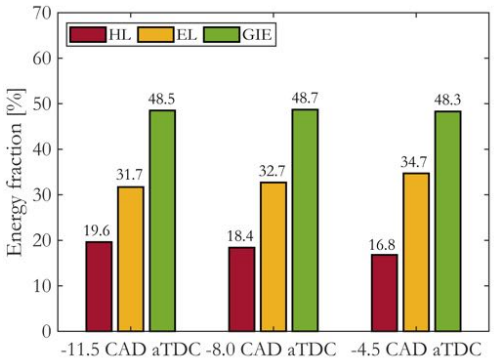

Figure 4.7: Energy distributions versus SOA in CAD aTDC using square rates in mode A30. Fuel pressure is 1700 bar and the EGR rate is 24%. Combustion losses are 0.2% in each point and are excluded for clarity.

The observed GIE maxima are established by balanced wall heat transfer and exhaust losses as diesel injection timing is varied. This is visualized in Figure 4.7, where fuel energy distributions are depicted of square rate experiments in mode A30 at three different SOA settings. Advancing the injection event primarily increases the heat losses, due to a longer residence time at elevated pressures and temperatures, while the latter is decreased as a result of a larger effective expansion ratio. For the optima found in Figure 4.6, the start of combustion is phased several crank angles before top dead center, and thus a certain portion of heat is released at a thermodynamically unfavorable interval. This is where, potentially, a ramped injection profile can have a beneficial effect on GIE. By gradually building up the rate of injection, the fuel fraction that is burned before TDC is reduced. This can further maximize efficiency in two ways. Firstly, heat transfer losses are reduced as both temperature and pressure rise relatively slowly in the first stages of combustion. Secondly, since less heat is released before TDC, compression work decreases. By a following increase of the injection rate just after TDC, the expansion stroke can be utilized as efficiently as possible. The square rate results in Figure 4.6 will be used as baseline and are compared to ramped injection performance in the following.

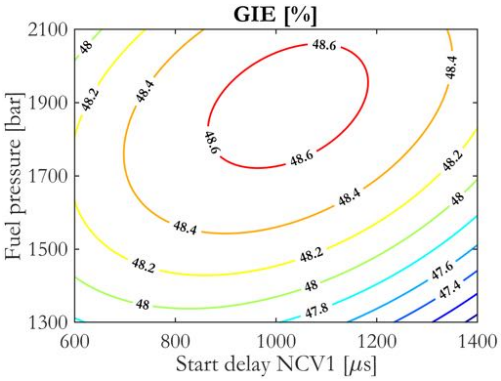

Figure 4.8: Response surface of GIE at A30 versus fuel pressure and the NCV1 start delay. SOA of NCV2 is -14 CAD aTDC, while the EGR rate equals 24%.

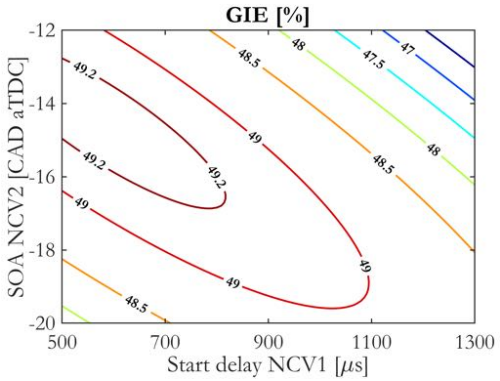

Figure 4.9: Response surface of GIE at B30 versus SOA of NCV2 and the start delay of NCV1. Fuel pressure is set to 1900 bar and the EGR rate is 24%.

4.3.2 Ramped rate optimization

Ramped injection strategies are tested using an additional operating parameter: the start delay of NCV1 with respect to the SOA of NCV2 (see Figure 4.4). Addition of this parameter results in a doubling of possible interaction effects. To investigate which operating parameters - or factors - and related interactions are most influential on GIE, a 4-factor ANOVA test is performed on the experimental data, similar to the approach of De Cuyper et al. [50]. This statistical test also quantifies the experimental error. Results of mode A30 are presented in Table 6.4. The ANOVA results indicate that the influence of EGR rate is insignificant, as its effect barely stands out from the error. The start of fuel injection, represented by the SOA of NCV2, and the fuel pressure are most dominant in affecting GIE. Moreover, the interplay of these two factors also significantly contributes to the variation in the data. These findings were perhaps already intuitively expected, and more interest after all goes out to the effect of the ramp duration. The influence of the NCV1 start delay on GIE, however, is more subtle, but surely noticeable. It is especially the interaction of the ramp duration (start delay of NCV1) with common rail pressure that has an apparent impact, although just not statistically significant at this confidence level. Analyzing this interaction in a response surface can give insight in the underlying mechanisms.

A response surface plot of GIE as function of fuel pressure and NCV1 start delay is shown in Figure 4.8. The associated load-speed point is mode A30. A region of peak GIE is observed at fuel pressures between 1800 and 2000 bar, and NCV1 start delays between 900 and 1100 μs. This plateau is elliptical, due to the interaction of these two factors. A lower fuel pressure requires the start delay to be reduced, while a longer ramp time is allowed at higher fuel pressure. Reasons for the specific location of optimal performance can be sought in the distribution of fuel energy. Analysis of the individual loss channels revealed that when the ramp duration is increased, heat transfer loss linearly follows. On the other hand, exhaust losses are only slightly affected in the start delay range of 600 to 800 μs, but this is followed by a steeper incline as the delay is extended further. Rising exhaust losses overtake the decreasing heat transfer losses around 1000 μs, thereby establishing an optimum. Later on in this chapter, aROHR traces and corresponding energy distributions will be compared to investigate how the ramp duration influences the combustion process.

Analogous to the preceding discussion, a 4-factor ANOVA was performed on the B30 results (see Table 4.8). The variance of these data reveals that a strong interaction is present among the start delay of NCV1 and the SOA of NCV2. Hence, the interaction of these factors and their effect on GIE

Table 4.7: GIE 4-factor ANOVA table for mode A30 using ramped injection rates. sDelay1 = start delay of NCV1, SOA2 = start of actuation of NCV2, pFuel = fuel pressure, EGR = rate of exhaust gas recirculation.

Source	SS	d.f.	MS	F-stat	p-value
pFuel	1.6091	1	1.6091	27.74	3.76e-6
SOA2	1.6049	1	1.6049	27.67	3.85e-6
SOA2·pFuel	0.3540	1	0.3540	6.10	0.0173
sDelay1·pFuel	0.2138	1	0.2138	3.69	0.0612
sDelay1	0.1225	1	0.1225	2.11	0.1531
EGR	0.0786	1	0.0786	1.36	0.2505
sDelay1·SOA2	0.0420	1	0.0420	0.72	0.3996
sDelay1·EGR	0.0101	1	0.0101	0.18	0.6773
SOA2·EGR	0.0009	1	0.0009	0.02	0.9020
pFuel·EGR	0.0008	1	0.0008	0.01	0.9085
Error	2.6098	45	0.0580		
Total	6.6464	55			

Table 4.8: GIE 4-factor ANOVA table for mode B30 using ramped injection rates. Double horizontal lines separate statistically significant factors and interactions from the rest.

Source	SS	d.f.	MS	F-stat	p-value
pFuel	7.9013	1	7.9013	97.24	8.05e-13
SOA2	5.2210	1	5.2210	64.25	3.27e-10
sDelay1	3.9573	1	3.9573	48.70	1.09e-08
sDelay1·SOA2	2.217	1	2.217	27.28	4.36e-06
EGR	0.4252	1	0.4252	5.23	0.0269
SOA2·pFuel	0.2608	1	0.2608	3.21	0.0799
pFuel·EGR	0.0394	1	0.0394	0.48	0.4898
sDelay1·pFuel	0.0363	1	0.0363	0.45	0.5075
sDelay1·EGR	0.0009	1	0.0009	0.01	0.9145
SOA2·EGR	0.0000	1	0.0000	0.00	0.9897
Error	3.6565	45	0.0813		
Total	23.7158	55			

will be more closely investigated in a response surface plot; this is illustrated in Figure 4.9. It can be seen that the region of maximal GIE is again shaped elliptically, but to an even larger extent compared to Figure 4.8. By advancing the SOA of NCV2, more tolerance is created for increasing the ramp duration. Optimal ramp durations are much shorter than those seen in mode A30. In part, the higher engine speed is causing this effect. Matching the ramp durations for both modes in the crank angle domain requires shorter NCV1 start delays given the higher engine speed in B30. Still, this only explains about a 150 µs offset, while the GIE maxima are approximately 400 µs apart. Explanations are again found by analyzing the energy loss channels. The strong rise in exhaust losses when increasing ramp durations, which was also observed at A30, already commences at start delays longer than 600 µs. This soon cancels any positive effect of reduced heat losses, and thus an optimum is settled at shorter start delays.

Figures 4.8 and 4.9 evidence that ramped profiles can attain GIEs that are near identical to those of square rates. Although GIE was not increased compared to the square rate baseline, ramped rates may be useful for reducing NO_x levels instead. Figure 4.6 already introduced tradeoffs of GIE and $ISNO_x$ for ramped injection schemes at both modes. GIE optima are shown with markers for comparison of the two rate shapes. Along each ramped rate curve the ramp duration is varied by adjusting the NCV1 start delay according to the values depicted in Tables 4.3 and 4.5. Fuel pressures are set to 1900 bar, and the EGR rates equal 24% in both modes. The SOAs of NCV2 are fixed at -14 and -15 CAD aTDC in A30 and B30, respectively, as these led to the best efficiency. Peak GIE is reached just below 6 g/kWh NO_x in A30, which matches with results obtained using square rates. Distributions of fuel energy are seen to be very similar as well. Ramped injection was expected to reduce NO_x by lowering the initial temperature rise rate, hence lowering the temperature history throughout the cycle. However, an increase in the fuel pressure and slight advance of combustion phasing were needed to reach equal GIE. These measures ultimately worked as a counterbalance.

In mode B30, on the other hand, peak efficiency is obtained at 4.8 g/kWh of NO_x versus 5.6 g/kWh for the square rate optimum. This amounts to a reduction of about 15%. Contrary to mode A30, fuel pressure could be kept the same, omitting any counter effects. Heat transfer losses are somewhat lower when compared to the square rate results, hinting at lower local temperatures throughout the cycle. This observation concurs with the reduction of NO_x emissions. A steep decline in GIE is seen when the ramp duration is increased further, stressing the need for meticulous start delay selection when utilizing ramped injection rates, especially at elevated engine speeds. The results in Figure 4.6 hint that a critical engine speed will be reached where ramped rates cannot attain high GIE, as the optimal ramp duration is significantly reduced with an engine speed increment of only 225 rpm. Table 4.9 summarizes the optimal parameter settings, associated integral combustion metrics and emissions of NO_x and PM. Each column represents one of the optimized injection strategies, as indicated by markers in Figure 4.6.

4.3.3 Ramp duration effects on the rate of heat release

The previous analysis indicated that GIEs in ramped and square rate operation are near identical. In this section, it is further analyzed why that is, and how GIE may be increased further. Apparent rates of heat release (aROHR) are plotted in Figure 4.10 to investigate how ramp durations affect the combustion event. A direct comparison is made to a square injection profile in otherwise equal operating conditions. Actuation schemes in arbitrary units are shown below the aROHR traces in corresponding line types and colors. Note that all injection strategies result in an identical start of combustion. It is observed that the well-known premixed peak is strongly reduced when a ramped injection strategy is used, particularly for longer ramp durations. This is often considered a positive effect, as combustion noise and NO_x emissions have been reported to decline [77]. Here, it also appears to affect the intensity of pressure oscillations, which are notably present for

Table 4.9: Overview of optimal operating parameter settings, integral combustion metrics, indicated efficiency and specific emissions for both load-speed points using square and ramped rates.

Parameter	A30 square	A30 ramped	B30 square	B30 ramped	Units
Start delay NCV1	0	1000	0	600	µs
SOA NCV2	-9	-14	-12	-15	CAD aTDC
Fuel pressure	1800	1900	1900	1900	bar
EGR rate	24	24	24	24	%
CA50	2.7	2.3	1.5	2.4	CAD aTDC
BD	15.5	17.5	16.4	17.5	CAD
GIE	48.7	48.7	49.2	49.3	%
$ISNO_x$	5.8	5.9	5.6	4.8	g/kWh
ISPM	0.004	0.03	0.003	0.02	g/kWh

the square rate trace despite equal filter settings as compared to the ramped rates. The height of the premixed peak dictates the initial rise rates of pressure and temperature. By lowering this first peak, maximum temperatures are lowered and NO_x formation is readily mitigated. It was hypothesized earlier, that this may also result in less compression work and lower heat transfer losses, hence increasing GIE. However, the heat release rate in the diffusive burn phase is also lowered. As a consequence, combustion extends further into the expansion stroke, thereby decreasing the useful work extraction.

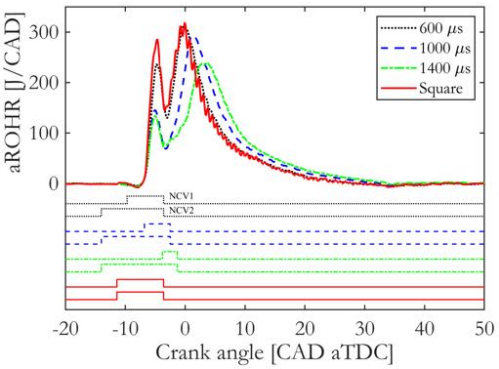

Figure 4.10: Rates of heat release for varying ramp durations and a square profile in A30. Fuel pressure is 1700 bar, and EGR equals 24% for all traces.

The aforementioned observations are most notable when the ramp duration is increased from 1000 to 1400 µs. Two reasons are noted. First, given the fact that the maximal flow rate is the same for all scenarios, extending the ramp phase inevitably leads to a longer injection duration. Second, it is at this point unclear how the needle position affects spray formation and mixing. Since fuel is throttled into the nozzle sac, the effective injection pressure is consequently lower than the common rail pressure. This has an evident impact on the ignition delay as shown in Figure 4.11, which depicts a scatter plot of all DOE runs listed in Tables 4.2 to 4.5. Burn durations (BD) are defined as the interval between the crank angles at which 10% and 90% of the total heat is released (CA10 and CA90). The definition of ignition delay differs somewhat between square and ramped injection rates. It is defined as the interval between the first SOA that occurs and CA5. Since ramped rates are initialized with an actuation of NCV2, that particular SOA is used as starting point in that case. The slow upward motion of the needle seems to cause an extension of the ignition delay, as the pressure in the nozzle sac gradually builds up. An overall offset of 3 CAD is seen in A30, while this offset increases to 4 CAD for B30. These longer igni-

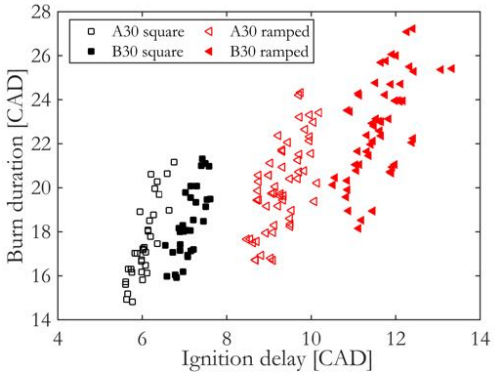

Figure 4.11: Burn duration as function of ignition delay for all experiment runs. Note that ramped injection rates result in much longer ignition delays and overall longer burn durations.

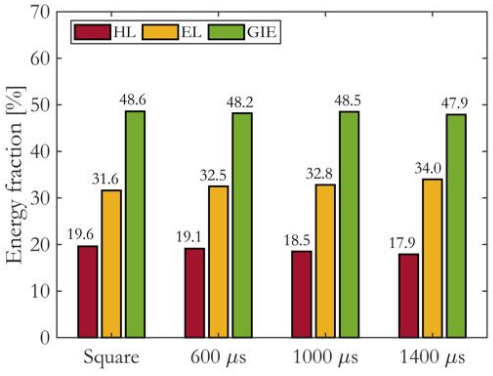

Figure 4.12: Fuel energy distributions for different NCV1 start delays belonging to the aROHR traces presented in Figure 4.10. Combustion losses are 0.2% for all injection rate shapes and are excluded for clarity.

tion delays clearly correlate with an extension of the burn durations. It is argued that continuously shaping injection rates should provide the capability of controlling the successive heights of the premixed and diffusive peaks largely independent of each other. This would really result in the capability to reduce compression work and heat transfer, while also maximizing the effective expansion ratio. A prerequisite is that ignition delays need to be sufficiently short (at least comparable to square rates), such that the burn rate can be adjusted from an early point in the combustion event.

4.3.4 Energy loss channels and emissions

To support the discussion of the effects of ramped injection on GIE and related loss channels, fuel energy distributions are presented in Figure 4.12. The experimental conditions at which these results are obtained correspond to the aROHR traces in Figure 4.10. Heat transfer losses are found to decline almost linearly as the ramp duration is increased, which relates to tempered temperature rise rates as the ramp duration is increased. Exhaust losses are in turn lowest for the square rate case, owing to the relatively short burn duration. When the ramp duration increases from 600 to 1000 μs, exhaust losses follow only marginally. That changes, however, when ramps longer than 1000 μs are applied and combustion extends too far into the expansion stroke. The excessive ignition delays play a crucial role in this, because a considerable amount of fuel is injected during this period which will burn late and slow. This severely extends the burn duration with an obvious impact on exhaust losses.

Figure 4.13 displays indicated specific emissions corresponding to the results shown Figures 4.10 and 4.12. Note that ISNO$_x$ values are divided by 10 for sake of readability. These NO$_x$ levels follow the trend of heat losses to lower values; both are largely governed by local temperature. The ramp duration affects these temperatures not only by decreasing the height of the premixed peak, as evidenced by Figure 4.10, but clearly also lowers the intensity of the diffusion-limited combustion phase. Soot emissions are extremely low when using a conventional square injection profile, well below EURO VI legislative levels. A ramp of 600 μs still complies with these levels, but longer ramp durations result in a substantial increase of soot emissions. This is to a certain extent ascribed to a lower degree of mixing of fuel and air, because fuel pressure in the nozzle sac is lower during the ramp up. This causes more soot to be formed in the spray [78]. The burn duration extension also affects the global gas temperature and might deteriorate soot oxidation. Later in the cycle, the burnout phase progresses slower, which clearly in-

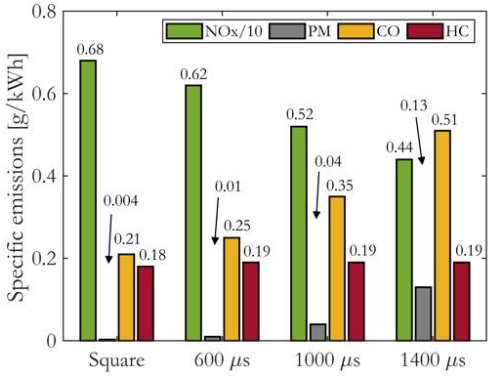

Figure 4.13: Indicated specific emissions belonging to the aROHR traces of Figure 4.10. ISNO$_x$ values are divided by a factor of 10 for readability.

creases carbon monoxide emissions too. Contrarily, unburned hydrocarbons are unaffected by the injection rate shape; combustion losses thus remain largely constant.

There are several caveats to mention related to the tests in this chapter. First of all, the compression ratio of the test engine has been lowered to facilitate contrasting requirements for conventional diesel combustion and low temperature combustion, to allow both to be researched. This obviously has an effect on the TDC temperature, and thus affects the ignition delay. It is expected that when contemporary compression ratios reaching well over 17 are applied, severe extension of the ignition delay is limited. Second, this work focused solely on low load operation. While the load-speed points under consideration are deemed significant contributors to the average fuel consumption of long-haul trucks, future work needs to be extended to higher loads. Higher loads will result in increased cycle-averaged temperatures of piston, liner and cylinder head, which will boost TDC temperature. With the reducing effect that this has on ignition delay, control over the burn rate should be secured at an earlier point in the combustion event. Moreover, it is in some reports suggested that rate shaping strategies are more effective at elevated loads entirely. In [83], for example, square injection rate is proposed at low load, which eventually needs to transition to ramped rates in the medium load regime and boot profiles at full load. The full load regime was argued to be best suited for rate shaping, because of major improvements to the NO_x and efficiency tradeoff. These improvements were ascribed to a comparatively more isobaric combustion using ramped or boot rates instead of a square profile. Third, the DFI7 injector is besides ramped rates also capable of producing aforementioned boot rates, which have not been taken into account in this work. Boot rates can be created using a third NCV actuation, and allow to rapidly reach a reduced flow 'plateau' before activating maximum flow rate. As the throttling effect in the first stages of injection is less severe, ignition delays are expected to be shorter. This will consequently give more initial burn rate control.

4.4 Conclusions and outlook

This work experimentally compared square and ramped injection rate shapes using Delphi's DFI7 injector at a relatively low load and two representative engine speeds. The aim was to improve engine performance with regard to GIE and NO_x by applying ramped injection rates instead of traditional square profiles. The experiment data, and regression analysis based on that, revealed that ramped fueling rates can attain high GIE in both load-speed points, essentially equal to square rate values. The levels of NO_x at which peak efficiencies were reached, however, differed between engine speeds. When operating at 1200 rpm, maximum GIE of the two injection rate shapes were attained at virtually equal engine-out NO_x. An elevated engine speed of 1425 rpm, contrarily, rendered a ramped rate effective in lowering NO_x emissions at peak GIE. This opens up possibilities to further optimize efficiency by other means.

Rate of heat release analysis revealed a considerable extension of the ignition delay when ramped injection rates were applied. It is thought that the processes of fuel atomization and evaporation are adversely affected, and that these are the cause of the longer ignition delays. The spray behavior influences both the engine efficiency and emissions.

Effects of the ramped injection on the prevailing spray behavior should therefore be carefully considered. Increased soot emissions are such a challenge when utilizing ramped rates, as these were seen to rise substantially. The injection strategies may be expanded with a post injection as countermeasure. Burn durations were seen to extend as well. While ramped rates were effective in minimizing the premixed combustion peak, independent control over the separate combustion phase burn rates was overall limited. Reducing premixed intensity proved to be inseparable from slower diffusion-limited and late-stage combustion. Ideally, the burn rates in these phases should be controlled independent from each other to fully exploit the capabilities of injection rate shaping.

Several measures can be investigated in future work to improve the effects of rate shaping on engine efficiency. The ignition delay can be reduced by increasing the compression ratio. Follow up tests need to be conducted with a typical compression ratio for conventional diesel combustion; the test engine in this work had a lower compression ratio to facilitate requirements of low temperature combustion. At low loads, a short pilot injection may be added to force an earlier start of combustion and thus make more use of an injection profile that follows. Boot rates or steeper ramps may be explored, for these are expected to reduce the ignition delay to a significant extent as well.

Initial nozzle sac pressure will be higher compared to tests in this chapter resulting in improved atomization and evaporation of fuel. The experiments should also be extended to higher loads, since problems of long ignition delays are anticipated to be less harsh, and hence the possibilities to control combustion are enhanced. The key message is that rate shapes need to be carefully selected for a particular combustion chamber geometry, load and speed point and additional operating conditions. Further exploration of DFI7's capabilities is necessary to find its potential of extracting valuable efficiency points.

4.A Injection rate shapes

The DFI7 has been returned to Delphi after the engine experiments discussed in this chapter. The fuel injection rate shapes associated with the experiments were measured by a Delphi test engineer on a hydraulic test rig and the measurement results are included here for reference. Figure 4.14 and Figure 4.15 display the square and ramped injection rates for mode A30. For the square rates, five traces are plotted corresponding to five tested fuel pressures. For the ramped rates, nine traces are shown in total, resulting from the combinations of fuel pressure and ramp duration settings. Figure 4.16 shows the square rate traces for mode B30, while Figure 4.17 displays the related ramped rate traces.

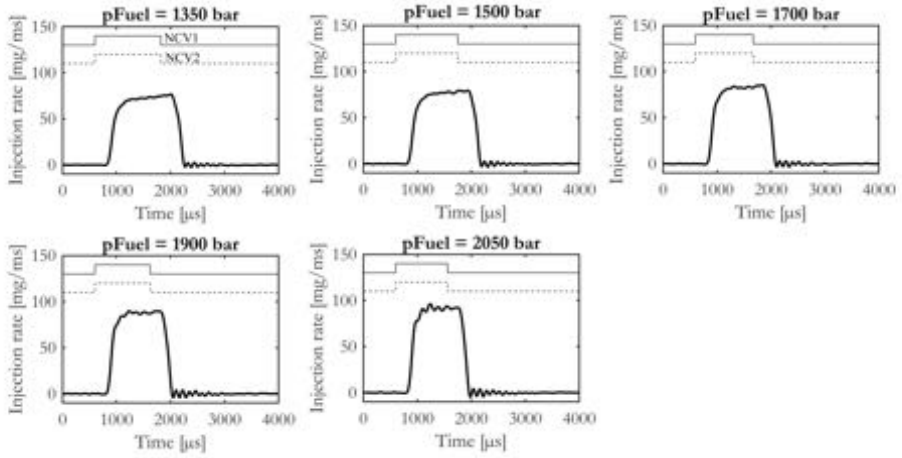

Figure 4.14: Square injection rate shapes for mode A30. pFuel = fuel pressure.

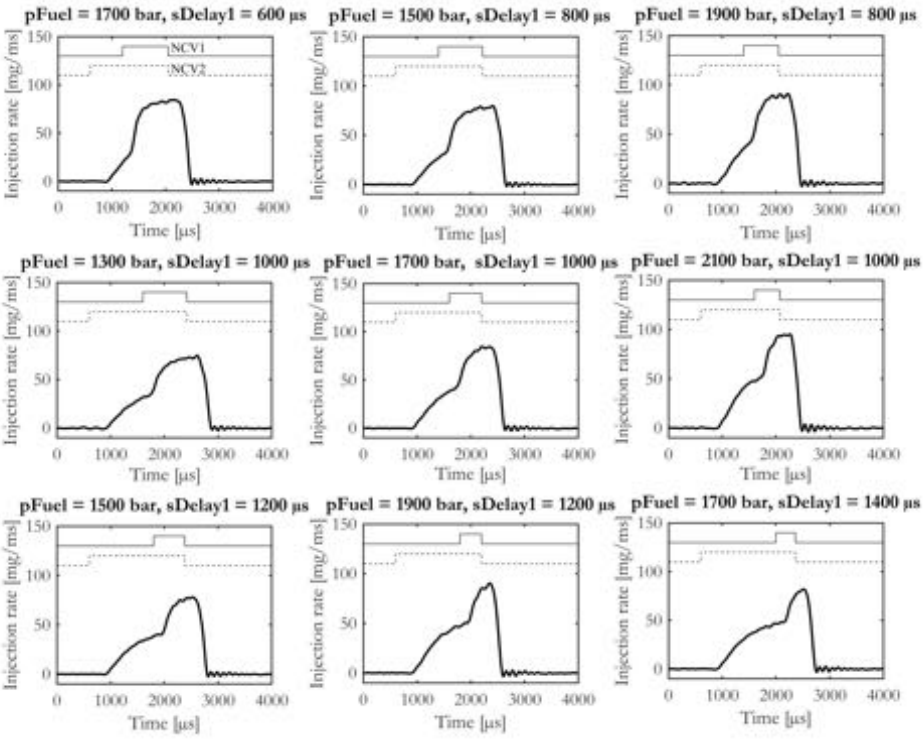

Figure 4.15: Ramped injection rate shapes for mode A30. sDelay1 = start delay of NCV1.

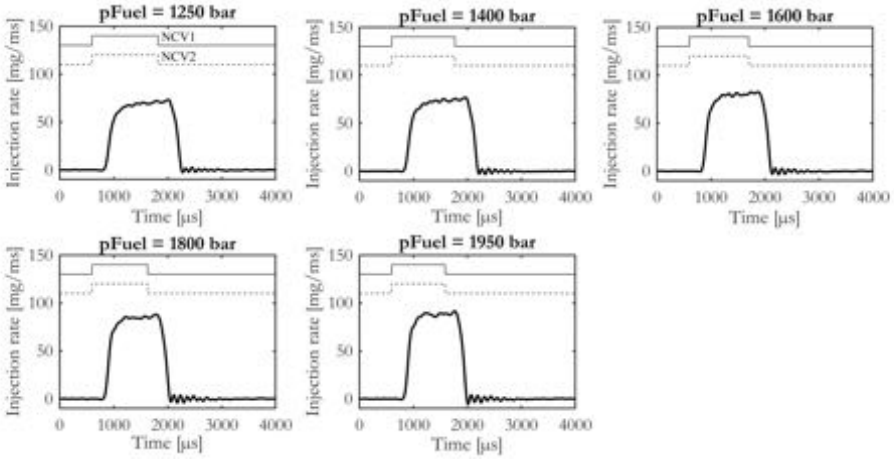

Figure 4.16: Square injection rate shapes for mode B30.

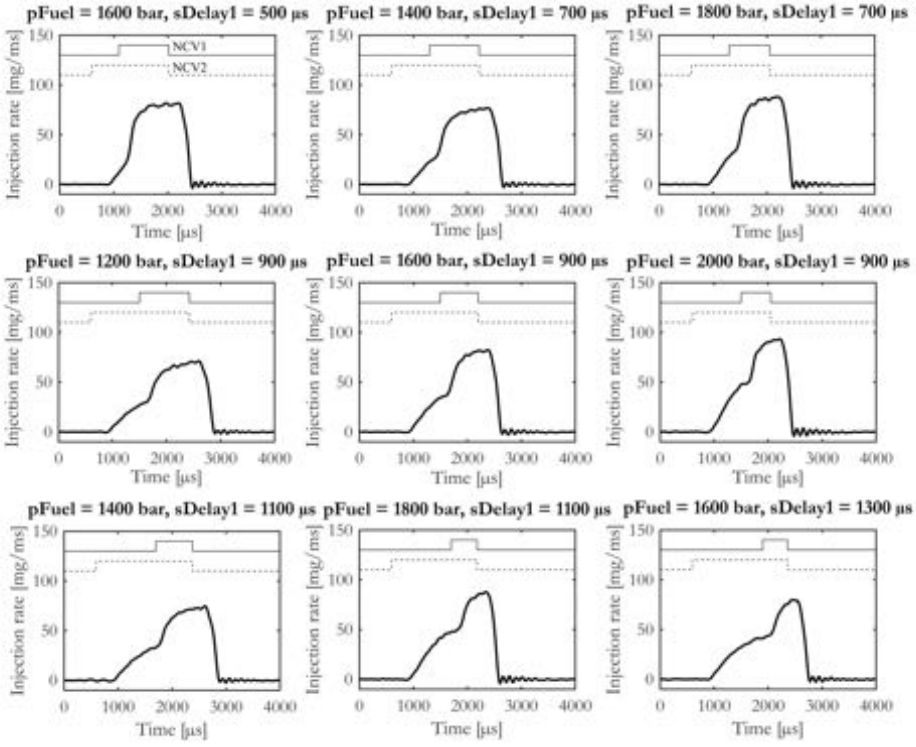

Figure 4.17: Ramped injection rate shapes for mode B30.

Chapter 5

Optimizing the use of conventional fuels

Introduction

Upcoming CO_2 legislation in Europe is driving heavy-duty vehicle manufacturers to develop highly efficient engines more than ever before. Further improvements to conventional diesel combustion, or adopting the reactivity controlled compression ignition concept are both viable options to comply with mandated targets. In this chapter, these two combustion regimes are compared by performing a thorough gross indicated efficiency optimization on both, and investigating fundamental differences in their performance. Attention is directed towards fuel energy distributions to quantify separate loss channels; where are potential efficiency points left to gain? An analysis of crank angle resolved data is done to further identify the differences between the two regimes. The experiments presented in this chapter aim to provide insight into the capabilities of both combustion regimes to increase efficiency and hence comply with future legislation.

The contents of this chapter have been published as Willems, R.C., et al., "A Comparison of Low-Load Efficiency Optimization on a Heavy-Duty Engine Operated With Gasoline-Diesel RCCI and CDC," Proceedings of the ASME 2019 Internal Combustion Engine Division Fall Technical Conference, Chicago, Illinois, USA, October 20–23, 2019. doi:10.1115/ICEF2019-7149 [84].

5.1 Literature review

Fueled by the 2015 Paris Agreement, new short-term CO_2 emission targets have been set for heavy-duty vehicles in the European Union, mandating a 15% tailpipe reduction relative to 2019 for new trucks by 2025 [14]. In addition, a reduction of at least 30% with respect to 2019 is scheduled for 2030. While it is unlikely that such abatements will come solely from improvements to the internal combustion engine, it is certain that engine efficiency will play a major role in the development of trucks for years to come. Given the small timespan, an appealing approach to develop efficient engines is utilizing existing technologies as much as possible, from engine hardware and fuel retail point-of-view alike.

Among possible strategies, adopting reactivity controlled compression ignition (RCCI) is particularly interesting, for its potential to increase thermal efficiency, reduce the emissions of nitrogen oxides (NO_x), and for its improved control capabilities compared with alternative low temperature combustion (LTC) concepts [29, 30]. RCCI differs from other combustion processes in that it utilizes two fuels of different reactivities to control the onset and duration of the combustion event [27]. Typically, a low reactive fuel is injected via the intake manifold (e.g. gasoline), whereas a high reactive fuel is directly administered into the combustion chamber (e.g. diesel). Direct injection is hereby advanced to the extent that the ignition and ensuing combustion processes are determined by chemical kinetics. In conventional dual fuel operation, contrarily, the ignition process is instead mixing-controlled, by injecting

high-reactivity fuel much closer to top dead center (TDC) [85]. While in RCCI a certain degree of fuel stratification exists too, there is sufficient time for mixing of air, fuel and recirculated exhaust gas prior to combustion, such that excessive formation of soot and NO_x is prevented. Although direct injection of both fuels is also possible [86], the option of employing a port fuel injection system is attractive. Many years of development have resulted in a robust technology that could in principle be implemented right away, or even retrofitted. This is equally true for direct injection equipment, for its wide use and ongoing development in diesel engines. By combining these two fuel injection systems, the intended RCCI engine essentially becomes a technological hybrid between spark- and compression ignition engines.

From fuel perspective, RCCI can in principle be done with any combination of fuels, as long as there is sufficient difference in their respective reactivities, allowing appropriate control over the combustion event and extension of the operable load range. The reader is referred to Chapter 1 for more information about RCCI. Utilizing readily available retail fuels would be favorable on short term, since the necessary infrastructure is already in place. The combination of diesel and gasoline has been demonstrated in literature to work well over a reasonable load range [87], and to enable very high gross indicated efficiencies [87, 88, 89]. Long term fuel solutions may include synthetic variants like gas-to-liquid (GTL) fuels [90] or hydrotreated vegetable oils (HVO) [91] as high reactivity fuel. Alcohols from potentially sustainable sources, such as ethanol [91, 92, 93] or blends thereof with conventional fuels [94, 95, 96] have been researched as low reactive fuel candidates.

Despite notable progress developing RCCI on a laboratory level, the concept did not yet break through to larger production scales. The NO_x and soot reduction capabilities of RCCI have been demonstrated numerous times [97, 98, 99], but reported efficiencies differ notably between publications. In particular, researchers at the University of Wisconsin-Madison have reported indicated efficiencies reaching up to almost 60% [100], which has drawn the attention of an increasing number of other groups. However, to the author's knowledge, reports of gross indicated efficiency exceeding 55% in other laboratories are scarce [101]. Recent efforts have focused more on brake efficiency. By combining different dual fuel concepts, both efficiency and load range can be maximized. In [102], for example, 48% brake efficiency is achieved by optimizing the entire engine, from a combustion as well as a hardware perspective.

Conventional diesel combustion (CDC) has all the while maintained its firm position in the heavy-duty sector, mainly because of superior reliability, controllability, and surely also significant efficiency enhancements. Current efforts to further increase CDC efficiency include shaping the rate of heat release either by using multiple injections or by continuously adjusting the fuel mass flow within a single cycle [77]. The results in Chapters 3 and 4 already demonstrated some of the possibilities. Despite that CDC is plagued by high engine-out NO_x, notable advancements in selective catalytic reduction has ensured an upward trend in efficiency [103].

This chapter aims to maximize and compare gross indicated efficiencies (GIE) on the single-cylinder, heavy-duty XEC engine operated with both gasoline-diesel RCCI and CDC. It will serve as an initial evaluation of the separate capabilities of these operating modes to aid in complying with upcoming CO_2 mandates, without needing to considerably modify engine hardware components or depend on developments in fuel retail infrastructure. For RCCI experiments, the ratio of gasoline to diesel fuel, timing of a single direct injection event and the rate of exhaust gas recirculation (EGR) are of primary interest. The latter two parameters, complemented with fuel pressure, are considered in CDC mode, although the rate of EGR is merely used to target certain NO_x levels. Emphasis will also be put on heavily boosted operation, to investigate the effects of elevated charge mass on efficiency in both combustion regimes. European specification gasoline (EN228) and diesel (EN590) are used for RCCI tests. The latter fuel is obviously employed in the

Table 5.1: DOE factors and levels for CDC experiments.

CDC	$-\alpha$	-1	0	1	α	Unit
DI SOA	-14	-11	-8	-5	-2	CAD aTDC
Fuel pressure	700	950	1200	1450	1700	bar
Intake pressure	1.1	1.4	1.7	2.0	2.4	bar
EGR rate	3	11	19	27	35	%

CDC experiments. By using the design of experiments (DOE) method and response surface analysis, both regimes will be thoroughly optimized for the heavy-duty engine employed in this work. Attention is furthermore directed to quantifying energy loss channels in both optimized modes, to assess where potential improvements could be made. The reader is referred to Chapter 2 for more details on the DOE procedure and calculation of energy distributions.

5.2 Experimental approach

A single, relatively low load targeting 8 bar gross indicated mean effective pressure (IMEP) at an engine speed of 1200 rpm is selected for the experiments. CDC experiments are conducted for direct comparison with RCCI operation. All CDC tests are performed with an approximate fuel quantity of 83 mg/cycle to target roughly 25% engine load. Intake manifold temperature is set to 40 °C, and exhaust pressure is set to 0.5 bar above the intake manifold pressure to drive EGR. To limit the number of experimental runs needed for optimization and to be able to study the interaction effects between operational parameters, DOE is applied. In recent years, the amount of academic studies on combustion engines using DOE has been growing, although specific approaches differ [65, 46]. Here, a central composite design (CCD) is applied following the theory of Box, Hunter and Hunter [48].

Table 5.1 depicts the operating parameters (factors) and their corresponding settings (levels) varied in the CDC tests, where SOA refers to the start of (electrical) actuation of the solenoid injector. The total number of experimental runs for a CCD equals $2^k + 2k + C$, where k is the number of factors and C is the amount of center points. For the matrix shown in Table 5.1, k equals 4 and the selected amount for C is 12, giving a total of 36 runs. For the RCCI experiments, it was decided to run all full factorial and axial points twice and set the number of center points to 6, to distribute the confidence intervals more evenly over the parameter space. This resulted in a total of 34 runs for the matrices shown in Tables 5.2 and 5.3.

The RCCI experiments are separated into two sets. First, experiments are run at a 1.7 bar intake manifold pressure with variations in the mass percentage of PFI fuel in the total fuel quantity, timing of the diesel injection and EGR rate. The selected intake pressure is typical for a contemporary turbocharger at this particular load (center point in Table 5.1), hence these experiments can provide insight into the capability of RCCI to increase efficiency under similar conditions. Note that EGR rate requirements for RCCI could well be different compared to CDC, and exhaust enthalpy might differ also, both of which contribute to the eventual capacity of a turbocharger to supply the demanded boost pressure. It is thus a hypothetical case, but does make for a reasonably fair comparison given the gross indicated metrics under study in this work. Second, an intake manifold pressure variation is performed while keeping the EGR rate set at a relatively high level of 48%. Preceding experiments indicated that this rate was needed to reduce charge reactivity such that combustion could be phased closer to TDC. Table 5.3 shows the factors and levels for the second set of RCCI measurements. Note that the domain of

Table 5.2: DOE factors and levels for RCCI tests with varying EGR rate. Intake pressure is set to 1.7 bar.

RCCI set 1	$-\alpha$	-1	0	1	α	Unit
PFI rate	71.5	75	80	85	88.5	wt.%
DI SOA	-83.5	-80	-75	-70	-66.5	CAD aTDC
EGR rate	31.5	35	40	45	48.5	%

Table 5.3: DOE factors and levels for RCCI tests with varying intake pressure. EGR is kept constant at 48%.

RCCI set 2	$-\alpha$	-1	0	1	α	Unit
PFI rate	71.5	75	80	85	88.5	wt.%
DI SOA	-78.5	-75	-70	-65	-61.5	CAD aTDC
Intake pressure	1.5	1.7	1.9	2.1	2.3	bar

DI SOA values has been shifted with respect to Table 5.2. This was again done because of the first set of experiments. It showed a potential optimum in combustion efficiency in that region. Intake temperature and engine speed are set to 35 °C and 1200 rpm, respectively, and total fueling mass quantity (sum of diesel and gasoline) amounts to 90 mg/cycle. Slight variations in energy input, due to small differences in the lower heating values of both fuels, are thereby disregarded. Last, the common rail fuel pressure is controlled at 500 bar in all RCCI experiments. This injection pressure was found to work well in previous research [29].

For response surface analysis and optimization, regression polynomials are fitted to experimental data. DOE often yields multidimensional data sets with many interaction effects among tested factors. To somewhat ease interpretation of results, and search for the most influential factors and interactions effectively, a multi-factor analysis of variance (ANOVA) is done on the acquired data sets, analogous to the approach of De Cuyper et al. [50], by using the *anovan* function in MATLAB. Thereafter, the response surface analysis focuses on those factors and interactions that were identified by the ANOVA as most significant in affecting GIE. More information on ANOVA and the regression procedure is given in Chapter 2.

5.3 Results and discussion

5.3.1 CDC optimization

The CDC experiments are performed prior to the RCCI tests to construct a firm baseline optimized mode. The CCD depicted in Table 5.1 is run, and thereafter a 4-factor ANOVA is done on the acquired data. In this procedure, the influence of separate factors and their interactions on an output variable is statistically tested to quantify each effect, and to determine whether they stand out from experimental error. Main factors and 2-factor interactions are taken into consideration, and the response of interest is GIE. Results of the 4-factor ANOVA on the CDC data are presented in Table 5.4. The ANOVA indicates that, by far, the effect of intake pressure at the selected range is strongest on GIE, corroborated by its high mean squared value, high F-statistic and extremely low p-value. In addition, DI SOA and fuel pressure contribute significantly to variation in the GIE data. Regarding interaction effects, only the fueling parameters do contribute to some of the variation in GIE, although this effect is not significant at the chosen confidence level. Because intake manifold pressure has such an extreme effect on GIE, particular attention will be given to this operating parameter later on. First, an optimization of SOA and fuel pressure will be done at 1.7 bar in-

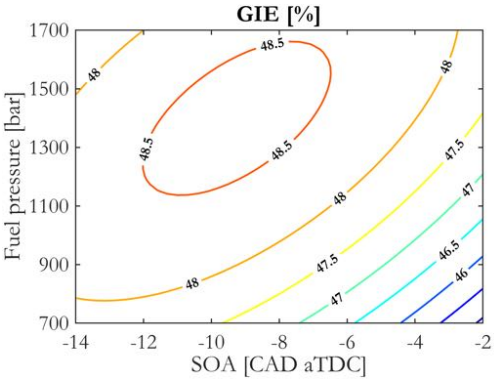

Figure 5.1: Response surface of GIE for CDC versus fuel pressure and SOA. Intake pressure is set to 1.7 bar. The model R^2_{adj} = 0.951.

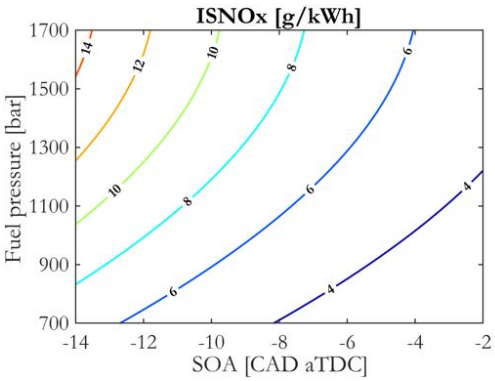

Figure 5.2: Response surface of $ISNO_x$ for CDC belonging to the GIE results depicted in Figure 5.1. The rate of EGR is set to 19%. The model R^2_{adj} = 0.995.

take pressure; a common level for the turbocharger normally employed on the production variant of this engine at this load and speed.

The response surface plot shown in Figure 5.1 illustrates a relatively large region where a peak GIE of 48.5% is obtained. This GIE plateau has an elliptical shape, owing to the interaction of injection timing and fuel pressure, which allows a slightly advanced SOA when operating with lower fuel pressure. When advancing injection beyond the optimum, compression work increases and heat transfer losses start to play a more dominant role. Contrarily, when SOA is retarded the effective expansion ratio decreases, directly resulting in less work being generated. The GIE response is also affected by the fuel pressure. Lowering fuel pressure results in an extension of the burn duration, with obvious impact on efficiency. Still, as Figure 5.1 already suggests, fuel pressure cannot be increased indefinitely. Again, heat transfer loss will start to dominate over efficiency gains, as an increase in fuel pressure both negatively impacts the convective heat transfer coefficient through increased turbulence and temperature rise during combustion due to faster combustion.

Figure 5.2 depicts the response surface of gross $ISNO_x$ belonging to the results in Figure 5.1. Rate of EGR for these results is set to 19%. Within the space of fueling parameters, engine-out NO_x levels can directionally be reduced by either lowering fuel pressure, or retarding injection. Both measures eventually impact on thermal efficiency as previously discussed, and thus a tradeoff is clear. Hence, the lowest NO_x level within the peak GIE plateau is sought to arrive at an optimum. By doing so, an SOA of -8 CAD aTDC and common rail pressure of 1250 bar are selected as optimal setting and will be analyzed in more detail later on.

5.3.2 RCCI optimization

To assess the capability of RCCI to increase GIE compared to CDC, a comparison is made at an equal intake pressure level of 1.7 bar as applied in the preceding optimization. The approach of analysis is largely identical. First, the DOE matrix depicted in Table 5.2 is run, and a 3-factor ANOVA is performed on GIE data; an overview is given in Table 5.5. Remarkably, only EGR is seen to have a truly significant effect on the efficiency. Most notably SOA, including its interactions with other factors, does not contribute much to variation in GIE. The MS values of these effects do not even surpass the mean squared error. The PFI rate, on the other hand, does have a noticeable effect, although not statistically significant at the selected confidence level. This also holds for the interaction between the PFI rate and the EGR rate. Thus, to investigate the response of GIE on the latter two

Table 5.4: 4-factor ANOVA table of GIE for CDC tests. The statistically significant factors are separated from the rest by double horizontal lines.

Source	SS	d.f.	MS	F-stat	p-value
pIntake	31.126	1	31.1263	118.13	5.81e-11
pFuel	2.5612	1	2.5612	9.73	0.0045
SOA	2.553	1	2.5530	9.69	0.0046
SOA·pFuel	0.6672	1	0.6672	2.53	0.1241
SOA·EGR	0.1683	1	0.1683	0.64	0.4316
pIntake·EGR	0.1181	1	0.1181	0.45	0.5092
SOA·pIntake	0.0929	1	0.0929	0.35	0.5580
EGR	0.0891	1	0.0891	0.34	0.5660
pFuel·EGR	0.086	1	0.0861	0.33	0.5728
pFuel·pIntake	0.0530	1	0.0530	0.20	0.6576
Error	6.5872	25	0.2635		
Total	44.1024	35			

factors, a response surface plot is shown in Figure 5.3. Here, it can clearly be seen that EGR has a very strong influence on efficiency. The response surface projects a steep upward slope of GIE as EGR rate is increased. The PFI rate of gasoline, as anticipated from the ANOVA, displays a limited effect. Still, the interaction between EGR rate and PFI rate of gasoline is obvious, mainly at the high end of the EGR domain. More specifically, combining a high EGR rate with a high PFI rate results in maximal GIE.

Reason for the strong reaction of efficiency to changes in EGR is clarified by the response surface plot of CA50 shown in Figure 5.4. The lowest EGR rates clearly lead to a very premature combustion event, with a detrimental impact on the thermal efficiency. It is only at the highest EGR rates tested, especially in combination with gasoline percentages well above 80% that combustion is phased somewhat close to TDC. But still, CA50 values in Figure 5.4 are seen to occur before top dead center. The European grade gasoline applied in this work, having a RON of 95, is apparently too reactive to be employed at this relatively low load, and at the concerning compression ratio. Difficulties in phasing combustion will only increase at higher loads. Yet, several measures to reduce charge reactivity could be considered. First, by reducing the intake manifold temperature the end of compression temperature is lowered too. However, intake temperature was already quite low at 35 °C. Lowering this number further would require heavy intercooling. Second, retarding the intake valve closure event also reduces TDC temperature, by lowering the effective compression ratio. An alternate cam shaft or, ideally, variable valve actuation could match valve timing requirements and fuel reactivity properties to phase combustion accordingly. Still, the selection of PFI fuel determines the eventual range in which combustion phasing can be adjusted. Sufficiently low base reactivity (i.e., high RON) remains an important prerequisite.

To investigate whether this combination of settings yields increased GIE, optimization runs were performed at 48% EGR and 88% gasoline. Figure 5.5 illustrates an overview of all RCCI experiments, DOE and optimization runs combined.

Table 5.5: 4-factor ANOVA table of GIE for the RCCI set at a 1.7 bar intake manifold pressure.

Source	SS	d.f.	MS	F-stat	p-value
EGR	35.5041	1	35.5041	145.02	2.28e-12
PFI·EGR	0.6614	1	0.6614	2.70	0.1118
PFI	0.5517	1	0.5517	2.25	0.1449
SOA·EGR	0.1128	1	0.1128	0.46	0.5030
SOA	0.1072	1	0.1072	0.44	0.5138
PFI·SOA	0.0169	1	0.0169	0.07	0.7949
Error	6.6101	27	0.2448		
Total	43.5643	33			

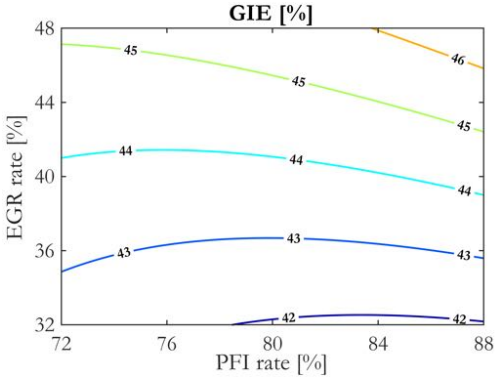

Figure 5.3: Response surface of GIE for RCCI versus EGR rate and PFI rate at 1.7 bar intake manifold pressure. SOA is set to -75 CAD aTDC. The model R^2_{adj} = 0.831.

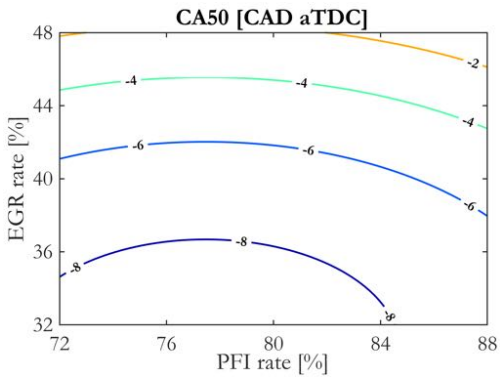

Figure 5.4: Response surface of CA50 for RCCI versus EGR rate and PFI rate. Remaining operating conditions are equal to those in Figure 5.3. The model R^2_{adj} = 0.936.

The results at elevated boost (red triangles), also shown in Figure 5.5, have yet to be discussed. It can again clearly be observed that EGR rate is the dominant factor with respect to efficiency in the first set of experiments (black squares). Note that EGR is the only factor in these experiments that affects the air-excess ratio, hence the arrow indication. Due to a retarding effect of the EGR rate on an otherwise premature combustion event, peak GIE is consequently found at the lowest air-excess ratio. At λ = 1.3 (EGR at 48%), the optimization is performed. The PFI rate of gasoline is first increased to 88%, and thereafter SOA is swept in between the axial points presented in Table 5.2. An optimum is subsequently found at -75 CAD aTDC (blue plus sign in Figure 5.5). While advancing DI SOA further resulted in a steady decrease of combustion efficiency, retarding the diesel injection advances CA50 to the point where thermal efficiency begins to decline. The peak GIE of RCCI at a intake pressure of 1.7 bar amounts to 47.9%, which is higher than the prediction observed in Figure 5.3. Although the regression anticipated the direction of increasing GIE well, accuracy of the prediction seems somewhat low. Reason for this is found in a relatively low adjusted R^2 value of the regres-

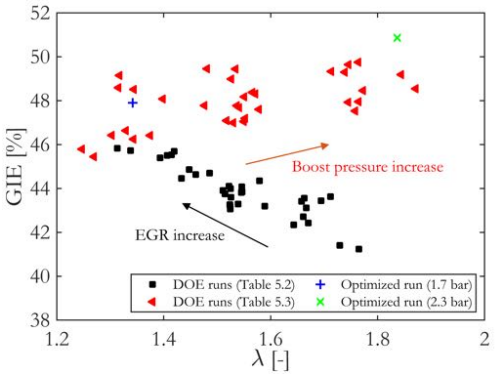

Figure 5.5: Overview of all GIE results as function of air-excess ratio (λ) in the RCCI experiments.

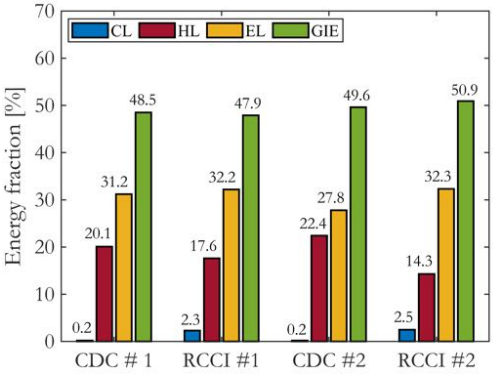

Figure 5.6: Fuel energy distributions for all four optimized combustion modes. Numbers 1 refer to low boost operation, whereas numbers 2 correspond to a high boost pressure.

sion model, which equals 0.831. Further, the confidence intervals slightly expand towards boundary regions of the response surface. Since both EGR rate and gasoline PFI rate are set to extreme values, accuracy of the prediction drops. The latter is a good reason to confirm predicted optima with additional experimental runs.

More important still, RCCI with gasoline and diesel is unable to improve efficiency compared to CDC for this particular intake pressure. To further investigate why this is, individual loss channels are assessed. Fuel energy fractions for the optimized modes are depicted in Figure 5.6, where numbers 1 denote optimization runs at 1.7 bar intake pressure. An overview of corresponding operating settings for each mode is shown in Table 5.6. RCCI is seen to mainly reduce heat transfer losses with respect to CDC, showing a 2.5% difference in favor of the former. Surprisingly, reducing the heat transfer losses is not translated into efficiency gains, but instead exhaust losses are slightly higher. In addition, the combustion losses account for another 2% difference, and as a result RCCI efficiency is 0.6% lower than that of CDC.

Figure 5.7 depicts the indicated specific emissions belonging to each of the optimized modes. Owing to the very high local temperatures in spray-driven combustion, CDC illustrates NO_x emissions that are an order magnitude higher than those of RCCI. The optimized RCCI mode results in NO_x emissions well below EURO VI legislative levels, albeit evaluated in gross indicated quantities. Matters look vastly different for CO and HC emissions, as RCCI is plagued by high levels of both. This is of course directly related to the low combustion efficiency, in turn caused by fuel being trapped in the crevice volume and overall fuel lean conditions. Indicated specific PM emissions are a factor of 2 higher for RCCI in comparison to CDC, which is at the least remarkable. Do note that particulate emissions could be notably higher than measured, because condensable organics are not effectively detected by the smoke meter. The combination of an early DI injection, low fuel pressure and low intake temperature in RCCI operation can at least partially explain this result. The in-cylinder charge is still quite cold upon the diesel injection resulting in bad evaporation, while a low common rail pressure does not atomize the diesel properly either. Local air-excess ratios depend on these rates of evaporation and mixing, resulting in relatively rich spots. Although the quantity of injected diesel is small and thus modest soot formation is expected, oxidation is inferior to that of CDC due to low local temperatures in RCCI combustion. It is furthermore thought that some droplets of diesel may deposit on the liner or piston surface, providing a potent source of particulates.

Table 5.6: Overview of operating parameters of all four optimized modes. Pressures in bar, temperature in °C, engine speed in RPM, PFI rate in wt.% and DI SOA in CAD aTDC.

Parameter	CDC #1	RCCI #1	CDC #2	RCCI #2
Intake pressure	1.7	1.7	2.3	2.3
Fuel pressure	1250	500	1250	500
EGR rate	19	48	19	48
DI SOA	-8	-75	-8	-62
PFI rate	n/a	88	n/a	88
Intake temperature	40	35	40	35
Engine speed	1200	1200	1200	1200
Gross IMEP	8.13	8.75	8.30	9.22

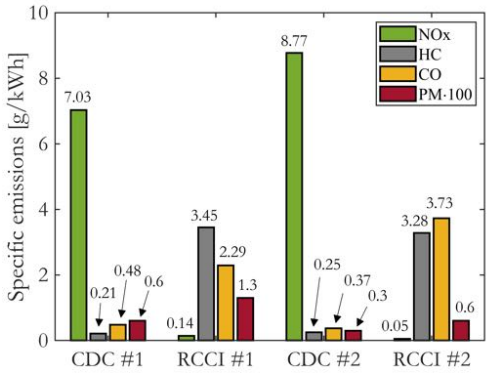

Figure 5.7: Gross indicated specific emissions for all four optimized combustion modes. Note that PM emissions are multiplied by a factor 100 for readability.

Results presented in the preceding discussion indicated that, despite superior NO_x levels, RCCI is surpassed by CDC on all other fronts. It was shown that excessive EGR rates were necessary to lower charge reactivity to an extent that the combustion event could be phased near TDC. In addition, large PFI rates of gasoline are needed too, leaving little possibility to control combustion phasing using DI injection timing. When comparing current results to reported GIE values in literature, especially those of researcher at the University of Wisconsin-Madison, large gaps are seen. In [87], for example, a GIE of 56% is reported on an engine and with operating conditions that show great similarities with the ones employed in this work. Still, one major difference can be noted between this work and those previously published results. While peak GIE in this work is obtained at an air-excess ratio of about 1.3, as illustrated in Figure 5.5, peak GIE in [87] is obtained at an AFR of 29 ($\lambda \approx 2$). This raises the question: what effect would heavy boosting have on efficiency? Table 5.4 already hinted at a strong effect of intake pressure on GIE in CDC. To investigate whether intake pressure can elevate efficiency in RCCI also, and to what extent, the DOE matrix depicted in Table 5.3 is run. As before, a 3-factor ANOVA is performed on the data, of which the results are depicted in Table 5.7. These results indicate that, by varying intake manifold pressure, the effect of the fueling parameters on GIE strengthens. It can be seen that both the effect of SOA and PFI rate on GIE are statistically significant under varying boost. This is substantiated by the results in Figure 5.5 (red triangles), that show an increased spread in GIE values at constant λ. Experimental results further evidence that increasing the intake pressure has a strong positive effect on GIE, for peak values already reach up to 50%.

It can be noted from Table 5.7 that the PFI rate and intake manifold pressure have about an equal effect on GIE, for the selected ranges in these experiments. Further, they also display a consider-

Table 5.7: 4-factor ANOVA table of GIE for the RCCI set at a 48% EGR rate.

Source	SS	d.f.	MS	F-stat	p-value
pIntake	15.8183	1	15.8183	49.51	1.45e-07
PFI	15.1474	1	15.1474	47.41	2.12e-07
SOA	2.8535	1	2.8535	8.93	0.0059
PFI·pIntake	1.1052	1	1.1052	3.46	0.0738
SOA·pIntake	0.2177	1	0.2177	0.68	0.4164
PFI·SOA	0.0248	1	0.0248	0.08	0.7827
Error	8.6256	27	0.3195		
Total	43.7925	33			

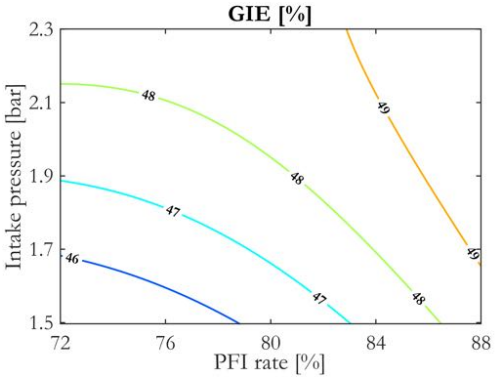

Figure 5.8: Response surface of GIE for RCCI versus intake pressure and PFI rate. The rate of EGR is set at 48%, while SOA is set to -70 CAD aTDC. The model R^2_{adj} = 0.868.

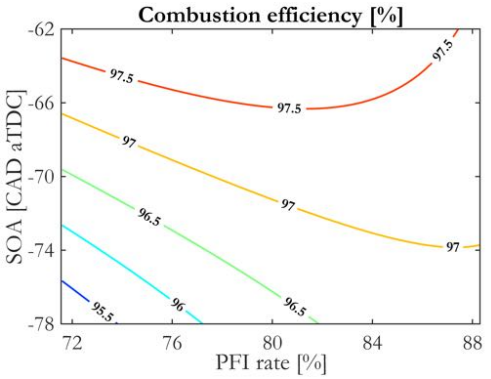

Figure 5.9: Response surface of combustion efficiency for RCCI versus SOA and PFI rate. Intake manifold pressure is set to 2.3 bar. The model R^2_{adj} = 0.894.

able interaction effect. To study the effects of these factors on GIE in more detail, a response surface is shown in Figure 5.8. The beneficial effect that increased intake pressure has on GIE is seen over most PFI rate values. Yet, for large amounts of gasoline the effect is diminishing, which is linked to decreasing combustion efficiency. The PFI rate again has a clear impact on GIE itself, which mainly relates to phasing. It is thus at the upper right corner of Figure 5.8 where peak GIE is found. This region is the target for further optimization.

SOA was found in Table 5.7 to be a significant contributor to variation in GIE data, although the interaction with other parameters proved insignificant. In an optimization effort, SOA was swept between -75 and -55 CAD aTDC to find the best compromise between the thermal and combustion efficiencies. To get an idea of where to schedule the diesel pulse, Figure 5.9 assesses the combustion efficiency response surface plot as function of both fueling parameters. Here, it is observed that the combustion efficiency mainly suffers at very advanced DI schedules. This is related to either overmixing, wall wetting or a combination of these two mechanisms. Too lean mixtures result in such low

temperatures that proper oxidation of fuel and combustion intermediates becomes problematic. Evidence of wall wetting is most obvious at low PFI rates, where DI duration extends and combustion efficiency descends quickly. By running with 88% of gasoline, it is possible to still target the region of peak combustion efficiency, which is predicted at 97.5%. An optimum in GIE was found at -62 CAD aTDC, with an intake pressure of 2.3 bar and an 88% PFI rate. The peak GIE value of 50.9% is depicted in Figure 5.5 (green cross). Attempts in elevating GIE by increasing boost levels further did not yield desired results. It was mainly combustion efficiency that was found to deteriorate under those over-lean conditions.

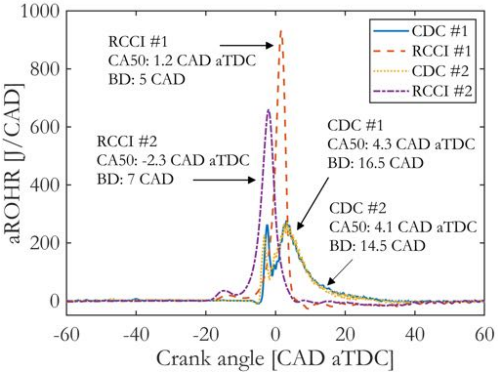

Figure 5.10: aROHR traces for all four optimized modes. Combustion metrics are included.

Similarly to RCCI, an optimization in CDC was done at an intake pressure of 2.3 bar. The resulting response surface plot from that optimization showed vast similarities with the plot shown in Figure 5.1, and an optimum was found at essentially the same settings for SOA and fuel pressure. The major difference compared to low boost operation is that GIE peaked at 49.5%; an increase of one percent point. To find out why the increase in GIE is higher for RCCI with respect to CDC, the distribution of fuel energy shown in Figure 5.6 is reviewed once more. The numbers 2 in this plot indicate the optimization runs of both CDC and RCCI at a 2.3 bar intake pressure setting. First, it can be seen that combustion losses are slightly higher for RCCI at a high boost level compared to low-boost operation. Figure 5.7 reveals that this is mostly related to a steep increase in CO, which in turn can be linked to even more lean combustion at elevated intake pressure, resulting in lower temperatures. Still, the increased combustion losses do not result in lower output of work. The heat loss fraction for high-boost RCCI indicates that in-cylinder heat transfer has decreased by more than 3%. This is the sole reason that GIE has risen up to 50.9%, as the exhaust losses have remained almost equal. CDC, on the other hand, is displaying reduced exhaust losses, while heat transfer losses have notably increased. This is corroborated by the results in Figure 5.7, where engine-out NO_x levels of CDC display an increase at elevated intake pressure. As local temperature is the main driver behind formation of NO_x and heat transfer alike, it can be expected from this observation that the in-cylinder temperature field has undergone a change. Diffusion-limited combustion ensures a high temperature at the periphery of the reacting jets and because of particular spray targeting and the resulting spray-bowl contact, these high temperatures can be found close to the surface areas where heat is lost. However, it cannot be univocally stated that this is the only mechanism affecting both formation of NO_x and heat loss. NO_x is naturally also governed by mixing of fresh air and hot combustion gases; a process which could well be altered by variations in boost pressure. Additionally, the convective heat loss coefficient may also be affected, potentially increasing the rate of heat transfer.

5.3.3 Analysis of in-cylinder traces

The question remains why RCCI is yet unable to decrease exhaust losses that could in turn maximize the GIE further. To investigate this, apparent rate of heat release traces of all four optimized modes are compared in Figure 5.10. The burn duration in the optimized RCCI runs, defined as the crank angle interval between CA10 and CA90, amount to 5 and 7 degrees for low and high boost operation, respectively. From an expansion ratio point of view, this is considered a positive feature with regards to efficiency. CDC

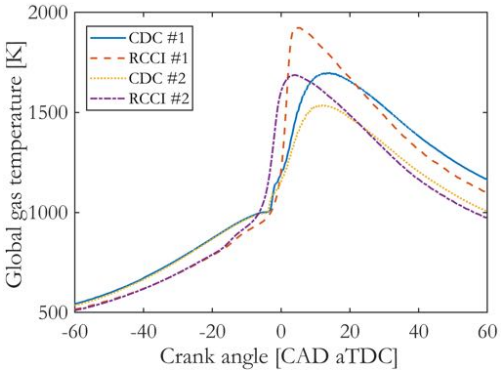

Figure 5.11: Global gas temperature traces for all four optimized modes.

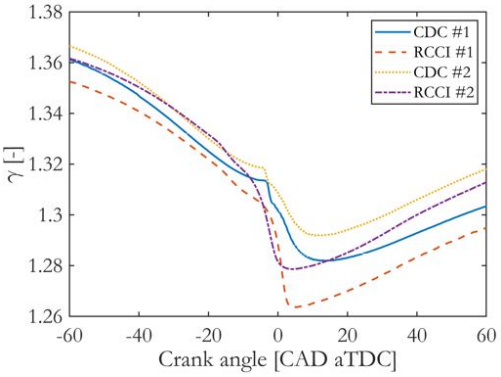

Figure 5.12: Ratio of specific heat capacities (γ) for all four optimized modes.

burn durations, on the other hand, total 16.5 and 14.5 degrees. When further analyzing combustion phasing, RCCI shows CA50 values of 1.2 and -2.3 CAD aTDC. High-boost operation clearly advances combustion phasing beyond an optimal value. It seems that the combination of extremely fast combustion and rather early phasing are the basis of the elevated exhaust losses of RCCI. More specifically, the peak global gas temperatures of RCCI surpass those of CDC by about 200 K. This is shown in Figure 5.11. These traces are inferred from in-cylinder pressure data using the ideal gas law. Despite that global temperatures during compression are lower for RCCI, being attributed to the charge cooling effect of gasoline evaporating in the intake flow, bulk temperatures during combustion overtake those of CDC at both boost pressure levels.

This difference in global temperature has an evident impact on the specific heat capacity ratio (γ) at and around TDC, which forces it down to lower values, as can be observed in Figure 5.12. These reduced values persist in the remainder of the expansion stroke, and apparently more energy is expelled into the exhaust as a consequence. The composition effect on γ only further decreases its values during the cycle, for RCCI is performed with very high EGR rates. CA50 should probably be phased somewhat later when operating with RCCI to suppress the decrease of γ, and thereby maximizing GIE. This could besides reduce heat transfer losses further, but a potential negative impact on the already inferior combustion efficiency is also lurking. Comparable differences in bulk temperature were found by Olmeda et al. [104] on a light-duty diesel engine. In their study, RCCI also displayed a similar reduction in heat transfer losses. These findings demonstrate the importance of peak versus bulk temperatures; heavy stratification like encountered in CDC has a largely different influence on heat transfer processes than the premixed character of RCCI. The NO_x formation rates are too affected by this temperature stratification, already hinted by the emission data in Figure 5.7. Despite considerably higher global temperatures in RCCI as revealed in Figure 5.11, local conditions are nevertheless favorable for suppression of NO_x formation.

5.4 Conclusions and outlook

This chapter aimed to optimize GIE on a heavy-duty engine operated with CDC and gasoline-diesel RCCI at one particular load-speed point that corresponds to highway cruising speed. It was found that, when intake pressure is limited to levels that are typical for a contemporary turbocharger at the load-speed point under study, CDC surpasses RCCI in terms of GIE. Besides, the indicated specific emissions were lower in CDC too, with the exception of extremely low NO_x emissions in RCCI operation. Energy

distribution diagrams indicated that, while heat transfer losses were considerably lower for RCCI compared to CDC, a combination of marginally higher exhaust losses and significant combustion losses rendered RCCI efficiency inferior. With a substantial increase of the intake pressure, RCCI proved to be performing much better, and actually exceed CDC GIE by about 1.5% point. The exclusive reason for this steep increase was even lower heat transfer losses; combustion and exhaust losses marginally increased compared to low-boost operation. From a practical viewpoint, however, the combination of very high boost pressure and an excessive EGR rate in RCCI operation is a limiting factor. In CDC, it was identified that the GIE primarily benefits from an exhaust loss decrease. In-cylinder heat losses actually increased, which consequently limits GIE gains in this mode. Thus, RCCI shows clear potential to enable a highly efficient process at elevated intake pressures. Efforts to identify where additional efficiency points can be gained pointed in the direction of phasing. Results revealed that high bulk gas temperatures, together with excessive EGR rates, limit the extraction of work because of a rather low in-cycle ratio of specific heat capacities. By somewhat retarding combustion, it is expected that this loss can be further minimized. Yet, the use of gasoline proved to be limiting, as phasing issues were ample, and only specific operational settings resulted in acceptable CA50 values. Valuable efficiency points can obviously also be gathered by reducing combustion losses. To have more control over phasing, and reduce the need for excessively high EGR rates, the next chapter focuses on applying a PFI fuel with a lower base reactivity. To remain within the area of practical fuels that are both suitable for RCCI and are commercially available, experiments will be done using E85. Its higher RON potentially facilitates to run without EGR at all, while having sufficient control over combustion phasing and provide fast combustion events for an efficient thermodynamic cycle. It is thought that these features together can further increase GIE.

Chapter 6

Shaping the heat release for optimal efficiency

Introduction

The preceding chapter indicated severe limitations in combustion phasing controllability with the use of gasoline as low reactivity fuel in RCCI combustion, despite the utilization of excessive rates of exhaust gas recirculation. The application of a fuel with a higher octane rating can be of aid, as the reactivity gradient between the two fuels is readily increased. This chapter investigates E85 as low reactivity fuel for optimal RCCI operation. It is a practical fuel candidate in the sense that the production and retail infrastructure is already in place. With the larger difference in fuel octane ratings comes more flexibility for fuel injection and air path settings. This opens up possibilities to tune the heat release. Regression results and rates of heat release are thoroughly analyzed to reveal the underlying relation of fuel reactivity stratification, the total charge dilution, the indicated efficiency and associated loss channels. A metric called the burn ratio is used to characterize the heat release shape and optimize the gross indicated efficiency.

The contents of this chapter have been submitted to Fuel as Willems, R., et al., "Heat release rate shaping for optimal gross indicated efficiency in a heavy-duty RCCI engine fueled with E85 and diesel".

6.1 Literature review

The drive for highly efficient and clean engines has moved research towards combustion concepts that provide ample time for mixing of fuel and air prior to ignition. Pioneering work in this field focused on essentially homogeneous, heavily diluted mixtures that are ignited by compression; a process known as homogeneous charge compression ignition (HCCI). These efforts opened up possibilities to achieve very low emissions of nitrogen oxides (NO_x) and soot, while retaining typical diesel engine efficiency. HCCI is governed by chemical kinetics and, hence, it suffers a lack of mixing-controlled combustion phasing that is common for conventional diesel combustion (CDC). To prevent premature ignition and violent combustion, considerable rates of exhaust gas recirculation (EGR) and boosted intake manifold pressures are used to lower the charge reactivity. These measures endow HCCI with a limited operable load range, also related to mechanical constraints, and high emissions of carbon monoxide (CO) and unburned hydrocarbons (UHC). Moreover, intake manifold pressure and EGR rate settings do not provide the timely response needed for transient engine operation. Various strategies have been proposed to deal with these issues, such as partial stratification of local air-excess ratios (λ) and tailoring of physicochemical fuel properties. Comprehensive overviews of such advanced HCCI engine operating strategies are given by Yao [20] and Saxena [21].

The idea of using two fuels of different reactivities to control ignition and combustion was first introduced by Inagaki [27]. Fuel reactivity is blended

to appropriate levels by port fuel injection (PFI) of a low reactivity fuel and direct injection (DI) of a high reactivity fuel. Timing of one or more DI events, scheduled well before the start of combustion (SOC), is used to create varying degrees of reactivity stratification allowing to tune the rate of heat release. The high reactivity fuel initiates combustion by low temperature reactions, producing enough heat and radical species to ignite the rest of the charge. This combustion concept was eventually termed reactivity controlled compression ignition (RCCI), and has been further developed in the last decade by various research groups [29, 30].

Conventional gasoline and diesel were initially applied in RCCI combustion, because their wide availability made them interesting fuel candidates. Researchers at the University of Wisconsin-Madison reported an extremely high peak gross indicated efficiency (GIE) of 56% at a moderate load [87], while emitting very low levels of engine-out NO_x and soot. It was furthermore demonstrated that this fuel combination works well over a reasonable range of gross indicated mean effective pressures (IMEP) from about 5 to 15 bar. Still, the intake valve closing (IVC) event had to be retarded at elevated loads to aid in combustion phasing control. Several other studies confirmed the NO_x and soot reduction capabilities of gasoline-diesel RCCI combustion [90, 97, 105, 106], but GIE values above 55% were not reproduced. Reasons for that offset may be sought in differences between light and heavy-duty engines [107] and base performance of an engine in CDC mode [108].

Control of CA50 using the diesel injection timing and gasoline percentage has been demonstrated to work acceptably up to moderate loads [109, 110]. Other means are necessary to maintain RCCI operation at higher loads [111], because gasoline reactivity proved to be insufficiently low for proper combustion phasing using merely fueling parameters. Strategies that involve lowering the effective compression ratio by IVC adjustments were shown to be adequate in extending ignition delays at elevated loads [112, 113]. This can be achieved by either installing an advanced variable valve actuation (VVA) system or changing the cam shaft entirely. This last option poses a tradeoff between low load combustion efficiency and high load operating limits. A pathway to extend the load range with apparently fewer compromises is applying a lower reactivity PFI fuel, as combustion can expectedly be optimized without engine hardware modifications.

Several studies have investigated higher RON fuels for application in RCCI combustion. At least two of such fuels already have a production and retail infrastructure in place: natural gas and E85 (i.e. a blend of 85% ethanol and 15% gasoline by volume). Both of these fuel candidates are expected to play a significant role in the future utilization of alternative fuels [91], both in existing and advanced engine concepts. Natural gas has been successfully applied as low reactivity fuel in heavy-duty RCCI operation [114, 115]. In these studies, EGR was shown to be redundant for controlling CA50 from low up to relatively high loads of 17 bar gross IMEP. This feature holds promise regarding brake efficiency, because of a potentially higher in-cylinder ratio of specific heat capacities and lower pumping losses. Increasing brake efficiency obviously aids the efforts to reduce CO_2, which is further facilitated by the favorable carbon to hydrogen ratio of methane. Unfortunately, the use of natural gas also brings about issues of CH_4 emissions, which have a significantly higher global warming potential and are extremely difficult to reduce using an oxidation catalyst. The latter especially holds at low loads, where exhaust gas temperature is low and the demand for reduction is high.

E85 received considerable attention in research on RCCI, which has shown some favorable aspects. Splitter [89] reported a peak GIE of 59% using PFI of E85 and DI of diesel, while the achievable maximum load was readily extended compared to their work with gasoline. In addition, lower EGR rates were required at all tested load points up to 16.5 bar gross IMEP, while NO_x emissions still remained well within legislative limits. The GIE was enhanced even further to values near 60% using a compression ratio of 18.7 and disabling the piston cooling [100]. The load expansion capabilities of E85 were corroborated by Curran [94] by

running tests on the light-duty federal test procedure. Still, concerns were raised on the comparatively low exhaust gas temperatures in RCCI operation that may pose aftertreatment issues and restrict turbocharger capacity. Aside from a load range extension, Benajes [96] also reported an improved CA50 control degree on DI timing by utilizing E85, ascribed to both a higher octane rating and latent heat of vaporization compared to gasoline. With respect to natural gas, E85 has the additional benefit of being liquid at atmospheric conditions, which alleviates storage and handling procedures. Its main component, ethanol, can furthermore be produced from a wide variety of sustainable resources and considerable progress is made in associated production methods [116].

6.2 Experimental approach

There are two main objectives set for the current chapter. First, rates of heat release (ROHR), and integral metrics derived thereof, are analyzed to increase the understanding of heat release behavior under various operational conditions. The goal is to relate key combustion characteristics to engine efficiency and related energy loss channels. Second, this chapter aims to optimize GIE through dedicated experiments on a single-cylinder engine setup using E85 and diesel as low and high reactivity fuels, respectively. Both fuel injection and air path settings are taken into account in the tests, and use is made of the design of experiments (DOE) methodology. In the following, the experimental design is first treated, after which the results are presented and discussed.

Tests are performed at a single, relatively low load point at approximately 30% of the rated torque at 1200 rpm. The arrangement of the engine setup does not allow for crank shaft torque measurements representative for the test cylinder alone, hence the total fuel energy input is kept constant instead. Gross IMEP thus varies with efficiency between experimental runs of different settings. The nominal stationary settings are summarized in Table 6.1. Although a single operating point provides only a limited view, the aforementioned

Table 6.1: Nominal stationary operating conditions.

Gross IMEP	8.5 $\pm$ 1 bar
Fuel energy input	3850 $\pm$ 100 J/cycle
Engine speed	1200 rpm
p_{exh}-p_{in}	0.3 bar
T_{in}	40 °C
$T_{coolant}$	85 °C
T_{oil}	90 ° C

$\geq$55% GIE values in literature were obtained at similar load settings as the one selected in this chapter, which makes it an interesting target for further research. Recent studies have opted for mode-switching to achieve maximum brake efficiency over the full operating map, although approaches differ between publications [117, 102]. These studies show that CDC can be used at low loads, as to prevent extreme combustion losses. At high loads, CDC may again be employed, or a switch to conventional dual fuel operation (i.e., with a diesel pilot close to TDC) can be done. The mid load range, as targeted in this chapter, proved to be most viable for optimal RCCI operation.

The DOE methodology is applied in the first set of experiments. Table 6.2 displays the fueling and air path parameters (factors) and their settings taken into account in the CCD experiments. The PFI rate of E85 is expressed as a weight percentage of the total fuel mass. A single DI strategy is applied in this chapter, where SOA refers to the start of actuation of the solenoid diesel injector. The intake manifold pressure is given in absolute values and the EGR rate is computed as the ratio of the volumetric concentrations of CO_2 in the intake and exhaust manifolds. The total number of experimental runs equals 2^k+2k+C, where k is the amount of factors and C is the number of center point measurements. For Table 6.2, k and C both equal 4, and the entire set was run twice, amounting to a total number of runs of 56.

Regression polynomials are fitted to the experimental data resulting from the CCD matrix. An

Table 6.2: Factors and levels used in the CCD experiments.

Factor	$-\alpha$	-1	0	1	α
PFI rate (E85) [wt. %]	65	70	75	80	85
SOA (diesel) [CAD aTDC]	-57.5	-50	-42.5	-35	-27.5
Intake manifold pressure [bar(a)]	1.6	1.8	2.0	2.2	2.4
EGR rate [%]	0	5	10	15	20

Table 6.3: Overview of R^2_{adj} values and prediction terms included in the models.

Model	R^2_{adj}	Main terms	Cross terms	Quadratic terms
Heat transfer loss	0.939	PFI, SOA, p_{in}	PFI·SOA, SOA·p_{in}	PFI^2, SOA^2, p_{in}^2
Combustion efficiency	0.923	PFI, SOA, p_{in}, EGR	SOA·EGR	PFI^2, SOA^2
Burn ratio	0.977	PFI, SOA, p_{in}	PFI·SOA, SOA·p_{in}	SOA^2

overview of the three polynomials that will be used in the response surface analysis is given in Table 6.3. It displays their adjusted R^2 values and the terms that are included in each equation. A second set of experiments consisting of SOA sweeps was run to optimize GIE and supplement more insight on relevant processes and metrics. These sweeps are discussed after the regression results.

6.3 Results and discussion

Increased interest in RCCI in recent years stems from its potential to attain high thermal efficiency at extremely low engine-out NO_x. To fully utilize these capabilities, a solid understanding of the combustion process is required. RCCI combustion is governed by chemical kinetics, the rate of which is predominantly dependent on how the combustible charge is prepared. This, in turn, relies on the fuel injection and air path settings. In the following, rate of heat release traces are analyzed, from which a combustion metric is derived called the burn ratio. It is demonstrated that this burn ratio relates to the rate of heat release shape, fuel reactivity stratification and GIE. Thereafter, a regression analysis is done to assess how heat transfer and combustion losses can be best balanced to optimize the GIE. It is shown how this is established using the available operational parameters. Finally, additional sweeps of SOA are presented to optimize GIE, and use of the burn ratio is proposed as an optimization guideline.

6.3.1 Impact of reactivity stratification on the rate of heat release

Mixture preparation is of utmost importance for the chemical kinetics and thermodynamic processes within the combustion chamber. This is discussed by Splitter et al. [118], who have used two distinctive equivalence ratios to describe the degree of fuel reactivity stratification and global charge dilution. The premixed equivalence ratio ($\Phi_{premixed}$), i.e., that of the charge prepared in the intake manifold, was used to specify the fuel reactivity stratification at a constant diesel injection timing. The global equivalence ratio (Φ_{global}), i.e., that of charge in the cylinder when the low and high reactivity fuels are mixed together, described the total charge dilution. It was found that lean global operation can increase GIE through reductions of heat transfer, but that stratification is necessary to find the best tradeoff between heat transfer and combustion losses. While $\Phi_{premixed}$ at a given Φ_{global} certainly is a measure for the reactivity span in the combustion chamber, it does not consider the time available for mixing of high reac-

tivity fuel after injecting it directly into the cylinder. This does, however, influence the local diesel concentration to a large extent [119]. In this chapter, the diesel injection timing is indeed varied and, thus, a measure of available mixing time is needed. The ignition dwell (*IDw*) is expressed by

$$IDw = CA10 - EOI \tag{6.1}$$

where *EOI* is the end of the direct injection event and *CA*10 is the crank angle at which 10% of the total heat is released, here taken as the start of combustion. The value of *IDw* is directly affected by the diesel injection timing via *EOI*, but also by the PFI rate, intake manifold pressure and EGR rate through changes in *CA*10. Note that local temperature also affects ignitability. Even if temperature stratification is negligible at IVC, wall heat transfer and fuel evaporation can induce temperature changes later in the compression stroke [122]. Yet, it is generally not considered a controllable process and will be excluded from this discussion.

Experiments were run according to the matrix in Table 6.2. Subsequent aROHR analysis revealed vastly different rate shapes under varying operational settings, which was then further investigated. It was observed that the aROHR can exhibit either a single-stage or dual-stage heat release rate, depending on the specific level of fuel reactivity stratification. A combustion metric called the burn ratio was defined that characterizes this feature, which is the ratio of the phase-specific burn durations after and before CA50,

$$R_b = \frac{CA90 - CA50}{CA50 - CA10} \tag{6.2}$$

Figure 6.1 shows various aROHR traces for an ensemble of R_b values taken from the data set, where a decreasing value of R_b marks the transition from dual-stage heat release rates towards a single peak. Note that the x-axis should not be interpreted as the crank angle domain, but rather allows for a side-by-side comparison of rate traces. For extremely high levels of fuel reactivity stratification, diesel fuel is locally concentrated, thereby creating regions of substantial reactivity. These regions will ignite first and burn rapidly, owing to the relatively fuel rich conditions and strong autoignition tendency of diesel. As a consequence, these heavily stratified conditions correlate to excessively advanced combustion, i.e., CA50 values well before TDC. Kokjohn, Musculus and Reitz [120] studied these ignition mechanisms through a combination of high-speed chemiluminescence imaging and modeling of chemical kinetics. They found that combustion starts in the squish region, and that the ignition delay gets progressively longer towards the combustion chamber center, thereby mainly following gradients in the concentration of the high reactivity fuel. Therefore, it is expected that under circumstances of considerable stratification, those regions with a low diesel concentration will burn late and slow. The dual-stage heat release rate seen in Figure 6.1 for $R_b > 1$ is ascribed to these mechanisms. As the diesel is given more time to mix with the already present premixed charge, the degree of fuel reactivity stratification goes down and the initial stage intensity decreases. Combustion phasing is concurrently retarded. Eventually, the aROHR shape develops into a single-stage heat release rate for moderate to low stratification levels. The single aROHR peak rises and the charge burns out faster, as mixing time is increased and lower values of R_b are attained. On the other hand, the first stage is seen to progress relatively slow for these well mixed cases, which may in part be attributed to specific chemical properties of ethanol. Sjöberg and Dec [121] found that in HCCI combustion, ethanol shows very little low and intermediate temperature heat release. Temperature rise rates are hence only moderate until high temperature heat release commences. Although experimental conditions in this chapter are different, it is probable that this plays a role in the first phase of combustion, given the large amount of ethanol present.

The preceding discussion emphasized the impact of the diesel mixing time (*IDw*) on stratification. The fuel injection parameters take on the most important role in controlling *IDw*, which are the DI SOA (diesel) and the PFI rate (E85). These pa-

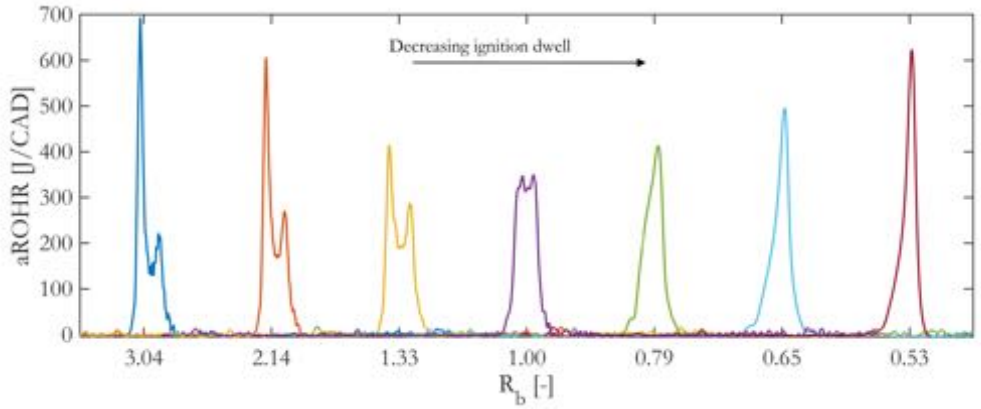

Figure 6.1: Rates of heat release (ROHR) for various burn ratios (R_b).

rameters will be used later on to control R_b and optimize GIE. Figure 6.2 shows a scatter plot of *IDw* and GIE as function of R_b for all DOE runs, thus including variations in all four operating parameters. It can be seen that a clear relation exists between the burn ratio and the ignition dwell. An exponential description appears quite suitable, which follows a general description for convective-diffusive mixing in a turbulent jet. This is further corroborated by the exponential fit and the associated R^2 value. However, there are some limitations to that description, as transient jet characteristics come into play after injection. Velocity in the center axis of the jet does not remain constant. Musculus and Kattke [123] studied the mixing behavior of diesel and air after the EOI by transient jet modeling. They found that mixing rates in the wake of the injection pulse increase just after EOI, due to an entrainment wave that quickly travels upstream and thereby speeds up mixing along the center axis of the entire jet. This can partially explain larger R_b values in the lower range of *IDw*, for the segregation of equivalence ratios is reduced faster. For larger values of *IDw*, and thus lower values of R_b, an increasing amount of momentum has been exchanged between the diesel jet and rest of the charge, which slows the diesel mixing rate over time.

GIE is also plotted in Figure 6.2, which displays an upward trend with decreasing R_b, showing the

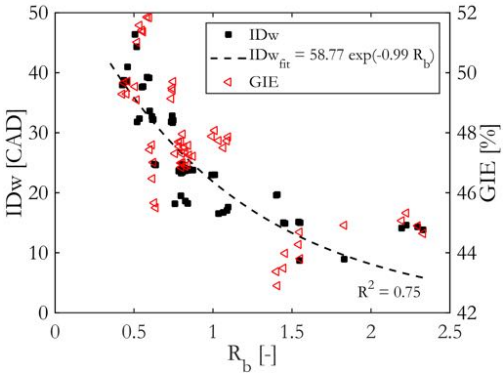

Figure 6.2: The ignition dwell (*IDw*) and gross indicated efficiency (GIE) versus the burn ratio (R_b) for all measured DOE points. An exponential fit and R^2 for *IDw* is included.

importance of fuel reactivity stratification. Using R_b as an indicator, it is clear that low levels of stratification, i.e., low R_b, result in high efficiency. But despite this clear trend, quite some spread in these GIE data remains. This is an indication that not only fuel stratification plays a role, but that some of the variance is explained by other mechanisms. In the next section, regression analysis is done to identify important operating parameters, and their interactions, relevant for maximizing GIE. It is discussed how these parameters relate to associated loss channels through fuel reactivity stratification and other governing mechanisms.

Table 6.4: Four-way ANOVA table of GIE data.

Source	SS	d.f.	MS	F	p
SOA	98.84	1	98.84	1294.97	2.34e-20
PFI	54.19	1	54.19	709.98	1.13e-17
pIntake	19.25	1	19.25	252.19	3.56e-13
SOA·pIntake	3.52	1	3.52	46.12	1.02e-6
PFI·SOA	0.87	1	0.87	11.41	2.80e-3
EGR	0.27	1	0.27	3.53	0.07
PFI·pIntake	0.18	1	0.18	2.37	0.14
pIntake·EGR	0.17	1	0.17	2.19	0.15
SOA·EGR	0.02	1	0.02	0.23	0.64
PFI·EGR	0.02	1	0.02	0.20	0.66
Error	1.60	21	0.08		
Total	178.92	31			

6.3.2 Identifying important parameters for efficiency optimization

A four-way analysis of variance (ANOVA) is first performed on the GIE data to discern important factors and interactions. The resulting ANOVA table is depicted in Table 6.4, where a double horizontal line separates statistically significant terms from the rest. The first column shows the factors and interactions that are tested and also includes an entry for the experimental error (i.e., variation that is not due to any of the tabulated factors and interactions) and total variation in the data. The second column depicts the sum of squares (SS) for each source. Mean squared (MS) values in the fourth column are computed by dividing SS by the degrees of freedom (d.f.) in the third column. F-values in the fifth column are calculated as the ratio of each MS values and the mean squared error, and finally, an F-test is performed at a 95% confidence level of which the resulting p-values are shown in the rightmost column. The results in Table 6.4 evidence that three factors have a particularly strong impact on GIE, namely SOA, the PFI rate and the intake manifold pressure. Furthermore, the interaction of the two fueling parameters, as well as the interplay between intake manifold pressure and SOA, prove to be significant.

The impact of fuel reactivity stratification on GIE was previously discussed and the importance is again stressed by the ANOVA results: both fueling parameters affect GIE to a large extent. Hereafter, it is investigated how fuel injection settings influence separate energy loss channels, through response surface analysis. RCCI is often linked to lower heat transfer losses as compared to CDC [104], but on the other hand suffers from higher combustion losses, especially at low loads. Hence, attention is directed to optimizing those particular loss channels using fueling parameter settings, and their relation to the formerly introduced burn ratio. Thereafter, a similar approach is used to study the effects of intake manifold pressure and SOA on these energy loss channels. The ANOVA table implies that this, too, is an important interaction effect and thus deserves further investigation. EGR is interestingly seen to be of insignificant in-

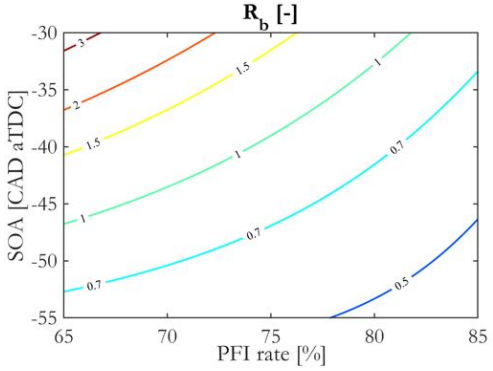

Figure 6.3: Prediction of burn ratio (R_b) as function of the PFI rate and DI SOA. The intake manifold pressure is set to 2 bar(a).

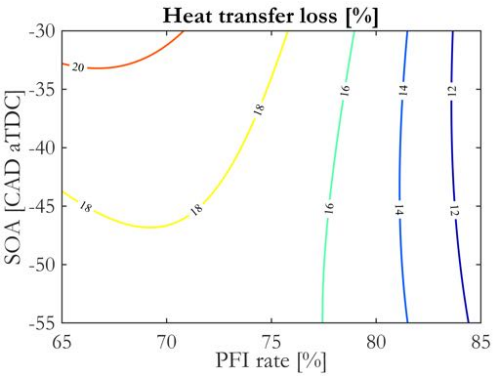

Figure 6.4: Prediction of heat loss percentage (HL) as function of the PFI rate and DI SOA. The intake manifold pressure is set to 2 bar(a).

fluence on GIE with respect to the other factors. Generally, EGR is applied to lower the charge reactivity as a means to control combustion phasing. Although it is thought that this effect is present, it is here only minor due to the relatively low EGR rates applied in the experiments.

6.3.3 Effects of fuel injection settings on reactivity stratification

Figure 6.3 shows a response surface plot of R_b as function of SOA and the E85 weight percentage. The intake manifold pressure is set to 2 bar in this plot, whereas the EGR rate has been entirely excluded from the regression polynomial due to a statistically insignificant effect. The largest values of R_b are found at the most retarded SOA and lowest E85 percentages, which is in line with the previous heat release analysis. This upper left region corresponds to heavily stratified conditions, since *IDw* is in its low range. As the diesel injection is advanced, or the relative amount of E85 is increased, the value of R_b reduces. Furthermore, a combination of the two measures proves most effective in lowering R_b owing to their interaction effect. As a results, the lowest burn ratios are found in the bottom right region of the response surface, where stratification is minimal.

A response surface plot of the heat loss percentage (HL) is shown in Figure 6.4. The selected intake manifold pressure corresponds to Figure 6.3. Reducing the degree of fuel reactivity stratification is evidently effective in lowering heat transfer losses, since a directional reduction of R_b correlates to a decline of HL. Two mechanisms are expected to play a role. First, as SOA is advanced the diesel is allowed more time to distribute, which reduces the local ignitability. Combustion phasing is thereby retarded, which has an evident effect on the temperature history. This can similarly be achieved by increasing the E85 percentage. Second, heat loss is governed by local temperatures at the surfaces where heat is actually transferred to the coolant. It thus matters where such high temperatures are reached. This is expected to be near the liner where most of the diesel has been forced to by spray momentum. By alleviating stratification through mixing, these local temperatures will be suppressed.

Fuel reactivity stratification also impacts on the combustion efficiency as can be seen in Figure 6.5, which is again plotted using an intake manifold pressure of 2 bar. Particular fuel injection settings provide an optimum of 97.5%. While heavily stratified conditions around an SOA of -30 CAD aTDC lead to the lowest combustion efficiency, the optimum is still located in a slightly more stratified region compared to the optimal setting for the heat transfer loss. And, hence, a trade-off is clear: preventing high heat transfer losses

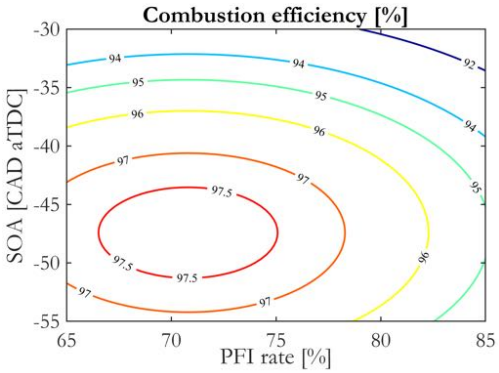

Figure 6.5: Prediction of combustion efficiency (1 - CL) as function of the PFI rate and DI SOA. The intake manifold pressure is set to 2 bar(a).

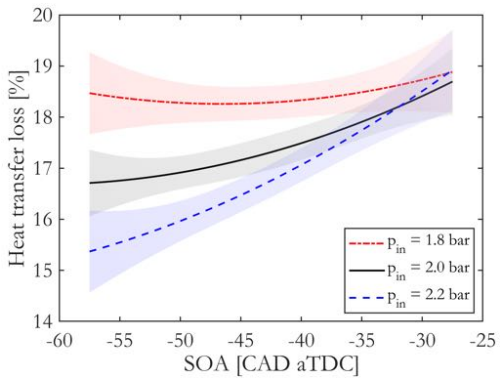

Figure 6.6: Prediction of heat loss percentage (HL) as function of DI SOA for three intake manifold pressures. The PFI rate is set to 75 wt.%. Shaded regions indicate 95% confidence intervals.

requires low stratification, while combustion efficiency pushes the optimal fueling settings towards slightly lower E85 percentages and retarded diesel injection timings. Careful calibration will be required to balance this tradeoff.

6.3.4 Interaction of direct injection timing and boost pressure

The ANOVA results in Table 6.4 show that intake manifold pressure has a strong impact on GIE. Furthermore, the interaction effect of SOA and the intake manifold pressure is also evident. Figure 6.6 presents regression curves of the heat loss percentages as function of SOA for three different intake manifold pressures. Shaded regions around the prediction curves illustrate a 95% confidence interval. In the previous discussion, it became clear that fuel reactivity stratification plays a key role in the total amount of heat loss, and the tradeoff that it displays with combustion efficiency. In Figure 6.6, the stratification is controlled only by SOA, since the E85 percentage is kept constant. Splitter et al. [118] found that low values of Φ_{global}, i.e., overall lean conditions, promote high efficiency. That, however, is here seen to only be partly the case. For the most retarded diesel injection timings, elevated boost pressures (low Φ_{global}) tend to exceed the heat transfer loss of lower intake manifold pressures. But as SOA is advanced, the differences between the cases enlarge in favor of heavily boosted conditions, although the effect subsides towards higher boost levels. This behavior exemplifies the strong interaction between SOA and intake manifold pressure, but also points out that there is another characteristic to take into account along with stratification. It raises the question: why is heat loss so strongly reduced at elevated boost pressure and advanced diesel injection? To answer that question, the effect of increasing the boost pressure on global temperature needs to be clarified. Figure 6.7 depicts global gas temperature traces inferred from the cylinder pressure via the ideal gas law for three intake manifold pressure settings. Increasing the intake manifold pressure results in a decrease of peak global gas temperature and in the remainder of the expansion stroke. Still, that does not directly mean that local temperatures are reduced as well, since the latter is coupled to the local equivalence ratio. Here, the degree of stratification again comes into play. Giving the injected diesel more time to blend by advancing SOA creates a more uniform, overall lean charge. Local temperatures then tend to settle towards the global gas temperature, which helps in suppressing heat transfer.

The effect of intake manifold pressure on combustion losses is investigated in Figure 6.8, where the combustion efficiency is plotted versus SOA for

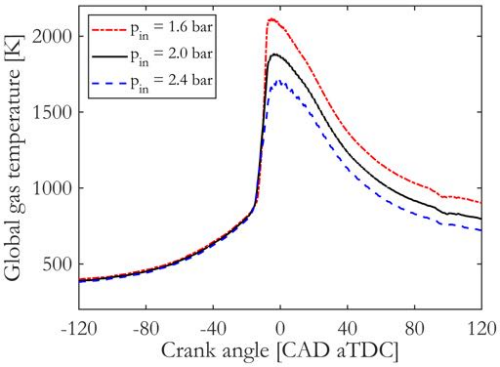

Figure 6.7: Global gas temperature versus crank angle for three intake manifold pressures. The SOA is set to -42.5 CAD aTDC, whereas the PFI rate equals 75 wt.%.

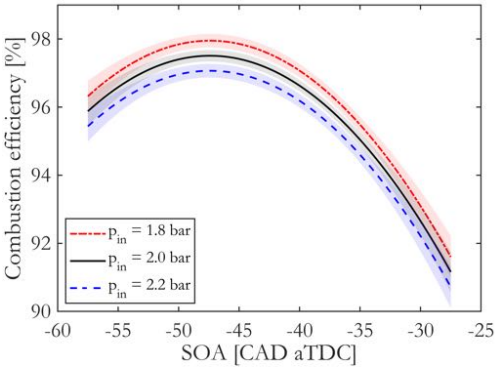

Figure 6.8: Combustion efficiency (1 - CL) as function of SOA for three intake manifold pressures. The PFI rate is set to 75 wt.%. The shaded regions indicate 95% confidence intervals.

three boost levels. The curves decrease with each increment of intake manifold pressure mainly due to a lower global temperature. This introduces another tradeoff with the heat transfer losses: boost pressure cannot be increased indefinitely, because of eventual excessive combustion losses. Once again, the need for careful selection of fuel injection and air path settings is clear.

6.3.5 GIE optimization

So far, it has been shown that fuel reactivity stratification plays a key role in finding a good compromise between heat transfer and combustion losses. Rates of heat release were shown to exhibit specific shapes according to the level of stratification, which was analyzed through a combustion metric called burn ratio (R_b). GIE generally increases as the value of R_b goes down, yet, R_b did not quite explain all variation seen in the GIE data. Further regression analysis revealed that stratification and total charge mass - varied through the intake manifold pressure - display a crucial synergy for balancing heat transfer and combustion losses. Particularly low heat transfer losses are found for high boost levels in combination with relatively early SOA settings. In the remainder of this section, SOA sweeps at various percentages of E85 are presented to find maximum GIE. The intake pressure is set to a relatively high value of 2.4 bar, which was a priori determined to provide the best results. External EGR is entirely omitted, since the ANOVA showed that it is statistically insignificant.

In the following, the burn ratio is suggested as a more direct predictor of peak GIE along variations in SOA, instead of the somewhat conventional use of CA50. Figure 6.9 depicts CA50 as function of multiple fueling combinations used in these sweeps. Many of the settings result in too advanced combustion phasing, even reaching -10 CAD aTDC. Only the highest two E85 percentages with sufficiently early SOA lead to CA50 values that are near TDC. As can be seen, the SOA range is not the same for all PFI rates, which was done to prevent misfires. This lack of tolerance to later combustion phasing was previously explained by an absence of low temperature reactions with ethanol combustion [121]. Hence, there appears to be only a small window of suitable CA50 values. Moreover, combustion phasing before TDC is rather counterintuitive when it comes to finding maximum efficiency, as from a CDC standpoint one would expect optimal phasing at several CAD after TDC. Besides, there is no real indication in these CA50 trends that the mixture is tending to misfire, yet it was found in the experiments that there is a very thin line between stable operation and complete misfires.

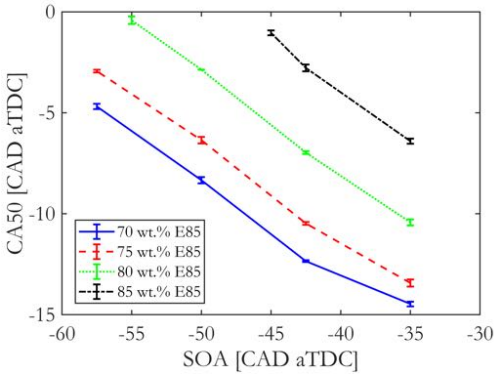

Figure 6.9: CA50 for various fueling parameter settings. The error bars show the standard deviation around the mean of three measurements. Further advance of SOA is limited due to misfires.

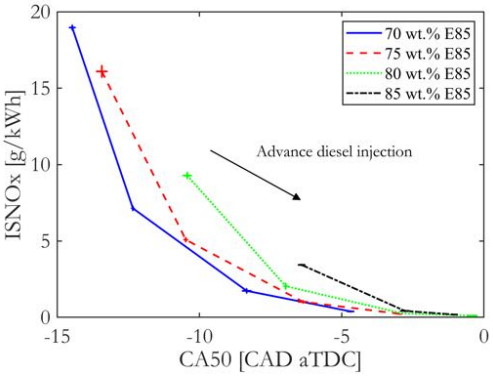

Figure 6.10: $ISNO_x$ as function of CA50 for different E85 percentages. The error bars show the standard deviation around the mean of three measurements.

Figure 6.10 shows the SOA sweep results in a NO_x versus CA50 plot. The NO_x emissions are included here because of their significant relevance in engine development. A very strong response to injection timing is seen in these NO_x data, which span a region between levels that comply with EURO VI (0.4 g/kWh) legislation and nearly 20 g/kWh. Combustion phasing again plays a crucial role, as the direction of NO_x increase corresponds to an advance of CA50. The effect of mixing time is also noticeable, since a constant CA50 gives rise to a larger amount of engine-out NO_x at higher E85 percentages. This is caused by the necessity to retard the diesel injection timing when the E85 percentage is increased, thereby leaving less time for mixing, which results in locally richer and thus hotter regions. All E85 percentages possess the ability to comply with EURO VI levels from an engine-out perspective, as long as the diesel is allowed sufficient time to mix.

The GIE results are plotted against R_b in Figure 6.11; R_b appears to be a good predictor of peak efficiency. For all E85 percentages, GIE is increased as R_b is reduced. At a certain point, the efficiency increase stagnates when the thermal efficiency and combustion efficiency settle in an optimal balance. The reasons for this were previously outlined. Figure 6.11 indicates that the decrease of R_b also stagnates when GIE peaks. Another look at Figure 6.1 is required to understand this behavior. The graph showed that when more time is available for mixing, the first phase of combustion (i.e., denominator of Equation 6.2) lengthens, whereas the second phase (numerator), contrarily, progresses faster. When the charge is overly mixed, however, the limit of this fast burnout is reached. The burn ratio decrease hence stagnates, and in some of the presented cases even rises again, which is shown in the zoom view included in Figure 6.11 to provide more detail.

The observed stagnation of both the GIE increase and R_b decrease is established when the combustion efficiency deteriorates to the point that potential thermal efficiency benefits (e.g., lower heat losses) cannot compensate this decline. This is shown in Figure 6.12 where energy distributions for the 80% E85 case are displayed. In the last step of SOA advance, R_b increases from 0.65 to 0.70, after it was reduced in the first two SOA steps. This R_b increment is accompanied with a notable increase of combustion losses, while heat losses remain nearly constant. The burn ratio, hence, does not only relate to the aROHR shape, it also predicts the position of peak GIE quite well when varying SOA. How these findings relate to higher loads and speeds, or other engine platforms, is yet unclear and needs to be addressed in future work.

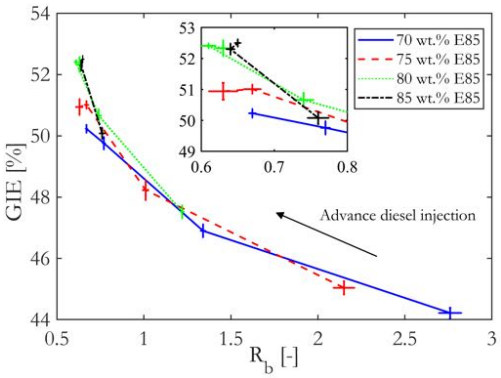

Figure 6.11: GIE as function of R_b for different E85 percentages. The error bars show the standard deviation around the mean of three measurements.

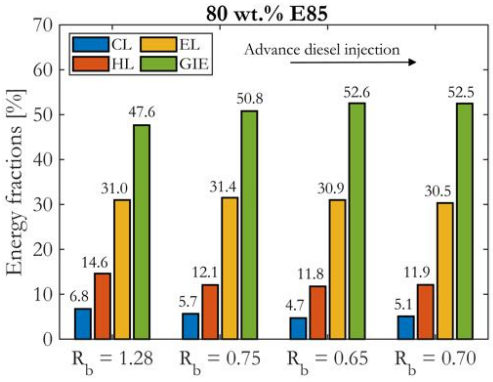

Figure 6.12: Energy fractions for various burn ratios (R_b) in an SOA sweep at a PFI rate of 80 wt.%. CL = combustion loss, HL = heat loss, EL = exhaust loss, GIE = gross indicated efficiency.

6.4 Conclusions

This chapter combined a heat release study with regression analysis to shed light on the influence of reactivity stratification on gross indicated efficiency and related energy loss channels in RCCI combustion. The main outcomes are:

- A distinctive combustion metric termed the burn ratio is introduced, which correlates well with fuel reactivity stratification, and is shown to characterize the heat release shape.
- The burn ratio is, through fuel reactivity stratification, linked to heat transfer loss and combustion efficiency.
- A strong reduction of heat loss is established through a combination of low reactivity stratification - thus low burn ratio - and high intake pressure, which proved crucial for maximizing the gross indicated efficiency.
- The burn ratio was used to identify the most favorable balance between heat loss and combustion efficiency, making it a practical metric for indicated efficiency optimization.

The results presented in this chapter confirm that E85 is a viable fuel for RCCI operation in heavy-duty engines operating in the mid load range. Peak GIE of 52.5% is reached at engine-out NO_x levels that comply with current legislation without the use of external EGR. Although not discussed in the body of the text, the soot emissions at peak GIE are well below legislative levels too.

Chapter 7

Mixing effects of the spray included angle

Introduction

The previous chapter showed that E85 is a very suitable low reactivity fuel for RCCI operation, with good heat release shaping capabilities and an increased gross indicated efficiency compared to gasoline. Furthermore, it was discussed that fuel mixing is of utmost importance for the preparation of an optimal charge in terms of the fuel reactivity stratification. While fuel balancing and the direct injection timing play a crucial role in that regard, engine hardware also requires an optimization. This chapter starts with a literature review to chart previous work and clarify what the current study adds. Up to now, all experiments have been done with standard engine components. The focus is now directed to the effects of the direct injection spray included angle on the mixture preparation. The tests are performed on a recently commissioned test setup based on a PACCAR MX-13 engine, which has a higher compression ratio than the DAF XEC engine. Hence, a comparison with the optimal settings from the XEC is done first, after which the baseline performance of the MX-13 is charted. The analysis again targets the relation of the fuel distribution, rate of heat release and the gross indicated efficiency. Figure 7.1 illustrates the different spray included angles that are considered in this chapter.

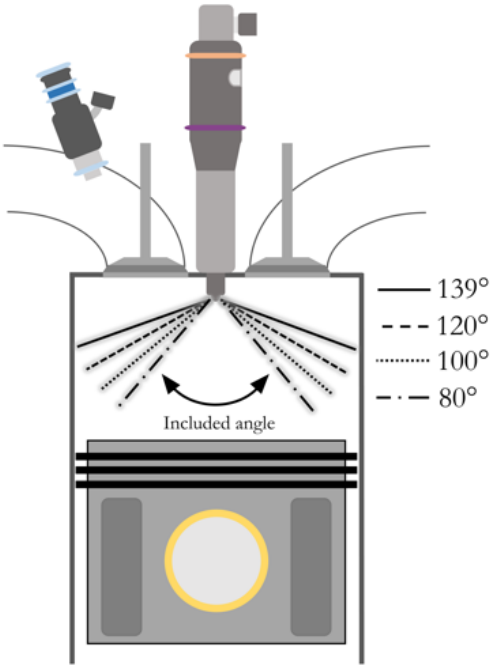

Figure 7.1: Illustration of the tested injectors with various spray included angles. The piston position corresponds to a crank angle of -65 CAD aTDC.

7.1 Literature review

The fundamentally different mixing processes in conventional diesel combustion (CDC) and reactivity controlled compression ignition (RCCI) require distinctive hardware designs. Both combustion regimes operate with an excess of air that in principle provides sufficient oxidizer for complete combustion. In CDC operation, however, all fuel

is injected directly into the cylinder close to top dead center (TDC), which requires mixing and combustion to take place concurrently on a time scale of several milliseconds. This necessitates an efficient design of the injector nozzle and piston bowl to utilize as much of the available air as possible in order to complete the combustion process in a timely manner. Over the years, this has led to many designs of diesel combustion systems, such as stepped-lip [124] and wave-shaped pistons [125], designed for improved mixing of fuel and air. There is a strong link between the motion of the reacting jet and the piston shape, giving rise to a staggering number of geometrical degrees of freedom in the design procedure. Besides, fuel injection parameters like timing and common rail pressure interact with these geometrical features as well, resulting in an even larger, multi-dimensional parameter space. To find optimal parameter settings, the use of the design of experiments (DOE) method is therefore widely applied in industry, but can also be found in an increasing number of academic studies. Benajes et al. [126] used DOE in conjunction with computational fluid dynamics (CFD) and experimental validation to optimize the combustion system and fuel injection parameters of a diesel engine operating in CDC. An innovative approach to improve mixing of fuel and air in CDC operation has recently been proposed by researchers at Sandia National Laboratories. Their ducted fuel injection (DFI) method involves injecting fuel through a small tube, much like the operation of a Bunsen burner, which creates leaner mixtures at the lift-off length that can lower or even prevent soot formation [127].

In RCCI operation, the mixture preparation must be optimized because of the delicate combination of local equivalence ratio (Φ), temperature and octane rating that govern the combustion process. Most of the mixing process takes place during the intake stroke, since low reactivity fuel is injected into the intake manifold. This creates an essentially homogeneous charge to which high reactivity fuel is added by direct injection (DI) early in the compression stroke. As such, the charge becomes partially stratified which allows control of the ignition moment and combustion duration. Because of these longer mixing times, fuel ends up in the crevices between the piston and cylinder liner and in the squish volume. In those places, it is relatively cold, and the chemical reactions cannot propagate sufficiently. The reactions stagnate, and as a consequence, large amounts of carbon monoxide (CO) and unburned hydrocarbons (UHC) are expelled into the exhaust. These regulated pollutants are reduced by aftertreatment, but excessive concentrations might pose difficulties for contemporary oxidation catalysts, especially at low exhaust gas temperatures [128]. Special piston designs have been proposed to reduce the squish and crevice-borne CO and UHC emissions. One approach is to increase the squish height, which directly reduces the crevice volume, while at the same time giving more space for reactions to propagate through the squish volume [129]. Additionally, the top ring land diameter can be reduced. While this actually increases the crevice volume, it can enhance local oxidation reactions, for the same argument: improved combustion propagation. Clearly, a tradeoff is present that needs careful balancing. More specialized piston designs employ a chamfered ring-land, which largely omits the crevice volume. Such a piston has been reported to reduce the UHC and CO emissions by 79% and 36%, respectively, at an intermediate load point. This increased the combustion efficiency to 99.5% [130].

Most studies on RCCI piston design focused on the optimal shape of the piston bowl. As long as the direct injection event is timed early in the compression stroke, the piston does not need to be shaped for guidance of the reacting jet like in CDC. On the contrary, a less sophisticated design may be more favorable due to a smaller piston surface area and a lower degree of piston-induced turbulence. Dempsey, Walker and Reitz [131] found a 2-4% point indicated efficiency increase by application of a shallow, wide piston design. At low loads, the indicated efficiency increase was due to a combination of improved combustion efficiency and lower heat transfer losses, while at higher loads the latter was the sole reason. When moving to higher loads, it might be necessary to move the diesel injection closer to TDC, as to stay within engine

constraints like peak pressure and maximum pressure rise rate. Benajes et al. [132] found that in those circumstances, a bathtub shape can lead to unacceptable soot levels and increased UHC compared to a stock piston. This was ascribed to the lower level of turbulence that is normally induced by spray-bowl contact. Still, they too reported improved thermal efficiency of an RCCI-optimized piston with respect to the stock variant, because of lower heat transfer losses resulting from a smaller piston bowl surface area.

To optimize fuel mixing, several studies focused on the hardware characteristics of fuel injection. Walker [133] investigated the application of gasoline direct injection (GDI) equipment in light-duty RCCI operation, because of the attractive economic aspects. Several injection pressures and spray included angles were put to the test, which indicated that mixing is improved both by widening the spray angle at a given fuel pressure or by increasing the fuel pressure at a given spray angle. A similar conclusion was drawn by Poorghasemi [134] through a comprehensive CFD study, which indicated that the distribution of diesel is enhanced by employing a larger spray included angle. A too narrow angle resulted in increased UHC and CO emissions stemming from the regions near the cylinder liner and the crevice volumes. In extreme cases, a narrow spray included angle was observed to result in pool-fire activity on the piston surface of an optical engine operating in a single-fuel low temperature combustion mode [136]. Still, a wide spray angle in combination with very early DI timing may result in wall impingement, leading to increased UHC emissions and unexpected combustion phasing behavior. Wissink et al. [135] observed such behavior in a light-duty RCCI engine and confirmed with CFD that wall wetting was indeed responsible for these trends. Injecting both fuels directly into the combustion chamber has been proposed by the same authors [86] to prevent wall wetting issues, while avoiding fuel ending up in the crevices as well. This approach opens up another control variable to extend the load range and optimize performance and engine hardware constraints.

Optical diagnostics are a powerful tool to shed light on reactivity stratification and the effects that it has on the combustion process. Several studies have been published that more or less observe the same behavior [137, 138]. Combustion generally starts near the cylinder liner and progresses towards the center of the combustion chamber, where conditions are typically most fuel lean and the local octane rating is highest. The rate at which chemical reactions progress towards the combustion chamber center depends on the degree of reactivity stratification. Tang et al. [139] performed spectrally-resolved measurements of RCCI combustion in an optical engine. They noted that, as fuel stratification was increased, emission bands of OH, CH, C_2 and CH_2O became more pronounced and appeared sequentially, while well-mixed cases showed very little spectral structure. This indicates that the spatiotemporal behavior of the combustion reactions differs under varying degrees of reactivity stratification. Kokjohn [120] combined optical diagnostics with chemical kinetics modeling and found that the location of ignition and progression of reactions mainly follows gradients in the primary reference fuel number, while gradients in the equivalence ratio had a smaller but still significant effect. Temperature stratification had an insignificant effect, at least under the conditions of that particular study.

This literature overview shows that considerable progress has been made in research to optimize engine hardware for RCCI operation. Especially the piston bowl design has received much attention, but some ambiguity remains on the impact of fuel injection specifications. This chapter focuses on the spray included angle of the direct injection equipment. It is investigated how this angle affects the gross indicated efficiency (GIE) and apparent rate of heat release (aROHR) through changes in the high reactivity fuel distribution.

7.2 Experimental approach

The experiments in this chapter are performed on a recently commissioned test setup based on a PACCAR MX-13 engine, which was previously in-

Table 7.1: Nozzle specifications for the injectors tested in this chapter. S = the standard nozzle that was also applied in all previous chapters.

Parameter	S	#1	#2	#3
Spray included angle [°]	139	120	100	80
Number of holes [-]	7	7	7	7
Hole diameter [µm]	195	180	180	180

troduced in Chapter 2; the reader is referred to that chapter for more details. Compared to the XEC platform, this engine has a higher compression ratio (17.2 versus 15.85) and a different cylinder head, but there are also similarities to note. First, despite the difference in compression ratio, the piston bowl has the same stock double-step design. Second, the diesel injector is (internally) the same Delphi DFI21, although the injector body differs between the two engines. The core of this chapter is a comparison of different spray included angles for RCCI combustion. The direct injection nozzle specifications are listed in Table 7.1. Nozzle S is the stock variant, which has been applied in all preceding chapters. Nozzles 1, 2 and 3 have a slightly smaller hole diameter compared to the standard version. This was done to improve fuel atomization at lower common rail pressures that are typical in RCCI mode. The number of holes is equal for all four nozzles. It was decided to perform SOA sweeps for each nozzle, instead of using the spray angle in a design of experiments (DOE) matrix, because randomization of test runs is practically impossible in cases where an hardware component is one of the independent variables. The injectors thus have to be tested one-by-one to remain within an acceptable timeframe. In-house blended E85 and EN590 specification diesel are applied as low and high reactivity fuel, respectively.

The experiments are divided into three parts. First, the baseline performance of the MX-13 engine in CDC mode is charted. Second, an initial exploration of the RCCI response is done by re-running the optimal settings of the XEC platform on the MX-13 setup. These tests are all performed using the standard fuel injection equipment (nozzle S in

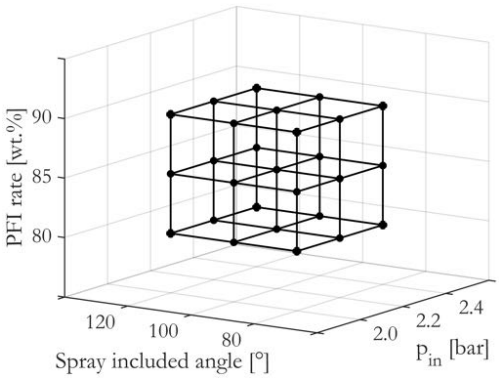

Figure 7.2: The test matrix for the experiments discussed in this chapter. An SOA sweep is performed at each of the nodes.

Table 7.1). Third, sweeps of SOA are performed with the three RCCI injectors (nozzles 1, 2 and 3). These sweeps are done with various settings of the intake pressure and PFI rate. A graphical overview of the experimental matrix is shown in Figure 7.2. At each of the black dots, an SOA sweep is done; the SOA range is -70 to -40 CAD aTDC with a step size of 5, except at a PFI rate of 90 wt.% which was done in the range of -65 to -35 CAD aTDC to prevent misfiring. The eventual goal is to increase GIE by optimizing the diesel distribution through spray targeting. How exactly an optimal charge is formed remains to be seen, but two hypotheses may be taken into consideration:

1. The E85 is approximately evenly distributed or has a higher concentration near the center of the combustion chamber, when the diesel injection event takes place. The coldest regions are the least reactive, which are expected near the cylinder liner. The diesel should be directed there using a relatively wide spray included angle.

2. The E85 is more concentrated near the cylinder liner and the charge becomes leaner towards the center. The diesel should be directed to the center of the combustion chamber to increase reactivity there, while the initial temperature rise is sufficient to properly combust the charge near the liner.

Table 7.2: Nominal stationary operating conditions and fuel specifications.

Gross IMEP	8.75 ± 1 bar
Fuel energy input	3950 ± 50 J/cycle
Engine speed	1200 rpm
p_{exh}	1.10 ± 0.02 bar
EGR rate	0%
$T_{coolant}$	87 °C
T_{oil}	96 °C
DI fuel	EN590 diesel
PFI fuel	E85

Several caveats need to be mentioned at this point. First, targeting the diesel jet towards the liner at low in-cylinder density brings about potential problems of wall wetting; this obviously has an adverse effect on the charge preparation. Second, enriching the charge near the liner will locally increase gas temperatures during combustion. Since heat transfer is governed by local temperature near the wall, it might be beneficial to prevent relatively rich regions near the liner. Last, since E85 is injected into just one of the two intake channels and the cylinder head has a low-swirl design, the distribution of E85 could be more skewed than postulated earlier. In that situation, it will be difficult to target the diesel in an optimal manner.

The experiments are performed at about 30% of the rated torque at 1200 rpm. Nominal stationary conditions are summarized in Table 7.2. An exhaust pressure of 1.10 ± 0.02 bar is used by fully opening the back-pressure valve. This was done since the Horiba gas analyzer was unavailable for the tests discussed in the current chapter, which made it impossible to monitor and log external EGR rates. However, since the XEC results indicated that the application of external EGR was not needed for combustion phasing control and efficiency optimization, this was not considered a major issue. However, lacking information about CO and UHC concentrations in the exhaust gas means that combustion losses cannot be inferred.

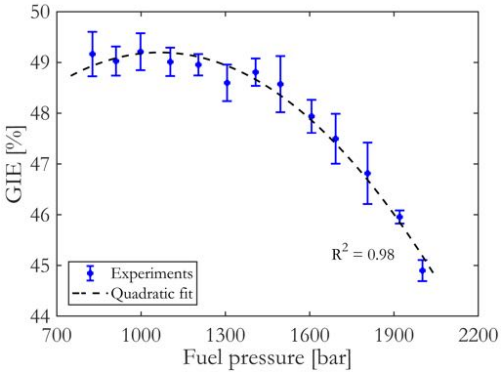

Figure 7.3: Gross indicated efficiency (GIE) versus fuel pressure in CDC mode. SOA is set to -8 CAD aTDC and the intake pressure equals 1.7 bar. The error bars indicate the standard deviation around the mean of three measurements.

7.3 Results and discussion

7.3.1 Baseline CDC performance

The performance of the MX-13 in CDC mode is first explored before investigating its RCCI capabilities. This is done to enable a proper comparison with the XEC platform; a GIE enhancement of RCCI with respect to CDC is not necessarily established with all engines. To get an idea of the GIE enhancing capabilities of RCCI on the MX-13 engine, a firm CDC baseline is required. In Chapter 5, an optimization was done on the XEC platform for both CDC and RCCI. This optimization was performed at two different boost pressures: 1.7 bar and 2.3 bar (revisit Figure 5.6). The former is a typical level for the capabilities of contemporary turbochargers, whereas the latter was selected to explore the GIE potential at heavily boosted conditions. Here, a similar exploration is done by sweeping the fuel pressure and SOA in CDC mode, again at two intake manifold pressures. While this is in no way an exhaustive optimization, it does provide compelling evidence of an increased GIE in CDC mode with this new engine compared to the XEC.

The MX-13 has a higher compression ratio as compared to the XEC (17.2 versus 15.85), hence the spe-

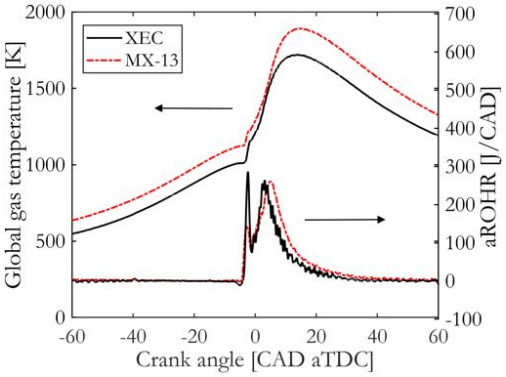

Figure 7.4: A comparison of global gas temperature and aROHR at 1.7 bar intake pressure in CDC mode. Fuel pressure for the XEC equals 1200 bar, whereas the MX-13 is operated at 1000 bar. SOA is -8 CAD aTDC in both cases and intake temperature equals 40°C.

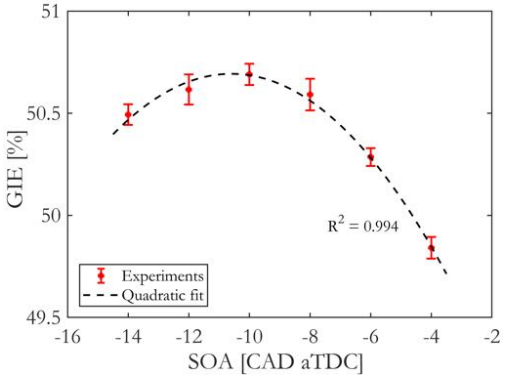

Figure 7.5: GIE versus SOA in CDC mode. The intake manifold pressure is set to 2.2 bar and common rail pressure equals 1100 bar. The error bars indicate the standard deviation around the mean of three runs.

cific requirements of the fuel injection settings are likely different. A fuel pressure sweep at an intake pressure of 1.7 bar is shown in Figure 7.3, including a quadratic fit to the experimental data. As the quadratic fit suggests, an optimum just over 49% GIE is found in the range of 900-1100 bar. This is a lower optimal fuel pressure range as was found for the XEC, which was in the 1200-1600 bar region, and yielded a peak GIE of 48.5%. The fuel pressure difference is ascribed to the increased cylinder pressures and associated temperatures during the cycle with a higher compression ratio, generally leading to higher heat transfer losses. Traces of the global gas temperature and aROHR are shown in Figure 7.4 for the optimal fuel pressure settings of both engines. The lower fuel pressure setting of the MX-13 results in a shifted peak of the diffusion-limited phase of combustion, resulting in a longer burn duration, providing a more favorable balance between heat transfer and the expansion ratio.

Many of the results in the previous chapters have shown that the intake manifold boost pressure is a key parameter for GIE optimization, regardless of the combustion regime. Here, a sweep of SOA in CDC mode at an intake manifold pressure of 2.2 bar is made to assess the performance of the MX-13 at heavily boosted conditions. The result of this SOA sweep is shown in Figure 7.5, again accompanied by a quadratic fit. The peak GIE reaches up to 50.7%, which is more than a percent point increase as compared to the high-boost optimum of the XEC engine.

7.3.2 Baseline RCCI performance

Before proceeding to the spray included angle investigation, an initial RCCI investigation is presented and discussed. This study provides an indication of the base performance and associated heat release shapes of the MX-13 engine in RCCI mode. The experiments on the XEC setup in Chapter 6 showed an optimum at a PFI rate of 80% and an SOA in the range of -50 to -55 CAD aTDC with an intake pressure of 2.4 bar and without external EGR. These settings were re-run on the MX-13 setup for comparison and the corresponding results are plotted in Figure 7.6. Note that the standard diesel injector was used in these tests (nozzle "S" in Table 7.1). The black line in Figure 7.6 displays the optimal aROHR of the XEC engine with a GIE of 52.5%. Additional combustion metrics are depicted in the frames with corresponding colors and line types. As was discussed in Chapter 6, the combustion of an optimal charge displays a relatively slow first phase, whereas the burnout of the fuel occurs rapidly. This results in a small value of the burn ratio (R_b) at optimal conditions. Recall that the burn ratio was defined as:

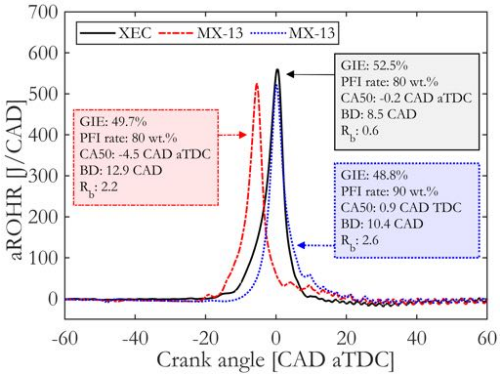

Figure 7.6: A comparison of rates of heat release recorded on the XEC and MX-13 engines. Common rail pressure is in all cases set to 500 bar, the intake pressure and temperature equal 2.4 bar and 40°C and SOA is -55 CAD aTDC. External EGR is 0%.

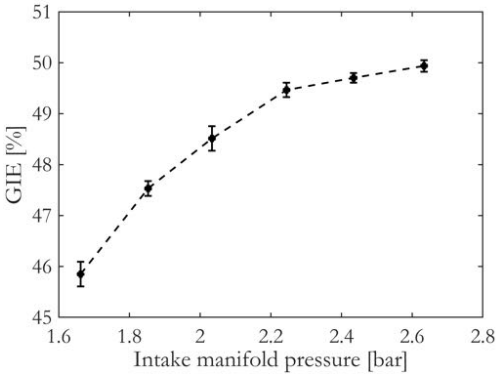

Figure 7.7: Gross indicated efficiency (GIE) versus intake manifold pressure. The PFI rate is set to 80% and the intake temperature equals 40°C. The common rail is pressurized to 500 bar, and SOA is -55 CAD aTDC.

$$R_b = \frac{CA90 - CA50}{CA50 - CA10} \tag{7.1}$$

By re-running these settings on the MX-13 setup, the red dashed-dotted line in Figure 7.6 is obtained, which resulted in a GIE of 49.7%. Combustion phasing has advanced to -4.5 CAD aTDC. This can be expected, given the higher compression ratio of the engine and thus higher compression temperature. It can be clearly seen that low temperature reactions occur several crank angles earlier, thereby initiating high temperature reactions at an earlier moment as well. It thus seems obvious that the lower GIE is a result of suboptimal combustion phasing. In addition, the total burn duration (CA90-CA10) is more than 4 CAD longer, together making it plausible that the thermal efficiency is lower. However, the aROHR traces suggest a less unequivocal explanation. If the final stage of combustion is observed in more detail, it can be seen that the aROHR tail is quite long for the MX-13 engine. It actually takes the red trace multiple crank angles more to burn out completely (i.e., reach aROHR = 0), despite the much earlier CA50. This could be an indicator of unacceptable combustion losses. For the red dashed-dotted MX-13 trace in Figure 7.6, the value of R_b is considerably higher than the black XEC trace; a direct consequence of the long combustion tail. Is this the result of wall wetting due to the diesel jet hitting the liner? Does an excessive amount of E85 end up in the crevice volume? Is the E85 concentrated in the piston bowl where an insufficient presence of diesel results in poor combustion? These questions need answering for further optimization of GIE. First, the effect of suboptimal phasing is counteracted by increasing the PFI rate to 90%. This results in the blue dotted aROHR trace in Figure 7.6. While the combustion phasing (CA50) is now almost equal to the XEC case, it can be seen that the start of combustion is delayed. Yet, the combustion duration is still longer owing to the lengthy tail. A reason for concern is the fact that the GIE has dropped almost a percent point with respect to the 80% PFI rate case. This is a crucial hint that combustion losses are causing the GIE offset between the XEC and MX-13 engines.

GIE generally increases with the intake manifold pressure. It was extensively discussed in the previous chapters that the beneficial effect of boosted RCCI operation comes from the reduction of heat transfer. Here, the effects of boosting on efficiency and the aROHR shape are studied on the MX-13 setup. Figure 7.7 shows GIE as function of the intake manifold pressure, displaying an increasing trend. The trend is curved and further

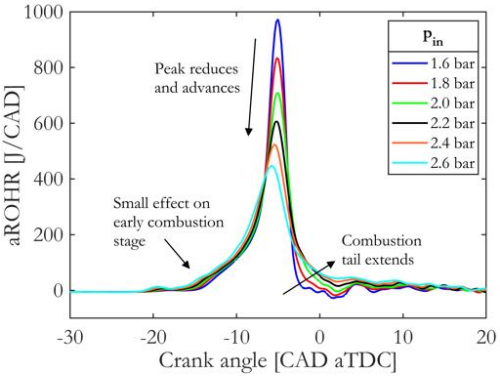

Figure 7.8: Apparent rates of heat release (aROHR) versus crank angle at various intake manifold pressures. Conditions correspond to the values of Figure 7.7.

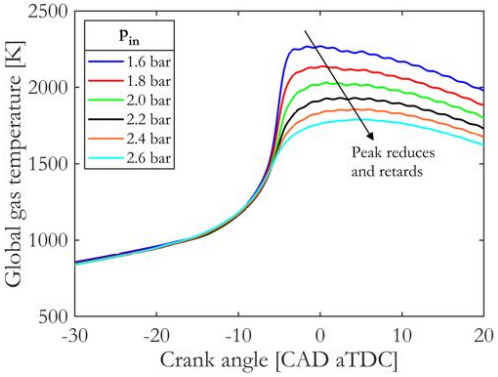

Figure 7.9: The global gas temperature versus crank angle at various intake manifold pressures. Conditions correspond to the values of Figure 7.7.

boosting after 2.2 bar is seen to provide only small benefits. Still, this behavior corresponds to results from the XEC platform, where increasing combustion losses counter the heat transfer benefit. Eventually, this will flatten the response for a further boost increase. The aROHR traces for the same boost variation are presented in Figure 7.8. Here, it can clearly be seen that the extended combustion tail is not always present. For the lowest boost level, peak aROHR is the highest and the charge burns out quickly, much like the optimal aROHR shape of the XEC setup. As the boost pressure is increased, however, the aROHR peak lowers and the burn duration extends. Most notably, the combustion tail lengthens drastically, whereas the initial phase is not much affected.

Previously, the question was raised what could cause this long combustion tail. Reviewing the options makes it unlikely that wall wetting due to the diesel jet hitting the liner is the cause. Two reasons are noted. First, similar behavior was not observed on the XEC setup, despite that the injector nozzle and piston bowl have identical geometries. Second, the tail actually diminishes when boost pressure is lowered. This is counter to the expected effect, as a lower in-cylinder density would make it more probable for the diesel spray to reach the wall. The fact that the tail is reduced at lower intake pressures suggests that there is a link with the global gas temperature, of which traces are depicted in Figure 7.9. It can be seen that the global gas temperatures reduce with an intake pressure increase. In previous analyses in Chapter 5 and Chapter 6, these lower temperatures were linked to strong reductions of heat transfer losses. This is an important quality of RCCI operation that needs to be fully exploited to maximize efficiency. However, here it is opposed by an extension of the late phase in the form of an evident tail. This can not only impact the efficiency of the thermodynamic cycle due to a longer burn duration, but it is probably also an indicator of poor combustion.

Another possibility is that a significant portion of the E85 is accumulated in the crevice volume between liner and piston, and therefore combusts poorly. By lowering the intake manifold pressure, global gas temperatures are considerably elevated. Combustion of fuel trapped in the crevices may be enhanced if local temperatures reach sufficiently high values. This reasoning can also be applied to the last proposition, where E85 is more concentrated in the center of the combustion chamber, while the diesel is mostly distributed downstream of the injector nozzle, near the cylinder liner. Raising the global gas temperature can significantly aid in combusting the low reactivity charge in the center of the combustion chamber. This effect is possibly further amplified by creating overall fuel richer conditions by lowering the intake pressure.

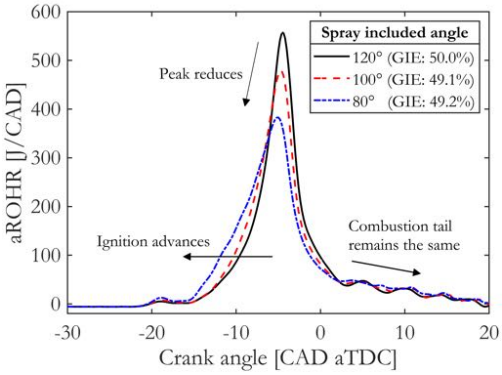

Figure 7.10: Apparent rates of heat release (aROHR) versus crank angle. Intake pressure is 2.4 bar, the PFI rate equals 80% and SOA is set to -60 CAD aTDC.

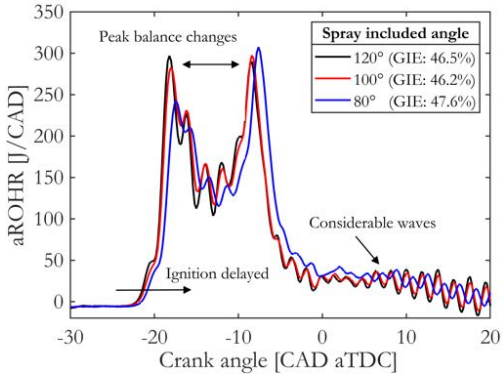

Figure 7.11: Apparent rates of heat release (aROHR) versus crank angle. Intake pressure is 2.4 bar, the PFI rate equals 80% and SOA is set to -40 CAD aTDC.

7.3.3 Spray included angle study

To further investigate from which part of the combustion chamber the long tail originates, the spray included angle is considered in the analysis. By targeting different parts of the combustion chamber (see Figure 7.1), the spatial distribution of diesel is altered. Specifically, by narrowing the spray angle, the diesel concentration will increase in the center of the combustion chamber relative to wider angles. It is expected that if a relatively high concentration of E85 is present in the center, thereby causing a slow burnout of the charge, a narrower spray angle will reduce the observed combustion tail. Figure 7.10 displays aROHR traces with three spray included angles ranging from 120° to 80° (nozzles 1, 2 and 3 in Table 7.1). The selected PFI rate of 80% is the lowest tested value, which corresponds to the largest amount of injected diesel and hence was expected to have the strongest interaction with the spray included angle. Furthermore, the highest intake pressure in the experiment matrix (2.4 bar, see Figure 7.2) is taken, since it was identified to exhibit the most pronounced combustion tail. Two evident trends are visible in Figure 7.10. First, the moment of ignition advances as the included angle is reduced, and second, the aROHR peak value reduces. The latter appears to some extent be a result of the former, since the burn duration is lengthened. Not many studies have directly addressed the influence of the spray included angle on combustion behavior, performance and emissions. Poorghasemi [134] performed CFD calculations with various angles and found an advance of combustion with narrower angles as well. They ascribed this trend to the hotter conditions in the piston bowl as compared to the temperatures near the cylinder liner. An alternate, or supplemental, explanation could be that mixing stagnates at an earlier point in the compression stroke because of a more confined movement of the diesel spray within the piston bowl, resulting in slightly richer spots. The combustion tail is unfortunately not affected by differences in the spray included angle, which eliminates the possibility to optimize this part of the combustion event using the spray angle, at least at the current conditions.

Changing the diesel injection timing could provide more insight into the relevant mechanisms for ignition behavior of these different angles. Figure 7.11 displays aROHR traces under the same conditions as in Figure 7.10, but at a retarded DI SOA of -40 CAD aTDC. The in-cylinder conditions are evidently more stratified than at an advanced SOA, since the aROHR traces display two clear peaks. Interestingly, the ignition trend has been reversed. The widest spray angle now results in the earliest ignition, whereas narrower angles retard ignition. The most notable effect occurs at an angle of 80°, where a shift in relative

peak heights can be seen. In Chapter 6, such a shift was related to a decrease in reactivity stratification by enhanced mixing. While fuel injection parameters can be adjusted to increase the mixing time, here equal parameter settings are applied for all traces. Thus, an enhancement of the mixing process must be induced by some other process. Revisiting Figure 7.1 learns that at an angle of 80° the center axis of the diesel spray targets the piston bowl rim. Whether significant spray-bowl contact occurs depends on the piston position at the start of injection: later injection will result in more contact-induced mixing. It is hence conceivable that the ignition retard is caused by a higher degree of mixing due to increased spray-bowl interaction. The lower GIE values at retarded SOA are to a large extent ascribed to the advance of combustion phasing. That the combustion event becomes quite violent at these advanced and stratified conditions is substantiated by the presence of considerable waves on these rate traces originating from the pressure signal. The fact that the tail of combustion is not affected by the spray included angle and SOA could be a consequence of fuel being trapped in the crevices.

Sweeps of SOA are performed with each of the injectors listed in Table 7.1. Ultimately, the goal is to find peak GIE with one of these nozzles. It is expected that targeting of the spray affects several important processes in charge preparation and combustion. First, a change in the spray included angle will affect the direction of the diesel jet. This has an impact on how diesel is distributed in the already present E85-air charge. As previously postulated, the charge reactivity is expected to be lowest near the cylinder liner due to lower temperature. The local charge reactivity could therefore benefit from the presence of diesel to raise the ignitability. On the other hand, a richer mixture results in higher local temperatures, which may increase heat transfer rates. Hence, a shallower spray angle is expected to bring some advantages as well. Moreover, the previous heat release analysis indicated that targeting the diesel jet towards the piston changes the mixing process through spray-bowl contact as well, especially at later injection timings. While this may not bring desired results at the current load point, it could be an important feature going towards full load where the injection timing often needs to be retarded, as discussed by Benajes [132].

In Chapter 6, the burn ratio (R_b, Equation 7.1) was used to optimize GIE using sweeps of SOA, where a minimal R_b yielded maximal GIE. The fuel reactivity stratification was linked to R_b using the ignition dwell (*IDw*), which showed good correlation. The results in the current chapter so far show that the combustion displays an evident tail (i.e., extremely slow burnout). This obviously impacts the thermal efficiency by extending the burn duration, but it also suggests poor combustion. It moreover renders R_b impractical for GIE optimization given its low sensitivity to fuel injection settings. Figure 7.7 displayed that the heat release can be shaped to resemble optimal conditions as seen on the XEC engine, but this requires considerably lower intake manifold pressures. By cause of higher heat transfer, according to the results in Chapter 5 and Chapter 6, these low boost conditions do not result in optimal efficiency. Hence, high boost pressure is applied with an inevitable combustion tail. The burn ratio therefore does not predict peak GIE on the MX-13 engine, as it is not a measure of fuel reactivity stratification, but is rather very much affected by slow burnout of the charge.

Therefore, GIE will be studied as function of CA50, as is shown in Figure 7.12. Each of the curves resembles an SOA sweep. At a PFI rate of 80%, the sweeps are done from -70 to -40 CAD aTDC, whereas at a 90% PFI rate the sweep ranges from -65 to -35 CAD aTDC. It is found that the 120° angle results in the highest efficiency at both 80% and 90% PFI rates. Furthermore, the 80% PFI rate setting using the 120° angle clearly outperforms the other combinations. The best balance between thermal and combustion efficiency is found at earlier CA50 values when the PFI rate is lowered. It is alarming to see that peak GIE is attained at 4 CAD before TDC. This suggests that the advance of combustion is necessary to elevate the global gas temperature; thermal efficiency is sacrificed to increase the combustion efficiency. Another indication of improper com-

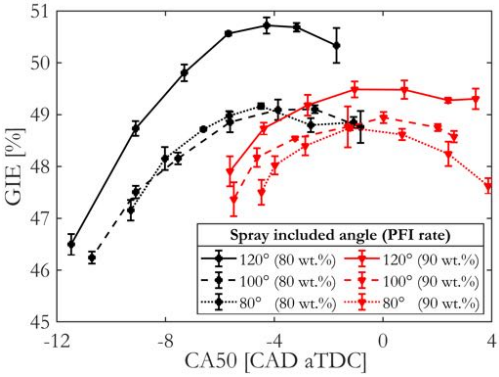

Figure 7.12: Gross indicated efficiency (GIE) versus CA50 in SOA sweeps for three spray included angles and at two PFI rates. The error bars indicate the standard deviation around the mean of five runs. The intake manifold pressure is set to 2.2 bar.

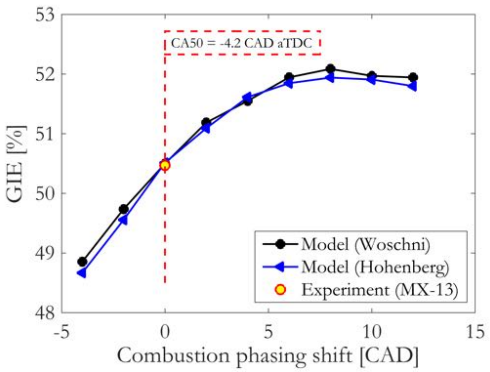

Figure 7.13: Modeled GIE versus a shift in combustion phasing. The curves are from a zero-dimensional thermodynamic model and are compared to the peak GIE in the experiments. Simulations by Bart Somers.

bustion is that the GIE curves are lowered when the PFI rate is increased, despite that combustion phasing is optimized from a thermodynamic viewpoint. The same observation was made in Figure 7.6. The by far prevailing explanation is that at higher PFI rates, more fuel gets trapped in the crevice volume, thereby lowering the entire curve.

The need to advance combustion phasing beyond a favorable value from thermodynamic viewpoint to limit excessive combustion losses raises the question what could be gained by a CAD shift of the ROHR further towards or after TDC. A small simulation study was performed to assess this thermal effect using a MATLAB model that solves the energy and mass conservation equations of a 0D open system, although here only the GIE is considered. The geometric parameters of the MX-13 engine are used to define the system dimensions. Two spatially-averaged heat loss models, i.e., the versions of Woschni [36] and Hohenberg [37], are considered to assess potential differences. The model furthermore assumes that the combustion efficiency remains equal under all circumstances; chemical kinetics are not included. The ROHR trace of the optimal experimental case from Figure 7.12 is inserted into the model. The intake pressure is adjusted until the pressure trace during compression is matched with the experiment and the intake temperature is adapted to obtain the same initial gas temperature at intake valve closing. The results can be seen in Figure 7.13; the model predicts the experimental GIE value well. The ROHR trace is subsequently shifted in the CAD domain by steps of 2 CAD. Earlier combustion phasing is seen to further decrease GIE, which is expected given the fact that the experimental CA50 value was -4.2 CAD aTDC. Delaying the combustion event evidently has a positive thermal effect on GIE in the simulation. With a shift of 8 CAD, the GIE peaks at 52% regardless of the applied heat loss model. Hence, the simulation results show that a 1.5% point of thermal efficiency can be gained in case the combustion efficiency would remain the same.

This chapter considers engine hardware in terms of the direct injector nozzle specifications. But aside from the fuel injection equipment, it is also necessary to monitor peak cylinder pressures, as it needs to be within constraints and eventually it also impacts the brake efficiency. The latter is affected through increased friction at the big end bearing. Typical modern heavy-duty engines are operated with peak cylinder pressures ranging in between 200 and 250 bar at full load. Figure 7.14 shows what peak pressures are reached with heavily boosted RCCI operation. These results correspond to the 120° spray included angle results at

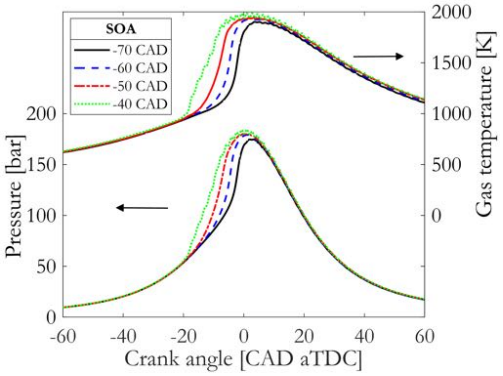

Figure 7.14: Global gas pressure and temperature as function of CAD. The traces correspond to the SOA sweep with a spray angle of 120° at a PFI rate of 80%. The intake manifold pressure equals 2.2 bar.

a PFI rate of 80%. Note that the intake manifold pressure is set to 2.2 bar, which is a considerable boost level given the approximate 30% load setting in these experiments. Together with the extremely advanced combustion phasing, peak pressures rise up to 180 bar. The most delayed SOA, associated with the most advanced CA50, results in the highest peak pressure. Still, the relative differences are small. Extending these heavily boosted conditions to full load would evidently cause problems. Simple linear extrapolation estimates a peak pressure of 600 bar at 100% load.

To keep peak pressures in RCCI operation within realistic and safe values, combustion phasing will have to be retarded. This could be achieved by switching to conventional dual fuel operation (i.e., a diesel pulse much closer to TDC) or switching to CDC. Another option is to reduce the relative boost level and to add dilution in the form of EGR. In Figure 7.14 global gas temperature traces are plotted for reference; it can be seen that changing SOA does not heavily impact on the peak values, although the temperature rise onset is advanced, which results in longer residence times at high temperature. This will - at least to some extent - alleviate the high combustion losses.

7.4 Conclusions and outlook

This chapter focused on the influence of the direct injection spray included angle on the GIE in RCCI operation via changes in the high reactivity fuel distribution. The experiments were performed on a new single-cylinder setup based on a PACCAR MX-13 engine. First, the base of performance of the engine in CDC and RCCI mode was explored. The CDC baseline was created to enable a proper comparison with the XEC engine in terms of GIE enhancements with RCCI. In CDC operation, the MX-13 displayed a considerable GIE improvement with respect to the XEC engine: 50.7% versus 49.6%. It must be mentioned that these explorations in CDC on the MX-13 engine did not comprise an exhaustive optimization; some tenths of percent points may still be gathered. In RCCI operation using the stock nozzle, the MX-13 showed fundamental differences in combustion compared to the XEC. A long rate of heat release tail was visible in the late combustion stage, which is thought to stem from poorly combusting fuel trapped in the crevice volume between piston and liner. This idea needs further investigation. It was found that a reduction of the intake pressure reduces the slow burnout by elevating the global gas temperature. It is thought that when the global gas temperature is increased, most of the crevice-trapped fuel is oxidized sufficiently fast. However, these lower boost levels did not yield higher GIE, since increased global temperatures also bring about higher rates of heat transfer, as results from previous chapters pointed out.

The tests were continued with high boost levels and the spray angle was changed to find if GIE could be enhanced. Sweeps of DI SOA were performed at different settings of the PFI rate, intake manifold pressures and with different spray included angles. The main outcomes are:

- A peak GIE in RCCI operation of 50.7% is attained at a spray included angle of 120° and an 80% PFI rate at an intake manifold pressure of 2.2 bar with an SOA setting of -60 CAD aTDC. The peak GIE in RCCI mode is virtually equal to that in CDC operation.

- The optimal spray included angle of 120° suggests that the optimal angle in RCCI mode is slightly narrower than for CDC operation, although this angle is still wide enough to direct the high reactivity fuel near the liner. The first formulated hypotheses in this chapter is expected to hold.
- Peak GIE is found at an extremely advanced CA50 value of -4.2 CAD aTDC. This is thought to be necessary to compensate for very high combustion losses; thermal efficiency is sacrificed to increase the residence time at a high global gas temperature.
- More indications that crevice effects are causing high combustion losses are found in the fact that GIE in RCCI mode drops significantly when the PFI rate is increased, though combustion is phased more favorable from a thermodynamic viewpoint.
- Ignition is affected in other ways for different spray included angles; early injection results in advanced ignition with a narrower spray angle, whereas late injection retards ignition with the same angle. Physical interaction between the diesel jet and piston bowl is believed to cause this contrasting behavior.

Outlook

Further investigation of the port fuel injection on this setup is needed to confirm the issues with distributing the low reactivity fuel in the combustion chamber. Resolving the long combustion tail is a prerequisite for further GIE enhancements. A PFI timing optimization is a first step in investigating this feature. The position of the injection valve can be switched to the other intake channel. Ideally, an injector is fitted in both channels that can be independently actuated. In that way, a sweep of the fuel balance between the two channels can be performed. This will provide crucial insight in the mixing process, but information about the unburned hydrocarbons and carbon monoxide from an exhaust gas analyzer is necessary. Solving the problems of the slow late phase of combustion is expected to increase GIE on three fronts: a direct increase of the combustion efficiency, less need to advance combustion phasing for compensation of combustion losses and an overall shorter burn duration. More insight of the influence of the spray included angle on the high reactivity fuel distribution needs to be obtained using computational fluid dynamics or optical engine experiments, to assess the formulated hypothesis.

Chapter 8
Concluding discussion and outlook

In this dissertation, several approaches have been discussed to increase the gross indicated efficiency of heavy-duty diesel engines within tolerable levels of emissions and mechanical constraints. Two combustion regimes were experimentally studied and compared: conventional diesel combustion and reactivity controlled compression ignition. The main goal was to improve the understanding of the combustion processes in these regimes. This final chapter summarizes the main results and discusses the potential of both regimes to drive the future of sustainable transport.

Design of experiments

Given the large number of operating parameters and associated interactions that influence engine behavior, a systematic experimental approach was required to obtain a comprehensive understanding of the combustion process. The design of experiments (DOE) method was therefore applied in this work to arrange the test runs, and statistical techniques were used to analyze the data. DOE has the advantage of testing multiple parameters with only a limited number of test runs. This method is different from sweeping one parameter at a time, which is the prevailing approach in research. However, considering only one parameter per sweep can lead to missing important interactions and necessitates considerably more runs to identify those interactions. The results in this dissertation showed that DOE is very effective for identifying underlying interactions and its use is highly recommended for future work and in the engine research community in general.

Conventional diesel combustion

Over the years, GIE enhancements in conventional diesel combustion (CDC) have been established by incremental improvements to the combustion system [5]. These improvements include, but are not limited to, increases of the compression ratio, increases of the injection pressure, optimized gas flows by cylinder head improvements and optimized combustion by improved designs of the piston bowl and injector nozzle. In particular, the advancements in fuel injection equipment have led to the emergence of injection strategies in which the fueling rate can be fine-tuned. This can either be achieved by multiple injections (digital rate shaping), or by tuning the injection rate without flow interruption (continuous rate shaping).

A specific double digital pulse strategy has been investigated in Chapter 3, which utilizes a post injection (i.e., a small fuel pulse after a main injection event). Previous research in literature showed that post injections are very effective in reducing soot emission, although the actual efficacy varies strongly between publications. Some of the published works also identified reductions of nitrogen oxides (NO_x) emissions and fuel consumption, while others did not. A general agreement on the effects of post injections is therefore difficult to distill, but some of the variation was expected to be influenced by the underlying operating conditions. However, broad investigations testing a variety of post-injection schedules and other operational settings were lacking. The experimental results in Chapter 3 indeed confirmed several complex interactions of the dwell (crank angle separation with the main injection), split (mass percent-

age of post-injected fuel in the total fuel amount) and other operational parameters like the main injection timing, common rail pressure, rate of exhaust gas recirculation (EGR) and intake manifold pressure. Post injections showed highest effectiveness for soot reduction at low air-excess ratios, i.e., low intake pressure or high EGR rate. A short-dwell, large-split post injection at low load showed the most promise for simultaneous reductions of fuel consumption and pollutant emissions. The takeaway message is that post injections need to be carefully balanced with other operating settings for optimal results.

A promising next step is employing fuel injection equipment capable of continuous fuel rate shaping. Only a limited amount of work on this topic is published to date. An advanced fuel injector, Delphi's DFI7, has therefore been tested and the results were discussed in Chapter 4. This unique double solenoid valve injector is capable of needle lift control, thereby changing the fuel rate within the same injection event. Ramped injection rates were created by delaying the start of actuation of one solenoid valve with respect to the other, while the ramp duration was varied by changing the start delay. Ramped rates were experimentally compared to conventional square profiles. The rationale behind these ramped rates is that the initial temperature and pressure rise rates inside the combustion chamber are tempered by gradually building up the fueling rate. This is thought to reduce compression work and heat transfer, while also mitigating NO_x formation, thereby providing a favorable shift in the NO_x and GIE tradeoff. The results indicated that ramped and square rates produce essentially equal GIE. At elevated engine speed, the peak GIE of ramped rates were shown to be attained at considerably lower NO_x emissions. Although heat transfer loss was shown to be reduced with the application of a ramped rate, a longer burn duration increased the exhaust loss, resulting in a peak GIE equal to that in square rate operation. However, analysis revealed that ramped rates only give limited control over the heat release shape with this combustion system. Vast extensions of the ignition delays were seen, which is thought to be linked to detrimental fuel atomization and evaporation. These outcomes provide valuable input for further research and development. Future work should focus on improving burn rate controllability by reducing the ignition delays. This can be done by increasing the compression ratio, elevating the ramp slope, applying a boot rate or adding a small quantity pilot injection. Above all, the results demonstrate that rate shapes need to be carefully selected for a specific combustion system and load-speed point.

Reactivity controlled compression ignition

Chapter 5 discussed an extensive comparison between reactivity controlled compression ignition (RCCI) and CDC with the use of conventional gasoline and diesel. It was found that at intake pressures comparable with modern turbocharger capabilities, CDC outperformed RCCI on almost all fronts, except for the specific NO_x emissions. The lower GIE in RCCI operation was mainly due to the excessive EGR rates necessary to properly phase combustion, which had an adverse effect on the specific heat capacity ratio. Despite considerably lower heat transfer loss, higher exhaust and combustion losses rendered RCCI inferior. The roles shifted in favor of RCCI at an elevated intake pressure, where an additional reduction of the heat transfer budget improved the performance of RCCI significantly. Although the combustion phasing was advanced beyond an optimum from a thermodynamic viewpoint, this also prevented a further increase of the combustion loss. This distinct balance between thermal and combustion efficiency sets RCCI apart from CDC. In very lean global conditions, it can be advantageous to sacrifice some thermal efficiency points to reach a higher GIE, even if that means timing the centroid of combustion (CA50) before top dead center. CDC substantially benefits from an increase of the intake pressure as well, although for a different reason. By boosting the intake air, CDC instead displayed a reduction of exhaust loss, while the heat transfer budget increased. This difference in the distribution of energy loss channels between the two modes, and the fact that RCCI performs superior at heavily boosted conditions,

are among the main outcomes of this dissertation. Regardless of the low NO_x and soot emissions in RCCI operation, which were both below EURO VI limits, the HC and CO emissions amounted to 3.7 and 3.3 g/kWh, respectively. These values will require a >95% catalytic conversion efficiency to bring them below mandated levels.

The use of gasoline proved to be inadequate for proper RCCI operation. Additional experiments discussed in Chapter 6 therefore focused on the application of E85 as low reactivity fuel. The larger reactivity difference between E85 and diesel provided a wider range of applicable fuel injection settings, which opened up more possibilities to control combustion phasing. A thorough analysis revealed that the rate of heat release displayed specific shapes at given degrees of reactivity stratification, which was in turn controlled by the fuel injection parameters. This shape was characterized by a combustion metric called the burn ratio (R_b):

$$R_b = \frac{CA90 - CA50}{CA50 - CA10} \tag{8.1}$$

The results showed that a rather gradual first stage of combustion followed by a fast burnout is most favorable for optimal GIE. This corresponds to an $R_b < 1$, although the actual optimal value will depend on specific operation conditions. In the load-speed point under investigation, it was found that a PFI rate of 80 wt.% and an SOA of -50 CAD aTDC at an intake manifold pressure of 2.4 bar resulted in a peak GIE of 52.6% with a R_b of 0.65. Further regression analysis showed that the burn ratio is linked to heat transfer and combustion efficiency; lower burn ratios resulted in lower heat transfer loss, but some stratification remained necessary for good combustion efficiency. As in the RCCI tests with gasoline, the regression results indicated that high intake manifold pressures are needed to maximize GIE, but an essential piece of information was added. Heavy boosting should be combined with sufficiently low reactivity stratification levels to fully exploit the low heat transfer capability of RCCI. In case high intake pressures are used in conjunction with late direct injection timing, the low heat transfer benefit is lost. These findings show good correspondence with previous work from the Wisconsin group [118]. Another important outcome is that the application of external EGR was not necessary for optimal combustion phasing with the use of E85. Finally, it was shown with sweeps of SOA at high boost and zero EGR conditions, that the burn ratio is a practical parameter for GIE optimization. The GIE optimum was attained while engine-out NO_x and soot remained below EURO VI regulated levels. Further optimization of combustion efficiency, and thus GIE, is expected with inclusion of the intake temperature in future experiments.

Engine hardware has to be optimized for a specific combustion mode, if that is possible, because it requires the same mode to be used over the entire load range. The combustion system for CDC has been improved considerably in the preceding decades. For RCCI, these incremental advances have yet to be made. Work by other research groups has already provided some insights with, for example, work on specialized piston bowls and chamfered ring lands. Chapter 7 had added experimental results with various spray included angles of the direct injector. These experiments were performed on a newly commissioned test setup, different from the results in the other chapters. The results suggest that an included angle slightly narrower than the original CDC nozzle is best suited for RCCI operation. The diesel appears to be best directed towards the outer regions of the combustion chamber, to counter the lower local temperatures and optimize the combustion efficiency. More importantly, the rates of heat release indicated poor burnout of the charge, which is thought to be linked to fuel trapped in the crevice between piston and liner. Ultimately, this led to a relatively low peak GIE in RCCI operation on this setup, even at high intake manifold pressures, because of two apparent reasons. The first one is low combustion efficiency, due to the poor combustion of fuel in the crevices. The second reason is that CA50 had to be advanced to approximately 4 CAD before top dead center to counteract these high combustion losses, which obviously limits the thermal efficiency at the same time.

An outlook for sustainable transport

The results in Chapter 3 and Chapter 4 showed that the balance between the GIE and pollutant emissions can be favorably shifted in CDC operation with the application of (digital) rate shaping techniques. This shift will be crucial for the advancement of CDC in heavy-duty diesel engines. Still, considerable efforts must be put in selecting appropriate combinations of fuel injection and air path settings and developing the necessary control strategies. Many important interactions have already been identified in this dissertation, for which the design of experiments method proved to be an extremely effective approach. The fuel rate shaping results also indicated that fluid dynamics and chemical kinetics play an important role in the response of the engine. The interplay of these aspects with the thermodynamic behavior are impossible to fully decouple in a metal engine experiment. It is thus of utmost importance that computational fluid dynamics and optical engine experiments remain on the research agenda for the interpretation of relevant physicochemical processes taking place inside the combustion chamber.

The different distributions of energy loss channels in the RCCI and CDC regimes seen in Chapter 5 can have large implications towards brake efficiency. Waste heat recovery is currently researched to push up brake efficiencies of future engines. Organic Rankine cycles are one of these promising technologies, which can be applied to both exhaust gas and coolant streams. Traditional turbomachinery is generally preferred for exhaust waste heat recovery in heavy-duty engines [140], but a large energy potential remains in the coolant stream in CDC operation. However, due to the smaller temperature range in the cooling system as compared to the exhaust stream, recuperation efficiencies are much lower [141]. This implies that a low heat rejection concept like RCCI has a benefit in terms of waste heat recovery, since there is less need to recuperate coolant energy and more waste energy is directed to the exhaust. Some of that waste energy is however stored in the unburned exhaust gas constituents, which need to be released first by an oxidation catalyst. This is in itself a challenge given the typical low combustion efficiency in RCCI operation, and the low exhaust gas temperature especially at low load. Research by other groups [142, 143] does show encouraging results for the application of oxidation catalysts in RCCI to lower the unburned hydrocarbon and carbon monoxide emissions at the tailpipe. The required >95% conversion efficiency was shown to be possible with already available equipment.

The reactivity difference between the PFI and DI fuels is a topic that has been debated much in literature. While these discussions are ongoing, it is worth noting that not only the reactivity difference is of importance, but also the base reactivity of the PFI fuel. The applicability of gasoline was observed in Chapter 5 to be limited not because of an insufficient reactivity difference with diesel, but because of its own relative high autoignition tendency. Hence, it would not have been useful to increase the DI fuel reactivity by applying a synthetic diesel with a higher cetane number. The use of E85 was evidently more useful for resisting premature autoignition. This has an important side effect. External EGR was omitted entirely for GIE optimization in the specific load-speed point under study, which in production engines eases the need to elevate the exhaust pressure for driving an EGR flow. This may ultimately improve the gas exchange process in RCCI operation and thus yield higher brake efficiency.

The results in Chapter 7 suggested that more investigation is needed to optimize the port fuel injection on the MX-13 setup. This can, for example, be done by changing the position of the port fuel injector or increasing the port fuel pressure. The spray included angle affects the high reactivity fuel distribution, which was found to impact the GIE in RCCI operation. Computational fluid dynamics studies are necessary to investigate the mixing processes in more detail. A viable alternative injection approach is investigating double direct injection, i.e., injecting both the low and high reactivity fuel directly into the combustion chamber. This provides an extra parameter for combustion efficiency optimization by better targeting of both the low and high reactivity fuel sprays.

Heavy boosting of intake air has not been a problem for the loads considered in this dissertation, but cylinder pressure data shows that peak pressures in RCCI can already exceed 150 bar at low load. Since typical peak firing pressures are in the range of 200-250 bar, a further increase of intake pressures for higher loads is limited. Moreover, additional losses due to increased friction in bearings might impact on brake efficiency as well. For these reasons, mode-switching is more frequently mentioned in literature [102, 144]. The idea is that RCCI transitions into conventional dual fuel operation at high loads to reduce peak pressures, pressure rise rates or even prevent more aggressive knocking behavior. Clearly, engine controls need to be developed that enable switching between these modes [85], which expectedly brings more complexity in the development of RCCI controls. Aside from high load operation, the low load region has its own challenges for RCCI operation. Due to the essentially premixed charge, the low gas temperatures associated with operating at the lowest loads give rise to excessively high emissions of carbon monoxide and unburned hydrocarbons. This not only has an adverse effect on the eventual brake efficiency, but introduces new challenges for the exhaust gas aftertreatment. Low load operation could thus benefit from CDC, given its high combustion efficiency, but compromises on engine hardware are inevitable to optimize combustion over the whole range of loads.

The envisioned mode-switching strategy does require an intricate control method; not only for stable combustion and an optimal thermodynamic cycle, but perhaps even more so because of complex thermal management in the entire scheme of turbocharging, aftertreatment and the aforementioned waste heat recovery. It is conceivable that in time exhaust energy and intake pressure will be decoupled by electric turbocharging [145]. This leaves more energy for aftertreatment of exhaust gas and relieves the issues of thermal management to some extent. To ascertain that the most possible waste energy is retrieved from the exhaust gas, a turbocompound system may be added [146]. This could be an electric variant to work in conjunction with a separate electric compressor.

In summary, RCCI shows potential to increase the GIE of heavy-duty diesel engines with respect to CDC at highway cruising conditions. The use of E85 is recommended over gasoline, because its lower reactivity allows better control over the combustion process. In addition, RCCI benefits from low heat rejection inside the combustion chamber, which could be beneficial for waste heat recovery. Still, several development steps need to be made, which will require a tremendous amount of resources. CDC has the benefit of being a robust and well-known principle, which works over the entire range of loads. Moreover, this dissertation showed that from the gross indicated point of view, there are still efficiency points left to be gained. It is also likely that engine hardware complexity will have to increase in pursuit of further enhancing brake efficiency, regardless of the operating mode. Whether that investment is worthwhile is largely up the sales market, but political factors play an undeniable role. In a political climate where decisions are in part made based on public opinion, it is the responsibility of the scientific community to inform people so that the best technology for the application may prevail.

The fuel flexibility of future engines will increase in importance, as the shift from fossil-based fuels to sustainable alternatives has already commenced. RCCI and CDC both show promise on that regard with the application of, for example, bio-alcohols and hydrotreated vegetable oils. Such sustainable alternative fuels can be locally produced on both large and small scales, which has the additional advantage of increasing the energy security of nation states. The prevalent association of internal combustion engines with fossil fuels needs to be turned around, for it is obsolete and draws away attention from the fact that vast CO_2 reductions can be made by switching to renewable fuels. CO_2 mandates based on a well-to-wheel analysis are the only appropriate solution. Diesel engines possess all the requirements to make freight transportation a sustainable sector.

Bibliography

[1] Mollenhauer, K., Tschoeke H., "Handbook of diesel engines," Springer, 2010, doi:10.1007/978-3-540-89083-6.

[2] Dohle U., "75 Years of Diesel Injection by Bosch," *MTZ* 64:6-8, 2003.

[3] Reiners N., Schwab W., "Turbocharging Of High Speed Diesel Engines," SAE Technical Paper 510106, 1951, doi:10.4271/510106.

[4] Watson, N., "Turbochargers for the 1980s-Current Trends and Future Prospects," SAE Technical Paper 790063, 1979, doi:10.4271/790063.

[5] Stanton, D., "Systematic Development of Highly Efficient and Clean Engines to Meet Future Commercial Vehicle Greenhouse Gas Regulations," *SAE Int. J. Engines* 6(3):1395-1480, 2013, doi:10.4271/2013-01-2421.

[6] Hoek, G., Krishnan, R.M., Beelen, R., Peters, A., et al., "Long-term air pollution exposure and cardio- respiratory mortality: a review," *Environ. Health* 12(43):1-15, 2013, doi 10.1186/1476-069X-12-43.

[7] Wolff, H., Perry, L., "Trends in Clean Air Legislation in Europe: Particulate Matter and Low Emission Zones," *Rev. Environ. Econ. Pol.* 4(2):293-308, 2010, doi:10.1093/reep/req008.

[8] Boogaard, H., Janssen N.A.H., Fischer P.H., Kos, G.P.A., et al., "Impact of low emission zones and local traffic policies on ambient air pollution concentrations," *Sci. Total Environ.* 435:132-140, 2012, doi:10.1016/j.scitotenv.2012.06.089.

[9] Cesaroni, G., Boogaard H., Jonkers, S., Porta, D., et al., "Health benefits of traffic-related air pollution reduction in different socioeconomic groups: the effect of low-emission zoning in Rome," *Occup. Environ. Med.* 69:133-139, 2012, doi:10.1136/oem.2010.063750.

[10] Wamelink G.W.W., de Knegt, B., Pouwels R., Schuiling C., et al., "Considerable environmental bottlenecks for species listed in the Habitats and Birds Directives in the Netherlands," *Biol. Convers.* 165:43-53, 2013, doi:10.1016/j.biocon.2013.05.012.

[11] Crowley, T.J., "Causes of Climate Change Over the Past 1000 Years," *Science* 289:270-277, 2000, doi:10.1126/science.289.5477.270.

[12] Parmesan, C., "Ecological and Evolutionary Responses to Recent Climate Change," *Annu. Rev. Ecol. Evol. Syst.* 37:637-669, 2006, doi:10.1146/annurev.ecolsys.37.091305.110100.

[13] Joshi, A., "Review of Vehicle Engine Efficiency and Emissions," SAE Technical Paper 2019-01-0314, 2019, doi:10.4271/2019-01-0314.

[14] The European Parliament and the Council of the European Union, "Regulation of the European Parliament and the Council of 20 June 2019 setting CO_2 emission performance standards for new heavy-duty vehicles," accessed via eur-lex.europa.eu with CELEX no. 32019R1242 on February 29, 2020.

[15] Li, L., Gong, Y., Deng, J., Gong, X., "CO_2 Reduction Request and Future High-Efficiency Zero-Emission Argon Power Cycle Engine," *Automot. Innov.* 1:43–53, 2018, doi:10.1007/s42154-018-0007-y.

[16] Annand, W.J.D., "Heat transfer in the cylinders of reciprocating internal combustion engines," *Proc. Instn. Mech. Engrs.* 177(36):973-990, 1963, doi:10.1243/PIME_PROC_1963_177_069_02.

[17] Borman, G., Nishiwaki K., "Internal-combustion engine heat transfer," *Prog. Energ. Combust.* 13(1):1-46, 1987, doi:10.1016/0360-1285(87)90005-0.

[18] Heywood, J.B., "Internal combustion engine fundamentals," McGraw-Hill, 1988.

[19] Dec, J., "A Conceptual Model of DI Diesel Combustion Based on Laser-Sheet Imaging," SAE Technical Paper 970873, 1997, doi:10.4271/970873.

[20] Yao, M., Zheng Z., Liu, H., "Progress and recent trends in homogeneous charge compression ignition (HCCI) engines," *Progr. Energy and Combust.* 35:398-437, 2009, doi:10.1016/j.pecs.2009.05.0011.

[21] Saxena, S., Bedoya I.D., "Fundamental phenomena affecting low temperature combustion and HCCI engines, high load limits and strategies for extending these limits," *Progr. Energy and Combust.* 39:457-488, 2013, doi:10.1016/j.pecs.2013.05.002.

[22] Dec, J., Sjöberg, M., "Isolating the Effects of Fuel Chemistry on Combustion Phasing in an HCCI Engine and the Potential of Fuel Stratification for Ignition Control," SAE Technical Paper 2004-01-0557, 2004, doi:10.4271/2004-01-0557.

[23] Agarwal K.A., Sing, A.P., Maurya R.K., "Evolution, challenges and path forward for low temperature combustion engines," *Progr. Energy and Combust.* 61:1-56, 2017, doi:10.1016/j.pecs.2017.02.001.

[24] Olsson, J., Tunestål, P., Haraldsson, G., Johansson, B., "A Turbo Charged Dual Fuel HCCI Engine," SAE Technical Paper 2001-01-1896, 2001, doi:10.4271/2001-01-1896.

[25] Ogawa, H., Miyamoto, N., Li, C., Nakazawa, S. et al., "Low Emission and Knock-Free Combustion with Rich and Lean Biform Mixture in a Dual-Fuel CI Engine with Induced LPG as the Main Fuel," SAE Technical Paper 2001-01-3502, 2001, doi:10.4271/2001-01-3502.

[26] Tomita, E., Kawahara, N., Piao, Z., Yamaguchi, R., "Effects of EGR and Early Injection of Diesel Fuel on Combustion Characteristics and Exhaust Emissions in a Methane Dual Fuel Engine," SAE Technical Paper 2002-01-2723, 2002, doi:10.4271/2002-01-2723.

[27] Inagaki, K., Fuyuto, T., Nishikawa, K., Nakakita, K. et al., "Dual-Fuel PCI Combustion Controlled by In-Cylinder Stratification of Ignitability," SAE Technical Paper 2006-01-0028, 2006, doi:10.4271/2006-01-0028.

[28] Kokjohn, S., Hanson, R., Splitter, D., Reitz, R., "Experiments and Modeling of Dual-Fuel HCCI and PCCI Combustion Using In-Cylinder Fuel Blending," *SAE Int. J. Engines* 2(2):24-39, 2010, doi:10.4271/2009-01-2647.

[29] Reitz, R.D., Duraisamy, G., "Review of high efficiency and clean reactivity controlled compression ignition (RCCI) in internal combustion engines", *Progr. Energy and Combust.* 46:12-71, 2015, doi:10.1016/j.pecs.2014.05.003.

[30] Paykani, A., Kakaee, A., Rahnama, P., Reitz, R.D., "Progress and recent trends in reactivity-controlled compression ignition engines", *Int. J. Engine Res.* 17(5):481-524, 2016. doi:10.1177/1468087415593013.

[31] Brunt, M., Rai, H., Emtage, A., "The Calculation of Heat Release Energy from Engine Cylinder Pressure Data," SAE Technical Paper 981052, 1998, doi:10.4271/981052.

[32] Brunt, M., Platts, K., "Calculation of Heat Release in Direct Injection Diesel Engines," SAE Technical Paper 1999-01-0187, 1999, doi:10.4271/1999-01-0187.

[33] Pedrozo, V., May, I., Dallo Nora, M., Cairns, A., Zhao, H., "Experimental analysis of ethanol dual-fuel combustion in a heavy-duty diesel engine: an optimisation at low load," *Appl. Energ.* 165:166-182, 2016, doi:10.1016/j.apenergy.2015.12.052.

[34] Spanjers, C.S., Beach, C.A., Jones, A.J., Dauenhauer, P.J., "Increasing flame ionization detector (FID) sensitivity using post-column oxidation-methanation," *Analytic. Methods* 9:1928-1934, 2017, doi:10.1039/c6ay03363f.

[35] Kar, K., Cheng, W.K., "Speciated engine-out organic gas emissions from a PFI-SI engine operating on ethanol/gasoline mixtures," SAE Technical Paper 2009-01-2673, 2009, doi:10.4271/2009-01-2673.

[36] Woschni, G., "A Universally Applicable Equation for the Instantaneous Heat Transfer Coefficient in the Internal Combustion Engine," SAE Technical Paper 670931, 1967, doi:10.4271/670931.

[37] Hohenberg, G., "Advanced Approaches for Heat Transfer Calculations," SAE Technical Paper 790825, 1979, doi:10.4271/790825.

[38] Chang, J., Güralp, O., Filipi, Z., Assanis, D. et al., "New Heat Transfer Correlation for an HCCI Engine Derived from Measurements of Instantaneous Surface Heat Flux," SAE Technical Paper 2004-01-2996, 2004, doi:10.4271/2004-01-2996.

[39] Bakker, P., Willems, R., Dam, N., Somers, B. et al., "Investigation of Late Stage Conventional Diesel Combustion - Effect of Additives," SAE Technical Paper 2018-01-1787, 2018, doi:10.4271/2018-01-1787.

[40] The European Parliament and the Council of the European Union, "Regulation of the European Parliament and of the Council of 18 June 2009 on type-approval of motor vehicles and engines with respect to emissions from heavy duty vehicles (Euro VI) and on access to vehicle repair and maintenance information," accessed via eurlex.europa.eu with CELEX no. 32009R0595 on March 12, 2020.

[41] Christian, R., Knopf, F., Jaschek, A., Schindler, W., "Eine Neue Messmethodik der Bosch-zahl mit Erhöhter Empfindlichkeit," *MTZ* 54:16-22, 1993.

[42] Northrop, W.F., Bohac, S.V., Chin, J., Assanis, D.N., "Comparison of Filter Smoke Number and Elemental Carbon Mass From Partially Premixed Low Temperature Combustion in a Direct-Injection Diesel Engine," *ASME. J. Eng. Gas Turbines Power* 133(10):102804, doi:10.1115/1.4002918.

[43] Gothekar, S., Vora, K., Mutha, G., Walke, N. et al., "Design of Experiments: A Systems Approach to Engine Optimization for Lower Emissions," SAE Technical Paper 2007-26-012, 2007, doi:10.4271/2007-26-012.

[44] Fridriksson, H.S., Hajireza, S., Tunér, M., Sunén, B., "A CFD Investigation of Heat Transfer in a Diesel Fueled PPC Engine Applying Design of Experiments," Proceedings of the ASME 2012 Internal Combustion Engine Division Fall Technical Conference, Vancouver, BC, Canada, September 23–26, 2012, doi:10.1115/ICEF2012-92059

[45] Sjoblom, J., Andric, J., Faghani, E., "Intrinsic Design of Experiments for Modeling of Internal Combustion Engines," SAE Technical Paper 2018-01-1156, 2018, doi:10.4271/2018-01-1156.

[46] Li J., Yang W.M., Goh T.N., An H., Maghbouli A., "Study of RCCI (reactivity controlled compression ignition) engine by means of statistical experimental design," *Energy* 78:777-787, 2014, doi:10.1016/j.energy.2014.10.071.

[47] Box G.E.P., Wilson K.B., "On the experimental attainment of optimum conditions," *J Roy Stat Soc B Met* 13:1-45, 1951.

[48] Box, G., Hunter, J., Hunter, W., "Statistics for experimenters: design, discovery, and innovation - 2nd edition," Wiley, 2005.

[49] Andersson, Ö., "Experiment! - Planning, Implementing and Interpreting," Wiley, 2012.

[50] De Cuyper, T., Demuynck, J., Broekaert, S., De Paepe, M., "Heat transfer in premixed spark ignition engines part II: Systematic analysis of the heat transfer phenomena," *Energy* 116:851-860, 2016, doi:10.1016/j.energy.2016.10.032.

[51] Chen, S., "Simultaneous Reduction of NOx and Particulate Emissions by Using Multiple Injections in a Small Diesel Engine," SAE Technical Paper 2000-01-3084, 2000, doi:10.4271/2000-01-3084.

[52] Badami, M., Mallamo, F., Millo, F., Rossi, E., "Influence of Multiple Injection Strategies on Emissions, Combustion Noise and BSFC of a DI Common Rail Diesel Engine," SAE Technical Paper 2002-01-0503, 2002, doi:10.4271/2002-01-0503.

[53] Desantes, J., Arrègle, J., López, J., García, A., "A Comprehensive Study of Diesel Combustion and Emissions with Post-injection," SAE Technical Paper 2007-01-0915, 2007, doi:10.4271/2007-01-0915.

[54] Vanegas, A., Won, H., Felsch, C., Gauding, M. et al., "Experimental Investigation of the Effect of Multiple Injections on Pollutant Formation in a Common-Rail DI Diesel Engine," SAE Technical Paper 2008-01-1191, 2008, doi:10.4271/2008-01-1191.

[55] Benajes, J., Molina, S., García, J., "Influence of Pre- and Post-Injection on the Performance and Pollutant Emissions in a HD Diesel Engine," SAE Technical Paper 2001-01-0526, 2001, doi:10.4271/2001-01-0526.

[56] Payri, F., Benajes, J., Pastor, J., Molina, S., "Influence of the Post-Injection Pattern on Performance, Soot and NOx Emissions in a HD Diesel Engine," SAE Technical Paper 2002-01-0502, 2002, doi:10.4271/2002-01-0502.

[57] Sperl, A., "The Influence of Post-Injection Strategies on the Emissions of Soot and Particulate Matter in Heavy Duty Euro V Diesel Engine," SAE Technical Paper 2011-36-0350, 2011, doi:10.4271/2011-36-0350.

[58] O'Connor, J., Musculus, M., "Post Injections for Soot Reduction in Diesel Engines: A Review of Current Understanding," *SAE Int. J. Engines* 6(1):400-421, 2013, doi:10.4271/2013-01-0917.

[59] Hotta, Y., Inayoshi, M., Nakakita, K., Fujiwara, K. et al., "Achieving Lower Exhaust Emissions and Better Performance in an HSDI Diesel Engine with Multiple Injection," SAE Technical Paper 2005-01-0928, 2005, doi:10.4271/2005-01-0928.

[60] Mingfa, Y., Hu, W., Zunqing, Z., Yan, Y., "Experimental Study of Multiple Injections and Coupling Effects of Multi-Injection and EGR in a HD Diesel Engine," SAE Technical Paper 2009-01-2807, 2009, doi:10.4271/2009-01-2807.

[61] Rakesh, B., Bakara, A.S., Sarware, A., "Effect of Fuel Injection Parameters and EGR on Exhaust Emission of a 3 L Diesel Engine," SAE Technical Paper 2015-01-2814, 2015, doi:10.4271/2015-01-2814.

[62] Horibe, N., Komizo, T., Sumimoto, T., Wang, H. et al., "Smoke Reduction Effects by Post Injection for Various Injection Parameters and Combustion Chamber Shapes in a Diesel Engine," SAE Technical Paper 2014-01-2634, 2014, doi:10.4271/2014-01-2634.

[63] Horibe, N., Komizo, T., Mamizuka, Y., Sumimoto, T. et al., "Analysis of Mixture Formation Process in a Diesel Engine with Post Injection," SAE Technical Paper 2015-01-1836, 2015, doi:10.4271/2015-01-1836.

[64] Montgomery, D., Reitz, R., "Optimization of Heavy-Duty Diesel Engine Operating Parameters Using A Response Surface Method," SAE Technical Paper 2000-01-1962, 2000, doi:10.4271/2000-01-1962.

[65] d'Ambrosio, S., Ferrari, A., "Potential of multiple injection strategies implementing the after shot and optimized with the design of experiments procedure to improve diesel engine emissions and performance," *Applied Energy* 155:933-946, 2015, doi:10.1016/j.apenergy.2015.05.124.

[66] Martin, J., Sun, C., Boehman, A., O'Connor, J., "Experimental Study of Post Injection Scheduling for Soot Reduction in a Light-Duty Turbodiesel Engine," SAE Technical Paper 2016-01-0726, 2016, doi:10.4271/2016-01-0726.

[67] Pandurangi, S., Frapolli, N., Bolla, M., Boulouchos, K. et al., "Influence of EGR on Post-Injection Effectiveness in a Heavy-Duty Diesel Engine Fuelled with n-Heptane," *SAE Int. J. Engines* 7(4):1851-1862, 2014, doi:10.4271/2014-01-2633.

[68] Naber, J., Siebers, D., "Effects of Gas Density and Vaporization on Penetration and Dispersion of Diesel Sprays," SAE Technical Paper 960034, 1996, doi:10.4271/960034.

[69] Graham, M., Crossley, S., Harcombe, T., Keeler, N. et al., "Beyond Euro VI - Development of A Next Generation Fuel Injector for Commercial Vehicles," SAE Technical Paper 2014-01-1435, 2014, doi:10.4271/2014-01-1435.

[70] Ritter, D., Korkmaz, M., Pitsch, H., Abel, D., Albin, T., "Optimization-based fuel injection rate digitalization for combustion rate shaping," 2019 American Control Conference (ACC), 2019, pp. 5103-5110.

[71] Montgomery, D., Reitz, R., "Effects of Multiple Injections and Flexible Control of Boost and EGR on Emissions and Fuel Consumption of a Heavy-Duty Diesel Engine," SAE Technical Paper 2001-01-0195, 2001, doi:10.4271/2001-01-0195.

[72] Dronniou, N., Lejeune, M., Balloul, I., Higelin, P., "Combination of High EGR Rates and Multiple Injection Strategies to Reduce Pollutant Emissions," SAE Technical Paper 2005-01-3726, 2005, doi:10.4271/2005-01-3726.

[73] Gambhir, H., Barman, J., Patchappalam, K., "Experimental Investigation on the Effect of Pilot and Post Injection on Engine Performance and Emissions," SAE Technical Paper 2018-28-0015, 2018, doi:10.4271/2018-28-0015.

[74] Willems, R., Bakker, P., Dreezen, R., Somers, B., "The Impact of Operating Conditions on Post-Injection Efficacy; a Study Using Design-of-Experiments," SAE Technical Paper 2018-01-0229, 2018, doi:10.4271/2018-01-0229.

[75] Willems, R., Willems, F., Simpson, T., Albrecht, B. et al., "Ramped Versus Square Injection Rate Experiments in a Heavy-Duty Diesel Engine," *SAE Int. J. Adv. & Curr. Prac. in Mobility* 2(3):1322-1336, 2020, https://doi.org/10.4271/2020-01-0300.

[76] Ganser, M., "Common Rail Injector with Injection Rate Control," SAE Technical Paper 981927, 1998, doi:10.4271/981927.

[77] Mohan, B., Yang, W., Chou, S., "Fuel injection strategies for performance improvement and emissions reduction in compression ignition engine - A review," *Renew. Sust. Energy Reviews* 28:664-676, 2013, doi:10.1016/j.rser.2013.08.051.

[78] Siebers, D., Higgins, B., "Flame Lift-Off on Direct-Injection Diesel Sprays Under Quiescent Conditions," SAE Technical Paper 2001-01-0530, 2001, doi:10.4271/2001-01-0530.

[79] Desantes, J.M., Benajes, J., Molina, S., González, C.A., "The modification of the fuel injection rate in heavy-duty diesel engines. Part 1: Effects on engine performance and emissions," *Appl. Thermal Eng.* 24:2701-2714, 2004, doi:10.1016/j.applthermaleng.2004.05.003.

[80] Desantes, J.M., Benajes, J., Molina, S., González, C.A., "The modification of the fuel injection rate in heavy-duty diesel engines. Part 2: Effects on combustion," *Appl. Thermal Eng.* 24:2715-2726, 2004, doi:10.1016/j.applthermaleng.2004.05.004.

[81] Kohketsu, S., Tanabe, K., Mori, K., "Flexibly Controlled Injection Rate Shape with Next Generation Common Rail System for Heavy Duty DI Diesel Engines," SAE Technical Paper 2000-01-0705, 2000, doi:10.4271/2000-01-0705.

[82] Coldren, D., Schuricht, S., Smith, R., "Hydraulic Electronic Unit Injector with Rate Shaping Capability," SAE Technical Paper 2003-01-1384, 2003, doi:10.4271/2003-01-1384.

[83] Tanabe, K., Kohketsu, S., Nakayama, S., "Effect of Fuel Injection Rate Control on Reduction of Emissions and Fuel Consumption in a Heavy Duty DI Diesel Engine," SAE Technical Paper 2005-01-0907, 2005, doi:10.4271/2005-01-0907.

[84] Willems, R.C., Willems, F.P.T., Deen, N.G., Somers, L.M.T., "A Comparison of Load-Load Efficiency Optimization on a Heavy-Duty Engine Operated With Gasoline-Diesel RCCI and CDC," Proceedings of the ASME ICEF2019, October 20-23, 2019, Chicago, USA, doi:10.1115/ICEF2019-7149.

[85] Indrajuana, A., Bekdemir, C., Feru, E., Willems, F., "Towards Model-Based Control of RCCI-CDF Mode-Switching in Dual Fuel Engines," SAE Technical Paper 2018-01-0263, 2018, doi:10.4271/2018-01-0263.

[86] Wissink, M., Reitz, R., "Direct Dual Fuel Stratification, a Path to Combine the Benefits of RCCI and PPC," *SAE Int. J. Engines* 8(2):878-889, 2015, doi:10.4271/2015-01-0856.

[87] Kokjohn, S.L., Hanson, R.M., Splitter, D.A., Reitz, R.D., "Fuel reactivity controlled compression ignition (RCCI): a pathway to controlled high-efficiency clean combustion," *Int. J. Engine Res.* 12:209-226, 2010, doi:10.1177/1468087411401548.

[88] Hanson, R., Kokjohn, S., Splitter, D., Reitz, R., "An Experimental Investigation of Fuel Reactivity Controlled PCCI Combustion in a Heavy-Duty Engine," *SAE Int. J. Engines* 3(1):700-716, 2010, doi:10.4271/2010-01-0864.

[89] Splitter, D., Hanson, R., Kokjohn, S., Reitz, R., "Reactivity Controlled Compression Ignition (RCCI) Heavy-Duty Engine Operation at Mid- and High-Loads with Conventional and Alternative Fuels," SAE Technical Paper 2011-01-0363, 2011, doi:10.4271/2011-01-0363.

[90] Ickes, A., Wallner, T., Zhang, Y., De Ojeda, W., "Impact of Cetane Number on Combustion of

a Gasoline-Diesel Dual-Fuel Heavy-Duty Multi-Cylinder Engine," *SAE Int. J. Engines* 7(2):860-872, 2014, doi:10.4271/2014-01-1309.

[91] Tuner, M., "Review and Benchmarking of Alternative Fuels in Conventional and Advanced Engine Concepts with Emphasis on Efficiency, CO_2, and Regulated Emissions," SAE Technical Paper 2016-01-0882, 2016, doi:10.4271/2016-01-0882.

[92] Asad, U., Zheng, M., Tjong, J., "Experimental Investigation of Diesel-Ethanol Premixed Pilot-Assisted Combustion (PPAC) in a High Compression Ratio Engine," SAE Int. J. Engines 9(2):1059-1071, 2016, doi:10.4271/2016-01-0781.

[93] Pedrozo, V., May, I., Zhao, H., "Characterization of Low Load Ethanol Dual-Fuel Combustion using Single and Split Diesel Injections on a Heavy-Duty Engine," SAE Technical Paper 2016-01-0778, 2016, doi:10.4271/2016-01-0778.

[94] Curran, S., Hanson, R., Wagner, R., "Effect of E85 on RCCI Performance and Emissions on a Multi-Cylinder Light-Duty Diesel Engine," SAE Technical Paper 2012-01-0376, 2012, doi:10.4271/2012-01-0376.

[95] Willems, F., Kupper, F., Ramesh, S., Indrajuana, A. et al., "Coordinated Air-Fuel Path Control in a Diesel-E85 RCCI Engine," SAE Technical Paper 2019-01-1175, 2019, doi:10.4271/2019-01-1175.

[96] Benajes, J., García, A., Monsalve-Serrano, J., Villalta, D., "Benefits of E85 versus gasoline as low reactivity fuel for an automotive diesel engine operating in reactivity controlled compression ignition mode," *Energ. Convers. Manage.* 159:85-95, 2018, doi:10.1016/j.enconman.2018.01.015.

[97] Leermakers, C., Van den Berge, B., Luijten, C., Somers, L. et al., "Gasoline-Diesel Dual Fuel: Effect of Injection Timing and Fuel Balance," SAE Technical Paper 2011-01-2437, 2011, doi:10.4271/2011-01-2437.

[98] Curran, S., Hanson, R., Wagner, R., Reitz, R., "Efficiency and Emissions Mapping of RCCI in a Light-Duty Diesel Engine," SAE Technical Paper 2013-01-0289, 2013, doi:10.4271/2013-01-0289.

[99] Imtenan, S., Varman, M., Masjuki, H.H. Kalam, M.A., et al., "Impact of low temperature combustion attaining strategies on diesel engine emissions for diesel and biodiesels: A review," *Energ. Convers. Manage.* 80:329-356, 2014, doi:10.1016/j.enconman.2014.01.020.

[100] Splitter, D., Wissink, M., DelVescovo, D., Reitz, R., "RCCI Engine Operation Towards 60% Thermal Efficiency," SAE Technical Paper 2013-01-0279, 2013, doi:10.4271/2013-01-0279.

[101] Soloiu, V., Moncada, J., Gaubert, R., Harp, S., et al., "GTL Kerosene and N-Butanol in RCCI Mode –Combustion and Emissions Investigation," Proceedings of the ASME 2018 Internal Combustion Engine Division Fall Technical Conference, San Diego, California, USA, November 4–7, 2018, doi:10.1115/ICEF2018-9585.

[102] Nieman, D., Morris, A., Neely, G., Matheaus, A. et al., "Utilizing Multiple Combustion Modes to Increase Efficiency and Achieve Full Load Dual-Fuel Operation in a Heavy-Duty Engine," SAE Technical Paper 2019-01-1157, 2019, doi:10.4271/2019-01-1157.

[103] Johnson, T., "Vehicular Emissions in Review," SAE Int. J. Engines 7(3):1207-1227, 2014, doi:10.4271/2014-01-1491.

[104] Olmeda, P., García, A., Monsalve-Serrano, J., Sari, R., "Experimental investigation on RCCI heat transfer in a light duty diesel with different fuels: Comparison versus conventional diesel combustion," *Appl. Thermal Eng.* 144:424-436, 2018, doi:10.1016/j.applthermaleng.2018.08.082.

[105] Curran, S., Prikhodko, V., Cho, K., Sluder, C. et al., "In-Cylinder Fuel Blending of Gasoline/Diesel for Improved Efficiency and Lowest Possible Emissions on a Multi-Cylinder Light-Duty Diesel Engine," SAE Technical Paper 2010-01-2206, 2010, doi:10.4271/2010-01-2206.

[106] Heuser, B., Ahling, S., Kremer, F., Pischinger, S. et al., "Experimental Investigation of a RCCI Combustion Concept with In-Cylinder Blending of Gasoline and Diesel in a Light Duty Engine," SAE Technical Paper 2015-24-2452, 2015, doi:10.4271/2015-24-2452.

[107] Kokjohn, S., Hanson, R., Splitter, D., Kaddatz, J. et al., "Fuel Reactivity Controlled Compression Ignition (RCCI) Combustion in Light- and Heavy-Duty Engines," *SAE Int. J. Engines* 4(1):360-374, 2011, doi:10.4271/2011-01-0357.

[108] Pedrozo, V.B., May, I., Guan, W., Zhao, H., "High efficiency ethanol-diesel dual-fuel combustion: a comparison against conventional diesel combustion from low to full engine load," *Fuel* 230:440-451, 2018, doi:10.1016/j.fuel.2018.05.034.

[109] Leermakers, C., Somers, L., Johansson, B., "Combustion Phasing Controllability with Dual Fuel Injection Timings," SAE Technical Paper 2012-01-1575, 2012, doi:10.4271/2012-01-1575.

[110] Ma, S., Zheng, Z., Liu, H., Zhang, Q., Yao, M., "Experimental investigation of the effects of diesel injection strategy on gasoline/diesel dual-fuel combustion," *Appl. Energ.* 109:202-212, 2013, doi:10.1016/j.apenergy.2013.04.012.

[111] Molina, S., García, A., Pastor, J.M., Belarte, E., Balloul, I., "Operating range extension of RCCI combustion concept from low to full load in a heavy-duty engine," *Appl. Energ.* 143:211-227, 2015, doi:10.1016/j.apenergy.2015.01.035.

[112] Ickes, A., Hanson, R., Wallner, T., "Impact of Effective Compression Ratio on Gasoline-Diesel Dual-Fuel Combustion in a Heavy-Duty Engine Using Variable Valve Actuation," SAE Technical Paper 2015-01-1796, 2015, doi:10.4271/2015-01-1796.

[113] Molina, S., García, A., Monsalve-Serrano, J., Estepa, D., "Miller cycle for improved efficiency, load range and emissions in a heavy-duty engine running under reactivity controlled compression ignition combustion," *Appl. Thermal Eng.* 136:161-168, 2018, doi:10.1016/j.applthermaleng.2018.02.106.

[114] Doosje, E., Willems, F., and Baert, R., "Experimental Demonstration of RCCI in Heavy-Duty Engines using Diesel and Natural Gas," SAE Technical Paper 2014-01-1318, 2014, doi:10.4271/2014-01-1318.

[115] Walker, N.R., Wissink, M.L., DelVescovo, D.A., Reitz, R.D., "Natural gas for high load dual-fuel reactivity controlled compression ignition (RCCI) in heavy-duty engines," Proceedings of the ASME 2014 Internal Combustion Engine Division Fall Technical Conference, Columbus, Indiana, USA, October 19–22, 2014, doi:10.1115/ICEF2014-5620.

[116] Cardona, C.A., Sánchez, O.J., "Fuel ethanol production: process design trends and integration opportunities", *Bioresource Technol.* 98:2415-2457, 2007, doi:10.1016/j.biortech.2007.01.002.

[117] Benajes, J., García, A., Monsalve-Serrano, J., Sari, R.L., "Fuel consumption and engine-out emissions estimation of a light-duty engine running in dual-mode RCCI/CDC with different fuels and driving cycles," *Energy* 157:19-30, 2018, doi:10.1016/j.energy.2018.05.144.

[118] Splitter, D., Wissink, M., DelVescovo, D., Reitz, R., "Improving the Understanding of Intake and Charge Effects for Increasing RCCI Engine Efficiency," SAE Int. J. Engines 7(2):913-927, 2014, doi:10.4271/2014-01-1325.

[119] Egüz, U., Maes, N.C.J., Leermakers, C.A.J., Somers, L.M.T., de Goey, L.P.H., "Predicting auto-ignition characteristics of RCCI combustion using amulti-zone model," *Int. J. Automot. Techn.* 14(5):693-699, 2013, doi:10.1007/s12239-013-0075-2.

[120] Kokjohn, S.L., Musculus, M.P.B., Reitz, R.D., "Evaluating temperature and fuel stratification for heat-release rate control in a reactivity-controlled compression-ignition engine using optical diagnostics and chemical kinetics modeling," *Combust. Flame* 162 (2015) 2729-2742. https://doi.org/10.1016/j.combustflame.2015.04.009.

[121] Sjoberg, M., Dec, J., "Ethanol Autoignition Characteristics and HCCI Performance for Wide Ranges of Engine Speed, Load and Boost," *SAE Int. J. Engines* 3(1):84-106, 2010, doi:10.4271/2010-01-0338.

[122] Bekdemir, C., Baert, R., Willems, F., Somers, B., "Towards Control-Oriented Modeling of Natural Gas-Diesel RCCI Combustion," SAE Technical Paper 2015-01-1745, 2015, doi:10.4271/2015-01-1745.

[123] Musculus, M.P.B., Kattke, K., "Entrainment waves in diesel jets," *SAE Int. J. Engines* 2:1170-1193, 2009, doi:0.4271/2009-01-1355.

[124] Leach, F., Ismail, R., Davy, M., Weall, A., Cooper, B., "The effect of a stepped lip piston design on performance and emissions from a high-speed diesel engine," *Appl. Energ.* 215:679-689, 2018, doi:10.1016/j.apenergy.2018.02.076.

[125] Zhang T., Eismark, J., Munch, K., Denbratt, I., "Effects of a wave-shaped piston bowl geometry on the performance of heavy-duty Diesel engines fueled with alcohols and biodiesel blends," *Renew. Energ.* 148:512-522, 2020, doi:10.1016/j.renene.2019.10.057

[126] Benajes, J., Novella R., Pastor, J.M., Hernández-López, A., et al., "Optimization of the combustion system of a medium duty direct injection diesel engine by combining CFD modeling with experimental validation," *Energ. Convers. Manage.* 110:212-229, 2016, doi:10.1016/j.enconman.2015.12.010.

[127] Gehmlich, R.K., Mueller, C.J., Ruth, D.J., Nilsen, C.W., et al., "Using ducted fuel injection to attenuate or prevent soot formation in mixing-controlled combustion strategies for engine applications," *Appl. Energ.* 226:1169-1189, 2018, doi:10.1016/j.apenergy.2018.05.078,

[128] García, A., Monsalve-Serrano, J., Villalta, D., Sari, R.L., "Performance of a conventional diesel aftertreatment system used in a medium-duty multi-cylinder dual-mode dual-fuel engine," *Energ. Convers. Manag.* 184:327-337, 2019, doi:10.1016/j.enconman.2019.01.069.

[129] Splitter, D., Wissink, M., Kokjohn, S., and Reitz, R., "Effect of Compression Ratio and Piston Geometry on RCCI Load Limits and Efficiency," SAE Technical Paper 2012-01-0383, 2012, doi:10.4271/2012-01-0383.

[130] Lim, J.H., Reitz, R.D., "Improving the Efficiency of Low Temperature Combustion Engines Using a Chamfered Ring-Land," *ASME. J. Eng. Gas Turbines Power* 137:111509, doi:10.1115/1.4030284.

[131] Dempsey, A., Walker, N., Reitz, R., "Effect of Piston Bowl Geometry on Dual Fuel Reactivity Controlled Compression Ignition (RCCI) in a Light-Duty Engine Operated with Gasoline/Diesel and Methanol/Diesel," *SAE Int. J. Engines* 6(1):78-100, 2013, doi:10.4271/2013-01-0264.

[132] Benajes, J., García A., Monsalve-Serrano, J., Boronat, V., "Dual-Fuel Combustion for Future Clean and Efficient Compression Ignition Engines," *Appl. Sci.* 7(36), 2017, doi:10.3390/app7010036.

[133] Walker, N., Dempsey, A., Andrie, M., Reitz, R., "Use of Low-Pressure Direct-Injection for Reactivity Controlled Compression Ignition (RCCI) Light-Duty Engine Operation," *SAE Int. J. Engines* 6(2):1222-1237, 2013, doi:10.4271/2013-01-1605.

[134] Poorghasemi K., Saray, R.K., Ansari, E., Irdmousa, B.K., et al., "Effect of diesel injection strategies on natural gas/diesel RCCI combustion characteristics in a light duty diesel engine," *Appl. Energ.* 199:430-446, 2017, doi:10.1016/j.apenergy.2017.05.011.

[135] Wissink, M.L., Kavuri, C., Curran, S.J., Kokjohn, S.L., "Spray-Wall Interactions in a Small-Bore, Multi-Cylinder Engine Operating With Reactivity-Controlled Compression Ignition," Proceedings of the ASME 2017 Internal Combustion Engine Division Fall Technical Conference, Seattle, Washington, USA, October 15–18, 2017, doi:10.1115/ICEF2017-3607.

[136] Martin, G., Mueller, C., Milam, D., Radovanovic, M. et al., "Early Direct-Injection, Low-Temperature Combustion of Diesel Fuel in an Optical Engine Utilizing a 15-Hole, Dual-Row, Narrow-Included-Angle Nozzle," *SAE Int. J. Engines* 1(1):1057-1082, 2009, doi:10.4271/2008-01-2400.

[137] Kokjohn, S., Reitz, R., Splitter, D., Musculus, M., "Investigation of Fuel Reactivity Stratification for Controlling PCI Heat-Release Rates Using High-Speed Chemiluminescence Imaging and Fuel Tracer Fluorescence," *SAE Int. J. Engines* 5(2):248-269, 2012, doi:10.4271/2012-01-0375.

[138] Tang, Q., Liu, H., Li, M., Yao, M., "Multiple optical diagnostics on the effect of fuel stratification degree on reactivity controlled compression ignition," *Fuel* 202:688-698, 2017, doi:10.1016/j.fuel.2017.04.136.

[139] Tang, Q., Liu, H., Yao, M., "Simultaneous Measurement of Natural Flame Luminosity and Emission Spectra in a RCCI Engine under Different Fuel Stratification Degrees," *SAE Int. J. Engines* 10(3):1155-1162, 2017, https://doi.org/10.4271/2017-01-0714.

[140] Sprouse C., Depcik, C., "Review of organic Rankine cycles for internal combustion engine exhaust waste heat recovery," *Appl. Thermal Eng.* 51:711-722, 2013, doi:10.1016/j.applthermaleng.2012.10.017.

[141] Zhou, F., Dede, E., Joshi, S., "Application of Rankine Cycle to Passenger Vehicle Waste Heat Recovery - A Review," *SAE Int. J. Mater. Manf.* 9(2):224-235, 2016, doi:10.4271/2016-01-0178.

[142] Prikhodko, V., Curran, S., Parks, J., Wagner, R., "Effectiveness of Diesel Oxidation Catalyst in Reducing HC and CO Emissions from Reactivity Controlled Compression Ignition," *SAE Int. J. Fuels Lubr.* 6(2):329-335, 2013, doi:10.4271/2013-01-0515.

[143] Benajes, J., Garcia, A., Monsalve-Serrano, J., Sari, R., "Evaluating the Efficiency of a Conventional Diesel Oxidation Catalyst for Dual-Fuel RCCI Diesel-Gasoline Combustion," SAE Technical Paper 2018-01-1729, 2018, doi:10.4271/2018-01-1729.

[144] Martin, J., Boehman, A., Topkar, R., Chopra, S. et al., "Intermediate Combustion Modes between Conventional Diesel and RCCI," *SAE Int. J. Engines* 11(6):835-860, 2018, doi:10.4271/2018-01-0249.

[145] Vitek, O., Macek, J., "Thermodynamic Potential of Electrical Turbocharging for the Case of Small Passenger Car ICE under Steady Operation," SAE Technical Paper 2017-01-0526, 2017, doi:10.4271/2017-01-0526.

[146] Aghaali H., Ångström, H.-E., "A review of turbocompounding as a waste heat recovery system for internal combustion engines," *Renew. Sust. Energy Reviews* 49:813-824, 2015, doi:10.1016/j.rser.2015.04.144.

Acknowledgments

Many people have contributed to the work described in this dissertation, in one way or another, for which I am truly grateful. First of all, I would like to thank my promotors and co-promotor for the opportunity to further develop my research skills and their support over the last four years. Bart, thank you for the freedom to follow my own path within the project and providing guidance whenever needed. I hope that the results of my work can help in shaping the future of the Zero-Emission Lab and upcoming projects. Niels, I particularly appreciated your fresh perspective on engine experiments, and I hope that you can keep combustion on the research agenda with many more television appearances. Frank, our regular talks on Friday morning and your constructive feedback have been of great value to my work.

The feedback of the user committee is gratefully acknowledged. I wish to thank Bogdan Albrecht for the many fruitful discussions and the opportunity to present my work at DAF Trucks. This exchange of knowledge was also done on several occasions with TNO Automotive. For that, I am much obliged to Erik Doosje, Cemil Bekdemir and Frank Kupper for the valuable meetings. The experiments described in this dissertation would not have been possible without the fuel injection equipment provided by Delphi Technologies. Many thanks to Tony Simpson and his colleagues for the support and advice throughout the project. I would like to thank Jan Roelofs for the outstanding work on the base engine of the new single-cylinder test setup. This setup was further realized by MeSa Engine Solutions.

I want to thank Mehrzad Kaiadi and Claes-Göran Zander for building the setup and their great support after commissioning. Keeping the engines up and running would not be possible without the support of the technical staff. I especially want to thank Theo de Groot for his help in and around the engine cells.

Several master and bachelor students have helped in setting up and executing the experiments, performing data analysis and creating new ideas. This is much appreciated. I particularly want to thank Robbert Dreezen for his help in getting started with the design of experiments method and regression analysis. Reading the book *Experiment!* by Öivind Andersson has been a real inspiration on that regard as well. I am honored that prof. Andersson, dr. Antonio García-Martínez and prof. David Smeulders take place in the committee.

The daily work would not have nearly been as exciting without many great colleagues. I want to thank PC, Robin and Noud for the good times during and outside of working hours. Thanks to (former) Progression Industry colleagues Jos and Michel for the good company and discussions. Although most of us have fledged (...fled?) by now, we will stay in touch. Also, thanks to Conrad, Thijs and other colleagues for the fun during our Thursday and Friday afternoon drinks. And a big thanks to Marjan for keeping the pack together. Allen, bedankt voor het lachen!

Finally, I want to thank my family and friends for all the encouragements. Above all, I want to thank Marloes for her unconditional love and support.

List of publications

1. Bakker, P.C., Willems, R., Dam, N., "Implementation of High-Speed Laser-Induced Incandescence Imaging in CI Engines," SAE Technical Paper 2016-01-0725, 2016, doi:10.4271/2016-01-0725.

2. Willems, R., Bakker, P.C., Dreezen, R., Somers, B., "The Impact of Operating Conditions on Post-Injection Efficacy; a Study Using Design-of-Experiments," SAE Technical Paper 2018-01-0229, 2018, doi:10.4271/2018-01-0229.

3. Bakker, P.C., Willems, R., Dam, N., Somers, B. et al., "Investigation of Late Stage Conventional Diesel Combustion - Effect of Additives," SAE Technical Paper 2018-01-1787, 2018, doi:10.4271/2018-01-1787.

4. Xia, L., Willems, R., de Jager, B., Willems, F., "Constrained Optimization of Fuel Efficiency for RCCI Engines", *IFAC PapersOnLine* 52-5:648-653, 2019, doi:10.1016/j.ifacol.2019.09.103.

5. Willems, R.C., Bakker, P.C., Dam, N.J., "Laser-induced incandescence versus photoacoustics: implications for qualitative soot size diagnostics," *Applied Physics B* 125:138, 2019, doi:0.1007/s00340-019-7248-2

6. Willems, R.C., Willems, F.P.T., Deen, N.G., Somers, L.M.T., "A Comparison of Load-Load Efficiency Optimization on a Heavy-Duty Engine Operated With Gasoline-Diesel RCCI and CDC," Proceedings of the ASME ICEF2019, October 20-23, 2019, Chicago, USA, doi:10.1115/ICEF2019-7149.

7. Willems, R., Willems, F., Simpson, T., Albrecht, B. et al., "Ramped Versus Square Injection Rate Experiments in a Heavy-Duty Diesel Engine," *SAE Int. J. Adv. & Curr. Prac. in Mobility* 2(3):1322-1336, 2020, https://doi.org/10.4271/2020-01-0300.

8. Seykens, X., Bekdemir, C., Han, J., Willems, R., et al., "CO2 neutral heavy-duty engine concept with RCCI combustion using seaweed-based fuels," SAE Technical Paper 2020-01-0808, 2020, doi:10.4271/2020-01-0808.

9. Willems, R., Willems F., Deen, N., Somers, B., "Heat release rate shaping for optimal gross indicated efficiency in a heavy-duty RCCI engine fueled with E85 and diesel," submitted to *Fuel*, 2020.

Curriculum vitae

Robbert Willems was born on April 15, 1989, in Apeldoorn, the Netherlands. He finished secondary education (HAVO) in 2007 at De Heemgaard in Apeldoorn. He studied automotive engineering at HAN University of Applied Sciences, Arnhem, where he obtained his diploma in 2012. In the following year, he completed the pre-master track at Eindhoven University of Technology (TU/e) and proceeded with the automotive technology master. He graduated in 2016 with his thesis *Shedding light on soot burnout in conventional diesel combustion by high-speed laser-induced incandescence imaging*. In that same year, he started a PhD project in the Power & Flow group at TU/e focused on improving the indicated efficiency of heavy-duty diesel engines. The results of that project are discussed in this dissertation.